O-GLCNACYLATION LEVELS REGULATE PRIMARY CILIARY LENGTH BY PROMOTING AXONEME DISASSEMBLY AND EXPLORING CHLAMYDOMONAS REINHARDTII AS A SYNTHETIC TEMPLATE

A Dissertation

by

JIE TIAN

Submitted to the Office of Graduate and Professional Studies of
Texas A&M University
in partial fulfillment of the requirements for the degree of

DOCTOR OF PHILOSOPHY

Chair of Committee,	Hongmin Qin
Committee Members,	Mark Zoran
	Wayne Versaw
	Kayla Bayless
Intercollegiate Faculty Chair,	Dirk Hays

December 2019

Major Subject: Molecular and Environmental Plant Sciences

ABSTRACT

The sensory organelle primary cilium is involved in sensing and transducing relevant signaling cascades in almost all cells of our body. These ciliary-mediated pathways impact cellular homeostasis and metabolism profoundly. However, it is almost entirely unknown whether the cellular metabolic state affects the assembly of cilia. This study investigates how O-linked β-N-acetylglucosamine (O-GlcNAc), a sensor of cellular nutrients, regulates ciliary length. Pharmacological or genetic inhibition of O-GlcNAcylation led to longer length cilia and vice versa. Further biochemical assays revealed that both α-tubulin and HDAC6 (histone deacetylase 6) were O-GlcNAcylated *in vivo*. *In vitro* enzymatic assays showed that O-GlcNAcylation of either tubulin or HDAC6 promoted microtubule disassembly, which potentially caused ciliary shortening. Taken together, these results uncovered a negative regulatory role of O-GlcNAc in modulating the ciliary microtubule assembly. The crosstalk between O-GlcNAc and cilium is likely critical for fine-tuning a cellular response to nutrients, such as glucose, amino acids.

Flagella of green algae, *Chlamydomonas reinhardtii*, have similar structure and function as mammalian primary cilia. Structurally, a flagellum consists of a microtubule-based axoneme surrounded by a specialized membrane extended from the cell membrane. An axoneme is composed of 9 doublet microtubules (DMTs) surrounded by two central singlet microtubules. The beating of the *Chlamydomonas* flagella relies on the force-generating motility appendages, including outer and inner dynein arms, radial spokes, and dynein regulatory complex (DRC) assembled onto DMTs in a highly specific and periodic manner. The highly organized and regularly arranged structures of DMTs make them an excellent natural template for synthesizing biomolecules by fusing target proteins with axoneme proteins. The concept was proven with

successful transport and localization of tagged inner junction protein FAP20 and radial spoke protein RSP3 into the inner junction and radial spokes of flagella. This project tested whether *Chlamydomonas* could be utilized as a template for synthetic biology by inserting fusion proteins FAP20-TEV-Beta-lactamase (Bla), estrogen receptor alpha (ERα) and RSP3-TEV-Bla, ERα. These results confirmed that flagella are capable of assembling protein arrays. The RSP3-TEV-Bla and FAP20-TEV-Bla attached on the isolated flagella axoneme are enzymatically active; the flagella-bounded beta-lactamase was able to recycle for reuse; repeated deflagellation and regeneration can be used to increase the yield of tagged protein; RSP3-ERα and FAP20-ERα are able to bind and remove estrogen compounds. Altogether, the data indicate that flagella axoneme can serve as a template to synthesize biomolecules.

ACKNOWLEDGEMENTS

I would like to thank my committee Chair, Dr. Hongmin Qin, and committee members, Dr. Mark Zoran, Dr. Wayne Versaw, and Dr. Kayla Bayless, for their guidance and support throughout the course of this research.

I would like to thanks Dr. Jing Li from Capital Normal University for generously providing constructs, antibodies, and ideas for the project of O-GlcNAc; Dr. Daan van Aalten from Dundee University for providing a tremendous amount of OGA and OGT inhibitors for the entire research.

CONTRIBUTORS AND FUNDING SOURCES

This work was supervised by a dissertation committee consisting of Dr. Hongmin Qin, and Drs. Mark Zoran and Wayne Versaw of the Department of Biology and Dr. Kayla Bayless of the College of Medicine at Texas A&M University Health Science Center.

The data for making Figure 3-5 was conducted by Shih-Hung Yang in Dr. Kung-Hui Chu's lab of the Division of Environmental, Water Resources, and Coastal Engineering, Zachry Department of Civil and Environmental Engineering.

All other work conducted for the dissertation was completed independently by the student.

Graduate study was supported by TAMU College of Science Strategic Transformative Research Program and TAMU Superfund Research Center 2018 Pilot Projects Program to Dr. Hongmin Qin.

NOMENCLATURE

Bla	Beta-lactamase
DMTs	Doublet Microtubules
ERα	Estrogen Receptor α
FAP20	Flagella Associated Protein 20
HBP	Hexosamine Biosynthetic Pathway
IFT	Intraflagellar Transport
MT	Microtubule
O-GlcNAc	O-linked β-N-acetylglucosamine
OGA	O-GlcNAcase
OGT	O-GlcNAc Transferase
PTM	Post-translational Modifications
RS	Radial Spoke
RSP3	Radial Spoke Protein 3
SG	GlcNAcstatin G
TG	Thiamet G

TABLE OF CONTENTS

Page

LIST OF FIGURES

Page

LIST OF VIDEOS

Video 3-2-1 cc125

Video 3-2-2 im5

Video 3-2-3 pf14

Video 3-2-4 FAP20-ER alpha

Video 3-2-5 FAP20-Bla

Video 3-2-6 RSP3-ER alpha

Video 3-2-7 RSP3-Bla

Real-time videos of the wild-type *cc125*, mutant strains *im5*, *pf14*, and rescue strains FAP20-ERα, FAP20-Bla, RSP3-ERα, RSP3-Bla are included as a separate file.

CHAPTER I

INTRODUCTION

Introduction I

Basics of primary ciliary

Primary cilia are microtubule-based hair-like structures that extended from the surface of cells. They were considered as vestigial organelles until recent publications revealed that they exist on most types of quiescent mammalian cells, such as smooth muscle, neurons, and pancreatic endocrine cells [1-4]. Primary cilia on different tissue types are distributed through various receptors, ion channels, and transporters on the ciliary membrane to transduce extracellular signals within the cell to regulate various vital processes, including development, organ function, and tissue homeostasis [2, 5, 6] (Figure 1-1). Localization and proper function of primary-cilium signaling receptors rely on proper ciliary formation. Hormone receptors somatostatin sst3 receptor (Sst3R), melanin-concentrating hormone receptor 1 (Mchr1), insulin receptor (IR), and leptin receptor (LepR) all localize to hypothalamic neuronal primary cilia. Mis-localization of these receptors on neurons results in hyperphagia-induced obesity and type II diabetes [7-10]. Abnormal formation or dysfunction of primary cilia causes a series of human diseases, such as retinal degeneration, polycystic kidney disease, Bardet-Biedl syndrome, and Joubert syndrome, which are collectively known as ciliopathies [11]. Therefore, it is crucial to understand how ciliary formation and ciliary length are regulated. The regulation of ciliary formation and ciliary length will be discussed in the following two sections.

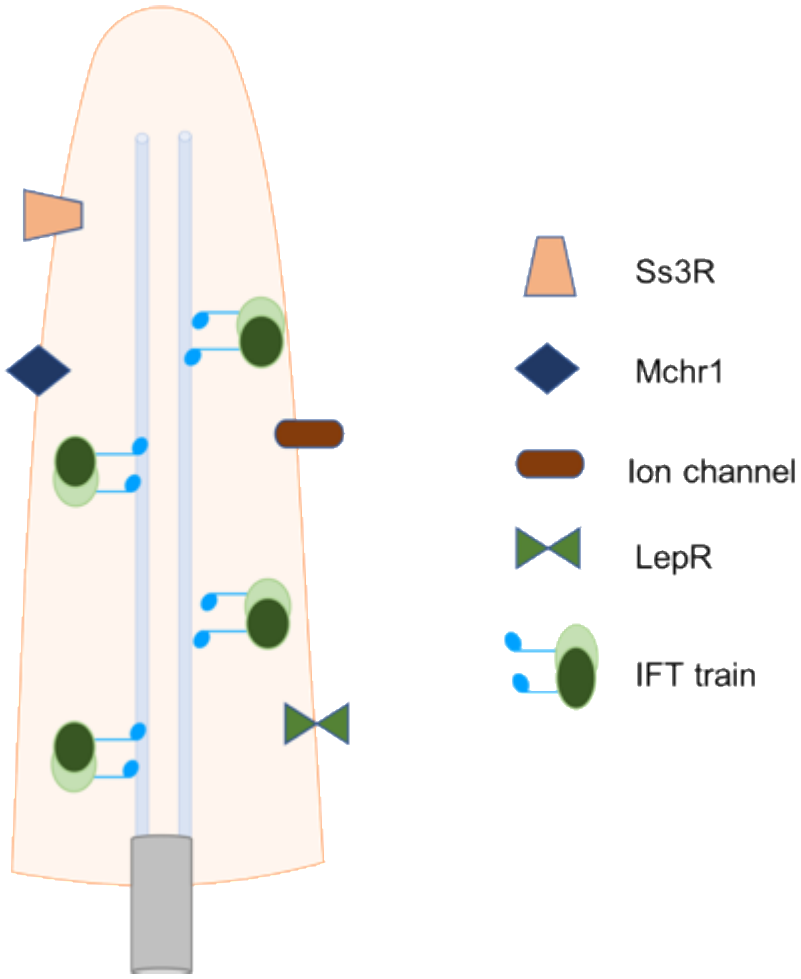

Figure 1- 1 Schematic presentation of primary cilium as a signaling hub.
The ciliary axoneme and membrane proteins were transported to the ciliary compartment by IFT trains. Primary cilia on different tissue types are distributed through various receptors, ion channels, and signal transporters on the ciliary membrane to transduce extracellular signals within the cell and to play roles in various vital processes, including development, cell cycle progression, and tissue homeostasis. Ss3R, somatostatin sst 3 receptor; Mchr1, melanin-concentrating hormone receptor 1; IR, insulin receptor; LepR, leptin receptor; IFT, intraflagellar transport.

Regulation of ciliogenesis

The first aspect is the regulation of cilia formation. Ciliogenesis is a process of cilia formation that occurs in an ordered set of steps. It starts with the transition of a mother centriole into a basal body, then the basal body migrating and docking at the apical plasma membrane, followed by a nucleating outgrowth of axonemal microtubules to give rise to a cilium [12-15]. Because protein

synthesis is restricted to the cytoplasm, elongation of the cilium is conducted by intraflagellar transport (IFT), which carries axoneme proteins and transports cargo from the basal body to the distal tip for construction [16-18]. Meanwhile, IFT is a bidirectional motor-driven complex that can also transport turnover proteins from the distal tip to basal body [17, 19, 20]. The axoneme is highly dynamic, undergoing assembly and disassembly constantly. When the cilium is elongated, the assembly rate is faster than the disassembly rate. When the cilium reaches steady state, the balance of the axoneme assembly and disassembly results in the final ciliary length [21, 22]. In summary, assembly and disassembly rate regulated by IFT is critical for determining ciliary length.

Although the mechanisms of how cells are triggered to initiate ciliary assembly or disassembly are still mostly enigmatic, recent findings provide insights into the regulation of ciliogenesis [21, 23]. First, ciliogenesis is highly dependent on cell cycle progression. The primary cilium is typically assembled during G1 or G0 phase and disassembled when the cell enters into mitosis [24, 25]. One possible explanation is that centrosome dynamics are precisely synchronized with the progression of the cell cycle [26, 27]. During the G1/S transition, centrioles need to translocate from the ciliary basal body to the cell interior to be duplicated, which will result in the resorbing of primary cilia [28]. Many centrosomal proteins such as CP110 and Cep97 that regulate cell cycle progression are also involved in ciliogenesis. Knocking out either CP110 or Cep97 prevents cytokinesis and formation of cilia [29]. Also, the mitosis regulator Aurora A and its upstream interaction protein HEF1 are localized to the basal body and are activated to promote ciliary disassembly. Further studies showed that HDAC6 acts downstream of Aurora A to deacetylate and destabilize axonemal tubulin, which leads to rapid cilium resorption [30, 31].

Besides, the transporter of ciliary proteins IFT is another factor controlling ciliogenesis. The IFT train size and speed are larger and faster, which can carry more axonemal precursors, in the growing cilia [21, 32]. Inhibition of *Chlamydomonas* IFT27, which is a Rab-like small G protein of IFT complex, results in disassembly of flagella as well as defects in cytokinesis [33].

Ultimately, many growth factors and genes involved in ciliopathies participate in the regulation of ciliogenesis. Many cultured mammalian cell types grow cilia upon serum starving promotes quiescence [25, 26]. One explanation attributed to this phenomenon is that serum starvation synchronizes cells in G0 phase to induce ciliogenesis. Serum starvation-induced autophagy activation may also produce cilia by removing ciliogenesis inhibition factors such as oral-facial-digital syndrome 1 (OFD1) from centriolar satellites. One finding showed that activation of autophagy rapidly degrades OFD1 at the centriolar satellites to induce ciliogenesis upon serum starvation. However, in the autophagy-deficient mutant cells, OFD1 accumulates at the centriolar satellites and impairs ciliogenesis [34]. Moreover, disruption of the intact phosphoinositide signaling pathway is another factor that promotes ciliogenesis. The classic tumor suppressor gene *VHL* gene is involved in phosphatidylinositol 3'-kinase (PI3K)/Akt signaling pathway. Typically, VHL is a hypoxia sensor, but VHL can function in promoting ciliogenesis. Deficiency of VHL in primary mouse embryonic fibroblasts causes loss of cilium [35-37]. PI3K is counteracted with VHL activity to restrict ciliogenesis. PI3K can also inactivate GSK3β through Akt-mediated phosphorylation to inhibit ciliogenesis [38]. These results indicate that GSK3β and VHL may have overlapping functions in promoting ciliogenesis. Overall, regulation of ciliogenesis is mainly regulated in three aspects, including cell cycle progression, IFT, and signaling pathways.

Ciliary length regulation

The second aspect is the regulation of ciliary length regulation. Primary cilia are sensory organelles that can be found on almost all vertebrate cells and possess sensory function [1]. Ciliary length varies extensively among different cells types. The length could range from 1 μm on vascular endothelial cells to approximately 200 μm on mammalian olfactory neurons, but ciliary length is constant for a given cell type [39, 40]. These observations suggest that ciliary length is subject to cell-type-specific regulation, and an optimal range is essential to ensure proper functionality of the cell. Indeed, the ciliary length is tightly regulated, either shorter or longer length of cilia leads to defects in function [41, 42]. In humans, the abnormal ciliary length correlates with various diseases, such as polycystic kidney disease [43, 44]. The mechanisms of ciliary length regulation have been studied extensively and can be briefly summarized into the following categories.

1. The assembly and disassembly balance regulate ciliary length

First, the ciliary length is regulated by a balance between axonemal assembly and disassembly, which is dependent on IFT machinery [22]. The IFT anterograde transports proteins from the base to the distal tips, which is catalyzed by kinesin motors; the IFT retrograde transports turnover proteins from the distal tip to the cell body, which is catalyzed by dynein motors [20]. IFT complex is composed of three sub-complexes: motor proteins, complex A, and complex B. Kinesin is a heterotrimeric complex consisting of two motor proteins KIF3A and KIF3B, and a nonmotor subunit KAP3. Dynein is the same as cytoplasmic dynein 2 [45-48]. IFT-A contains 6 known proteins and IFT-B contains at least 15 known proteins, which are not listed here [40]. IFT-A and IFT-B play distinct functions in maintaining flagellar assembly. IFT-A mutations

result in accumulation of IFT proteins in the stumpy cilia, while IFT-B mutations lead to short or deficient of ciliary assembly. The results suggest that IFT-B is more important for anterograde transportation, and IFT-A is more critical for retrograde transportation [21]. Recent findings indicate that BBSome may be another subset of IFT complex, which participates in transporting membrane proteins to the cilium [49, 50]. BBSome is composed of 7 BBS proteins (BBS1, BBS2, BBS4-9) [51]. Some BBS mutations may still assemble cilia but with minor functional defects, however, *bbs-1, 7, 8* loss-of-function mutations result in dissociation of IFT-A and IFT-B and complete ciliary defects [52-54].

It has been observed that axoneme assembly and disassembly happen continuously at the distal tip of flagella even after reaching their final length, which indicates that the axoneme is a highly dynamic structure [22]. When flagella reach a steady state, the assembly rate equals the disassembly rate at the distal tip and results in the final length of flagella [22, 55]. Disrupting the balance between axoneme assembly and disassembly by inhibiting IFT pathways induces cilia shortening gradually [22, 56]. The results indicate that the axoneme turnover is critical for the ciliary length regulation. Due to the disassembly rate is constant, the modulation of assembly rate is the key to regulate ciliary length. Findings showed that IFT is one factor participating in the regulation of the assembling rate. Reduction of IFT rate leads to shortening of ciliary length [22]. Moreover, *Chlamydomonas fla10* is a temperature permissive mutant, which mutated on the subunit of anterograde motor kinesis-2. Flagella of *fla10* cells gradually resorb when transferred to the restrictive temperature due to the deficiency of anterograde transport [57, 58]. The observation supports the previous finding that IFT contributes to axoneme assembling.

2. PTMs of axoneme regulate ciliary length

In addition, stability and assembly of axoneme are regulated by various types of post-translational modifications (PTMs) on the axonemal α- and β- tubulins, such as acetylation, detyrosination/tyrosination, polyglutamylation, and polyglycylation [59-62]. It is believed soluble α- and β-tubulin dimers are largely unmodified while highly post-translational modified when incorporated into MTs. Thus, various tubulin PTMs are accumulated in stable, long-lived microtubules, which has been observed in several studies [63-65]. The following three paragraphs discuss the modifications of acetylation, detyrosination, and polyglutamylation in regulation ciliary length.

Firstly, Tubulin acetylation is considered a hallmark of stabilized MTs and microtubular structures such as axoneme [66, 67]. Typically, acetylation occurs on lysine 40 (K40) of α-tubulin and towards the lumen of microtubule as soon as MT assembled [60, 68, 69]. Findings showed that tubulin acetylation is associated with long-lived MTs and promotes motor protein kinesin-I binding and trafficking on MTs [70, 71]. Acetylation of tubulin is mainly catalyzed by enzymes alpha-tubulin acetyltransferase 1 (αTAT1) and MEC17. Both αTAT1 and MEC17 acetylate K40 of α-tubulin. Disrupting either of the genes *αTAT1* or *MEC17* abolishes tubulin acetylation and labile MTs [72-75]. Ciliary axoneme acetylation is only catalyzed by αTAT1 [74]. By contrast, two enzymes catalyze tubulin deacetylation, histone deacetylase 6 (HDAC6) and SIRT2 (the human Sir2 orthologue). Both of them are members of the histone deacetylase family. Knockdown or pharmacological inhibition of HDAC6 increases tubulin acetylation and decreases MT growth rate [65, 76-79].

Furthermore, the PTM detyrosination is the first modification identified to regulate MTs dynamics [80]. Due to the C-terminal tail domains (CTTs) of α- and β-tubulins are both flexible domains locate on the surface of MTs, many microtubule PTMs happen on the CTTs, such as detyrosination [69, 81]. Most isotypes of α-tubulin contain a tyrosine at the C-terminal of MTs. This tyrosine is usually removed by tubulin tyrosine carboxypeptidase (TTCP), which exposes a C-terminal glutamic acid and stabilizes MTs through suppressing the plus end dynamics [82, 83]. The modification of tyrosine is catalyzed by tubulin tyrosine ligase (TTL) [84]. Despite the fact that TTCP prefers acting on microtubule polymers, TTL prefers tubulin dimers as a substrate to interfere with polymerization. Findings showed that overexpression TTL inhibits MT polymerization [85, 86]. This result is consistent with the observation that the detyrosination level in the newly assembled axoneme is much higher than the old axoneme [62, 67]. Overall, the findings indicate that detyrosination stabilizes axoneme while tyrosination promotes axoneme disassembly.

Lastly, polyglutamylation of α- and β-tubulins prominent in stable MTs such as axons of neuronal cells, mitotic spindles, and axoneme of primary cilium [87-89]. TTLL1 (TTL-like 1) and many other subtypes are the enzymes that catalyze the tubulin glutamylation [90]. For example, the observation that blocking glutamylation inhibits the motility of sea urchin sperm axonemes suggests that tubulin glutamylation is involved in regulating the ciliary dynein activity [91]. However, the mechanism of how tubulin glutamylation affects axoneme stability is still unknown.

In summary, precursor tubulin undergoes diverse PTMs during cilium assembly, which highlights the importance of tubulin PTMs in the axoneme assembly and stability. For instance, acetylation and detyrosination regulate axoneme stability by interacting with motors and plus-end capping proteins, loss-of-function of modifying enzymes studies showed glutamylation is the most critical one function in axoneme assembly and stability [92]. However, many other PTMs, such as phosphorylation, sumoylation, and ubiquitylation, are also worth investigation.

3. Signaling pathways regulate ciliary length

Finally, studies in many different systems have revealed broad-spectrum signaling molecules involved in ciliary length regulation [93, 94]. The observation that lithium treatment elongates cilium length suggests that cAMP plays a role in ciliary length regulation. Moreover, heterotrimeric G proteins, second messengers cAMP, cGMP, Ca^{2+}, and downstream effectors, such as protein kinase A and MAP kinase signaling, all affect ciliary length [95-99]. The best-studied signaling pathway in regulating ciliary disassembly is the one mediated through mitotic kinase Aurora A, which phosphorylates and activates downstream HDAC6 at the basal body to deacetylate tubulin, which in turn promotes ciliary disassembly. Serum stimulation induced expression and activation of HEF1 at basal body contributes to the stabilization and activation of Aurora A to modulate ciliary disassembly [30, 31]. Another set of mitotic kinases responsible for ciliary length regulation is the NIMA-related kinases (NEKs). There are 11 ortholog Nek genes in the human genome. Most of them have cell cycle-related functions while some such as Nek1 and Nek8 localize to centrosomes/cilium and function in regulating ciliary length [100-102]. Mutations in Nek1 and Nek8 lead to ciliary signaling defections and contribute to ciliary dysfunction, which is related to polycystic kidney diseases [103, 104]. In mice, loss of Nek8

produces extra-long renal cilia, while the loss of Nek1 induces significantly shorter length [44, 105, 106], indicating that abnormal ciliary length contributes to the pathology of kidney dysfunction.

Additionally, ciliary signaling pathways involved in the development, such as sonic hedgehog (Shh), Wingless (Wnt), and Notch, affect ciliary assembly or length control [107-109]. Inhibition of Gsk3β, which is a kinase function in the Wnt pathway to phosphorylate and degrade β-catenin, induces significantly elongated cilia both in *Chlamydomonas* and mammalian cells [110-112]. To date, there is still a growing list of signaling molecules that participate in ciliogenesis and ciliary length control.

Primary cilia as a signaling hub and their role in human diseases

Primary cilium as a cellular organelle plays important role in physiology. Primary cilia have a significant function in cell signaling because the ciliary membrane contains a variety of receptors, ion channels, and signaling transporters. Even some of their downstream effector molecules are localized to the cilium or basal body as well. Primary cilia are coordinating diverse key processes from development to tissue homeostasis, such as differentiation, cell cycle progression, apoptosis, and autophagy. Depending on the cell types, signaling pathways vary, including receptor tyrosine kinases (RTKs), Hedgehog (Hh), Wnt, Notch, neuronal receptors, planar cell polarity (PCP), and a platelet-derived growth factor receptor (PDGFR) [2, 113-118]. A single primary cilium can incorporate multiple signaling pathways and respond to different stimuli, such as morphogens, hormones, and growth factors [2]. When the growth and morphogens factors bind to their receptors on the ciliary membrane, different intracellular

signaling pathways will be activated. For instance, growth factor stimulated RTK results in activation downstream signaling pathways, such as MAPK cascade, PI3K-Akt kinase (AKT) kinase cascade, and Janus kinase (JAK)-signal transducer and activator of transcription (STAT) cascade [119]. In dermal fibroblast, PDGFRα in primary cilia modulates the activation of PI3K-AKT-Na^+/H^+ exchanger (NHE1) pathway to regulate cell migration [120, 121]. Also, the ciliary transforming growth factor β (TGFβ) is involved in left-right asymmetry regulation. Binding of Nodal- growth differentiation factor -1 (Gdf1) to TGFβ receptors result in the expression of target genes Lefty 2 and Pitx 2 to develop left-side morphogenesis [122, 123]. Many other factors, such as insulin growth factor (IGF), BBSome, leptin signaling, and hedgehog signaling, also transduce signaling to intracellular through primary cilia [124-126].

As discussed above, primary cilia transduce diverse extracellular signals into the cell. Therefore, it is not surprising that dysfunction of primary cilia causes a variety of human diseases, including left-right asymmetry defects, neurodevelopmental disorder, polycystic kidney disease (PKD), polydactyly, obesity, infertility, and cancers; as well as syndromes, such as Bardet-biedl syndrome (BBS), Alström syndrome (ALMS), Nephronophthisis (NPHP), Meckel syndrome (MKS), and Joubert syndrome (JBTS), are termed as ciliopathies [93, 127]. Many ciliopathies are caused by abnormal ciliary length or impaired ciliogenesis. Even a mild deviation from the normal range of ciliary length on a particular cell type is sufficient to generate pathogenic phenotypes. Therefore, understanding the mechanisms of ciliary regulation is critical for developing medicines and the treatment of ciliopathy disorders.

O-GlcNAcylation as one potential factor contributing to ciliary length regulation

A tremendous amount of research has shed light on the primary cilium and its crucial roles in maintaining tissue homeostasis and the pathogenesis of obesity and diabetes in the past decades. However, the genetic and molecular mechanisms of how primary cilium dysfunction is involved in the etiology of obesity and diabetes still lack investigations. O-GlcNAc, a modification using UDP-GlcNAc as a substrate derived from the hexosamine biosynthetic pathway (HBP), regulates energy homeostasis through participating in insulin and leptin signaling pathways [128, 129]. Several findings recently enlighten a potential interplay between O-GlcNAcylation and primary ciliary length. The work of Yu et al. showed that primary cilia were fewer and shorter in the diabetic mouse eyes, trachea, and skin cells compared to wild type. Increasing O-GlcNAcylation levels of RPE1 cells in culture medium impaired ciliogenesis [130]. The results indicate that higher O-GlcNAcylation levels decrease ciliary length and ciliogenesis, which is partially supported by the previous finding that glucose deprivation promoted primary cilium formation [131]. However, the mechanisms of how cellular O-GlcNAcylation levels regulate the ciliary length are lacking. Another study showed that obese individuals have shortened and compromised functional primary cilia of adipose-derived mesenchymal stem cells (ASCs) in humans [132]. Elevated activities of Aurora A and HDAC6 contribute to the shortening of ciliary length. Also, the deficiency of ciliary signaling Hh may impair ASCs differentiation to adipocyte in obese individuals [132]. Because the elevated O-GlcNAcylation is directly linked to many metabolic diseases including obesity and diabetes, the results imply that the escalated O-GlcNAc levels in the obese individuals contribute to the shortening of primary cilia [133, 134].

The principles of O-GlcNAc modification

O-linked β-N-acetylglucosamine (O-GlcNAc) modification was unexpectedly discovered by Gerald W. Hart when purifying galactosyltransferase in 1983 [135]. O-GlcNAc modification generally happens on 10-20% of all nuclear, mitochondria, and cytoplasmic proteins of the cell [136]. O-GlcNAc is involved in diverse cellular processes, such as transcription, translation, cell signaling, cytoskeletal network dynamics, stress responses, and proteasomal degradation [137]. O-GlcNAc has been found not only in all cellular compartments, but also ubiquitous in all investigated eukaryotes, ranging from fungi, plants, worms, and insects to humans [135].

The single pair of enzymes, O-GlcNAc transferase (OGT) and O-GlcNAcase (OGA), respond to the dynamic cycling of O-GlcNAc from serine/threonine residues of the target protein (Figure 1-2). OGT uses UDP-GlcNAc derived from the HBP as substrate donor to glycosylate target protein. O-GlcNAc is removed from target proteins by the enzyme OGA. The gene encoding OGT is evolutionarily conserved from plants to humans. The human *OGT* gene maps to chromosome Xq13.1, a region associated with Parkinson's disease [138]. Alternative splicing of the *OGT* gene results in three isoforms: the nucleocytoplasmic/full-length OGT (ncOGT, ~110kD), mitochondrial OGT (mOGT, ~90kD), and short form of OGT (sOGT, ~78kD), which target to the nucleus, mitochondrion, and cytosol respectively. All OGT isoforms contain an N-terminal domain with different numbers of tetratricopeptide repeats (TPRs), which mediate protein-protein interactions of the enzyme with the targeting proteins, and a C-terminal domain that is homologous to glycogen phosphorylase. The C-terminal domain contains the substrate of UDP-GlcNAc binding and catalytic sites [135]. Though a glycomic study of mouse brain

postsynaptic density revealed that about half of the O-GlcNAc modification sites have a PVS/TS/T or TTA motif, there is no preferred peptide sequence for binding to OGT [138].

The enzyme OGA is highly conserved in eukaryotic species, especially in mammals, but absent in prokaryotes and yeasts. OGA is encoded by the gene of *meningioma expressed antigen 5* (*MGEA5*) in mammals. There are two spliced isoforms of OGA (short and full-length). The full-length ncOGA localizes predominantly in the cytosol while the short form sOGA resides in the nucleus. Both isoforms contain the C-terminal glycosidase domain and the same first 662 amino acids. While the sOGA has an alternative carboxy-terminal sequence with 15 amino acids while ncOGA has a domain that homologous to the histone acetyltransferase (HAT) family at the C-terminal. However, the regulation of OGA activity is mostly a mystery. It is known that OGA can be O-GlcNAcylated and cleaved by activated caspase-1 at the site of Asp413, but such cleavage does not affect OGA activity [138].

Both OGT and OGA are ubiquitously expressed but with high expression in immune cells, brain, and pancreas. Maintaining homeostasis of O-GlcNAcylation is vital for its normal function in many cellular processes, such as transcription, translation, and signal transduction [135]. Dysregulation of O-GlcNAcylation homeostasis is contributing to the pathogenesis of a plethora of human diseases, including diabetes, neurodegeneration, and cancers [137, 139-143].

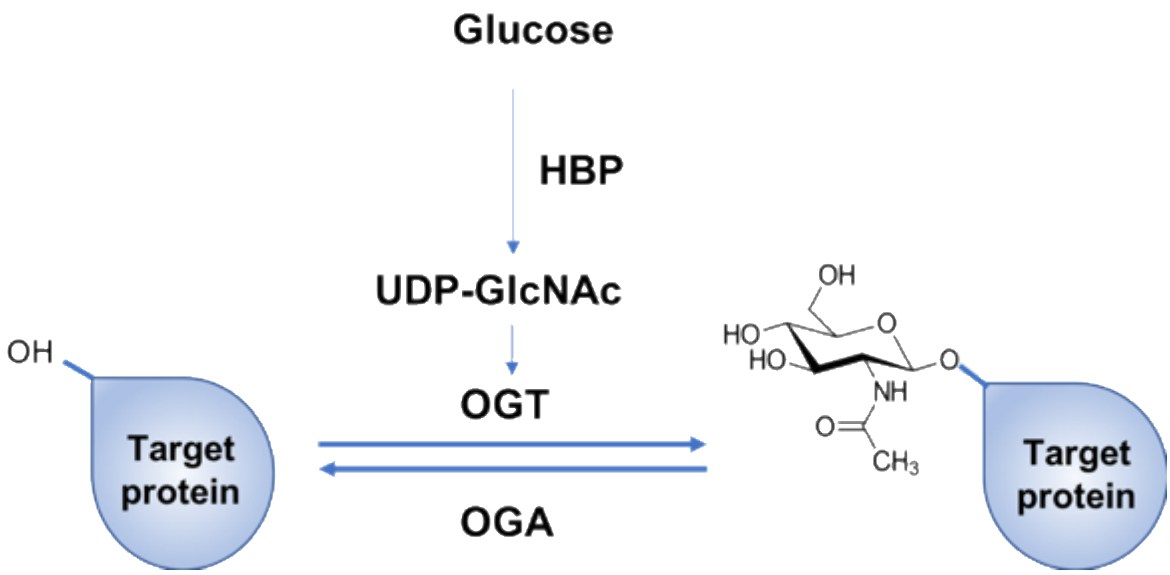

Figure 1- 2 Cycling of O-GlcNAc modification.
2-5% of glucose in taken by mammalian cells enters into the HBP directly. UDP-GlcNAc will be produced after many steps' reaction. The enzyme OGT uses UDP-GlcNAc as a substrate to catalyze glycosylation of the target protein. GlcNAc will be added on the Ser/Thr of the target protein. The modification is removed by the enzyme OGA. HBP, hexosamine biosynthetic pathway; OGT, O-GlcNAc transferase; OGA, O-GlcNAcase.

The regulation of dynamic cycling of O-GlcNAc

O-GlcNAc modification is one of the primary mechanisms for cells to sense the abundance of nutrients. About 2-5% of cellular glucose is converted to UDP-GlcNAc through the HBP [144]. The production of UPD-GlcNAc is the integration of HBP with the metabolism of carbohydrates, amino acids, fat, and nucleotides, which renders the concentration of UDP-GlcNAc highly dependent on nutrient flux and metabolite availability [129, 145, 146]. Meanwhile, the activity of OGT is highly responsive to UDP-GlcNAc concentrations. Therefore, the cellular O-GlcNAcylation level depends on the metabolic state of the cell and is considered as a nutrient sensor [147]. For example, increasing the intracellular level of UDP-GlcNAc leads to elevated O-GlcNAcylation levels [148, 149]. Besides, culturing mesangial cells in a high glucose medium

(25 mM) increases cellular O-GlcNAcylation levels compared to cells cultured in average glucose (5.5 mM) [150]. These examples support that O-GlcNAc is a cellular nutrient sensor.

Furthermore, O-GlcNAc interplays extensively with phosphorylation to regulate protein's activity. They share some common characteristics, such as both target Ser/Thr residues of the target proteins, are highly dynamic, and function in cellular processes like transcription, translation, cell division, and cell signaling [146]. When the global cellular O-GlcNAcylation level was raised through the treatment of OGA inhibitors, decreased phosphorylation on ~33% of phosphor-sites and increased phosphorylation on ~18% of phosphor-sites can occur [151]. The results indicate that elevated O-GlcNAcylation levels have different effects on phosphorylation modification at different sites. Indeed, there are generally three types of interplay between these two modifications. First, O-GlcNAcylation and phosphorylation may compete for the same modification sites on the target proteins. This competition alters the activity or stability of the proteins. For example, the anti-apoptotic protein Akt increases O-GlcNAc and decreases phosphorylation at Ser473 to promote apoptosis [152]. Second, the O-GlcNAc and phosphorylation modification occurs within a range of ~10 amino acids in many cases. The balance between O-GlcNAcylation and phosphorylation is likely to influence the target protein's function. For instance, O-GlcNAc modification of many cytoskeleton proteins is decreased upon activation of protein kinase C (PKC) and protein kinase A (PKA), while O-GlcNAc modification is increased when PKC is inhibited [138]. Last, the phosphorylation and O-GlcNAcylation on the same protein can be additional or synergistic. For example, increased O-GlcNAcylation of the Ser/Thr kinase Akt1 also increases Akt1 phosphorylation, which indicates Akt1 can be

simultaneously modified with O-GlcNAc and phosphorylation [153]. Other examples are also seen on insulin receptor substrate (IRS) and AMP-activated protein kinase (AMPK) [134].

At last, some kinases are involved in O-GlcNAc cycling regulation. Enzymes OGT and OGA are phosphorylated by various kinases to modulate their activity and interaction with their substrates, including calcium/calmodulin-dependent protein kinase IV (CaMKIV), glycogen synthase kinase 3 beta (GSK3β), and AMPK [146, 154, 155]. For instance, GSK3β phosphorylates and activates OGT on S3 or S4. However, this phosphorylation competes with O-GlcNAcylation to regulate OGT activity [155]. Also, inhibition of GSK3β will modulate O-GlcNAcylation profiles. On the one hand, many proteins have elevated O-GlcNAcylation levels, such as cytoskeletal and heat shock proteins. On the other hand, many other proteins have diminished O-GlcNAcylation levels, such as transcription factors and RNA-binding proteins [156]. In addition, AMPK is an energy sensor protein kinase in response to intracellular ATP levels. AMPK is positively regulated by O-GlcNAcylation, and in turn phosphorylate OGT on T444 regulates its substrate selectivity [154, 157]. GSK3β and AMPK are also kinases involved in ciliary length regulation, which further indicate the potential interplay between O-GlcNAcylation levels and primary ciliary length.

O-GlcNAc in metabolism homeostasis and in human diseases

O-GlcNAc as a nutrient sensor is highly sensitive to the availability of glucose, amino acids, fatty acids, and nucleotides, which will feed HBP flux to produce UDP-GlcNAc. However, OGT has different substrate specificity at different UDP-GlcNAc concentration. It has been clear that OGT and O-GlcNAc mediate different signaling pathways based on the nutrient state to impact

nearly all cellular processes and cellular physiology to maintain proper homeostasis [129, 144]. Dysregulation of nutrient homeostasis or nutrient excess leads to abnormal O-GlcNAcylation of proteins with corresponding effects on cellular processes and contributes to the etiology of humans diseases, such as diabetes, neurodegeneration, and cancers [144].

First, O-GlcNAcylation participates in regulating glucose metabolism. Altering the extracellular glucose levels modulates cellular O-GlcNAcylation levels via changing the flux of the HBP [158]. Meanwhile, O-GlcNAc regulates all enzymes' activities in the glycolytic pathways in turn. Elevated O-GlcNAcylation levels by OGT overexpression or OGA inhibition decrease glucose metabolism through promoting O-GlcNAcylation phosphofructokinase I (PFK1) on S529 to attenuate the activity of PFK1 [144]. Also, increased O-GlcNAc damps signaling pathways that promote glucose transport, such as mTOR, PI3K-Akt, and AMPK pathways [159-161]. Furthermore, O-GlcNAc down-regulates the insulin-signaling pathway and contributes to insulin resistant under a prolonged hyperglycemia condition [162, 163]. Several key proteins in the insulin-signaling pathway are O-GlcNAcylated, and the O-GlcNAc modification of them impairs the metabolic pathways of insulin receptor (IR)/IR substrate (IRS)-1, 2/PI3K/Akt [164]. The insulin-signaling pathway is mediated by primary cilia. For example, O-GlcNAcylation of IRS-1and IRS-2 may interplay with phosphorylation to regulate the activity of their downstream signaling cascades [165, 166]. Also, increased O-GlcNAcylation level through OGA inhibitor O-(2-acetamidO-2-deoxy-D-glucopyranosylidene) amino-N-phenylcarbamate (PUGNAc) treatment diminishes activation of Akt. Together with other studies, high O-GlcNAc attenuates insulin signaling and contributes to insulin resistance, which is a hallmark of type II diabetes [167-170]. Overall, these results indicate that increasing the flux of HBP, such as elevated UDP-GlcNAc,

prolonged hyperglycemia, and glucosamine treatment, raises O-GlcNAcylation levels and leads to insulin resistance and eventually type II diabetes [133, 171].

Furthermore, reduced O-GlcNAcylation contributes to the etiology of neurodegeneration, such as Alzheimer's disease (AD) and Parkinson's disease (PD). Due to the impaired glucose metabolism in AD brain tissue, decreased O-GlcNAcylation of numerous neural proteins contributes to the development of AD. The tau protein associated with microtubule is one of the most well-studied proteins [172-174]. Abnormal oligomerization of tau caused neurofibrillary tangles (NFTs) is one of the defining pathological features of AD [142]. The status of tau is regulated reciprocally by O-GlcNAcylation and phosphorylation. Decreased O-GlcNAc modification leads to hyperphosphorylation and aggregation of tau, which contributes to NFTs and pathologies of Alzheimer's disease [174]. Other hallmarks of AD are the accumulation of amyloid beta (Aβ) plaques in the extracellular space, synaptic loss, and dementia. The Aβ plaque is derived from amyloid precursor protein (APP), [175]. It has been shown that APP is O-GlcNAcylated. Increased O-GlcNAcylation impairs Aβ peptides levels and plaque formation in the brain and rescues memory impairment [176, 177]. Furthermore, the aggregation of α-synuclein, the key pathogenesis of Parkinson's disease, is partially due to the impaired O-GlcNAc cycling and leads to the neuronal death [178, 179]. Therefore, the development of OGA inhibitors as a therapeutic target might offer the opportunity to alter disease progression and provide useful treatment of neurodegenerative diseases [142, 144].

Lastly, total O-GlcNAcylation levels are elevated in cancer cells with the increased expression of OGT and decreased OGA [180]. The metabolism of glucose and glutamine is increased in cancer

cells, which suggests the dysregulation of cellular metabolism and is considered a hallmark of cancer cells [181, 182]. The elevated glucose and glutamine flux will feed in the HBP and contribute to O-GlcNAc mediated activation of AMPK and mTOR signaling pathways [183]. In addition, the key cell growth and metabolic regulator hypoxia-inducible factor 1-alpha (HIF-1α) were activated in cancer cells to facilitate aerobic glycolysis through up-regulating glucose transporter GLUT1 and hexokinase 2 (HK2). HIF-1α is not O-GlcNAcylated directly, however, HIF-1α is stabilized in elevated O-GlcNAcylation levels in breast cancer cells [180, 184, 185]. Several studies showed that primary cilia are decreased or lost in cancer cells [186]. The elevated O-GlcNAcylation levels may contribute to the activation of kinases, such as AMPK, mTOR, and HIF-1α, to promote ciliary disassembly in tumor cells. Overall, understanding more fully the ties between nutrient sensor O-GlcNAcylation and metabolism will provide novel approaches to the treatment of obesity, diabetes, neurodegenerative diseases, and cancer [144].

Tools for studying O-GlcNAc

With increased understanding of O-GlcNAc regulatory enzymes, several biological tools have been developed, including cell lines with genetic modifications to overexpress and knockdown the OGA/OGT enzyme. Importantly, pharmacological inhibitors such as OGA inhibitors PUGNAc, Thiamet G, GlcNAcstatin G, and OGT inhibitor Alloxan are now available [187] (Figure 1-3). PUGNAc is a non-selective inhibitor of the nuclear and cytoplasmic OGA, which induces insulin resistance and leads to Type II diabetes. In searching for highly selective OGA inhibitors, two specific and selective inhibitors, Thiamet G and GlcNAcstatin G, were later synthesized [188]. Alloxan is the first OGT inhibitor described, and OGT activity is inhibited in a dose-dependent manner with complete inhibition at a concentration of 1 mM [189]. All these tools are employed for this study.

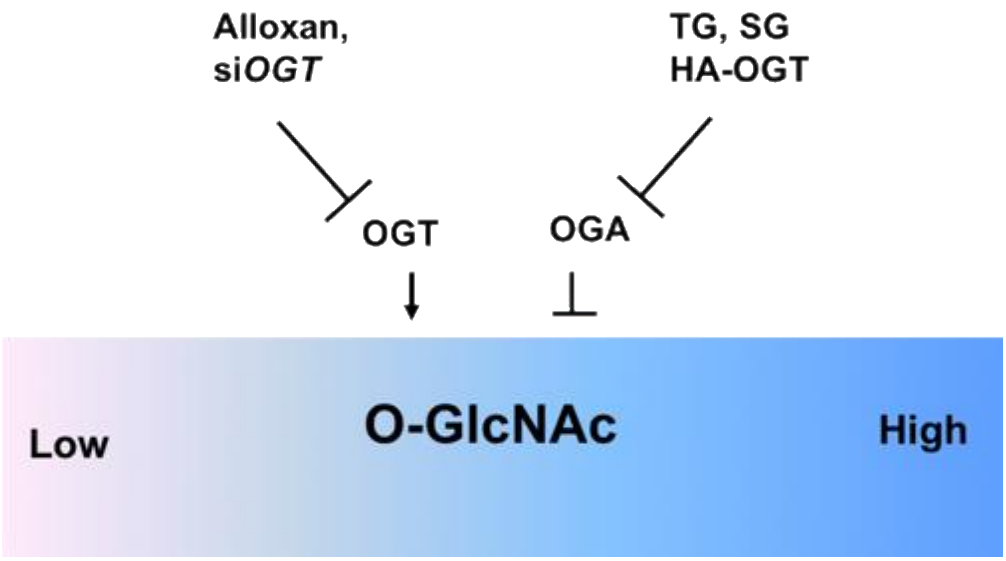

Figure 1- 3 Tools for studying O-GlcNAc.
Cellular O-GlcNAcylation levels can be manipulated either genetically or pharmacologically. Genetically overexpression and knockdown the enzyme OGT can elevate or attenuate O-GlcNAcylation levels. Inhibitors such as OGA inhibitors PUGNAc, Thiamet G, GlcNAcstatin G can increase O-GlcNAcylation levels, while OGT inhibitor Alloxan decreases O-GlcNAcylation levels. TG, Thiamet G; SG, GlcNAcstatin G.

Summary

Primary cilia are a microtubule-based organelle present on most mammalian cells. Various receptors and ion channels are localized on the ciliary membrane. The primary cilia function as a signaling hub to transduce extracellular signals, such as morphogens, hormones, and growth factors, to the intracellular and active the primary ciliary mediated signaling pathways. The proper ciliogenesis and ciliary length regulation are essential for the receptors localized to the primary cilia and play functions in transducing signal. Because primary ciliary mediated signaling pathways are mostly related to development, energy metabolism, and tissue hemostasis, the dysfunction of primary cilia usually causes metabolic-related disorders, such as obesity, diabetes, and cancers. These observations indicate that nutrient sensors may be factors that contribute to ciliary length regulation. The evidence presented the relationship between

primary cilia and nutrient status raise the possibility that the nutrient sensor O-GlcNAc as a potential contributer to ciliary length regulation. O-GlcNAcylation levels are tightly regulated by the availability of nutrients status, including glucose, amino acids, fatty acids, and nucleotides. Fluctuating O-GlcNAcylation levels regulate multiple cellular processes, such as transcription, translation, protein activity and stability, and autophagy. The ciliogenesis and ciliary length regulation factors, such as PI3K, AMPK, mTOR, Akt, GSK3β, and IRS1/2, are either O-GlcNAcylated directly, or their activity is regulated by O-GlcNAcylation. These investigations strengthen the hypothesis that O-GlcNAc plays a role in ciliary length regulation.

Introduction II

Synthetic biology and its applications

Synthetic biology is an interdisciplinary approach that takes advantage of biology, genetic engineering, and computer engineering to build artificial biological systems for pharmacology, medicine, agriculture, and environmental applications. In general, the purpose of synthetic biology is to design and construct novel artificial biological pathways, organisms or devices, or to redesign existing natural biological systems to deliver useful applications [190]. In the past decade, numerous synthetic gene circuits have been created and applied in biofuels, detectors for biomedical and chemical weapons, disease diagnosis, and genetic therapies [191].

One application of synthetic biology is in designing biosensors. Biosensors often refer to an engineered organism that can be used to detect the presence of chemicals. Bacterial biosensors combine the promoter/operator of a stress response gene with reporter genes to detect toxic metals [192]. One example is a sulfur-oxidizing bacterial (SOB) biosensor used for detecting toxic metals in water. When there are toxic chemicals present, SOB will be inhibited and cause an increase in pH and a decrease in electrical conductivity (EC), and the changes can be detected by EC and pH meters [193]. Other applications of synthetic biology are to produce industrial enzymes with high activity and novel biomaterials. The production of biomaterials is based on using microbes as molecular foundries to produce genetically encoded materials [194]. For instance, recombinant *E. coli* expressing phytochelatin synthase (PCS) and metallothionein (microtubule) can be used to synthesize diverse metal nanoparticles. PCS synthesizes varying sizes of oligoglutathione peptides PCS that can form a metal complex with Cd, Cu, Ag, and Hg. MTs are able to directly bind Cu, Cd, and Zn [195]. To date, bacteria, fungi, and viruses are

common hosts of biomolecular structures, such as virus capsids and bacteria encapsulants used for the synthesis of biomaterials. However, these structures have limited capacity and lack the ability to incorporate the biomolecules into highly predictable and ordered constructs. The highly organized and regularly arranged structures of *Chlamydomonas* flagella makes it an excellent natural template for synthesizing biomolecules by fusing target proteins with axoneme proteins.

Chlamydomonas as a model organism

The unicellular green alga *Chlamydomonas* is an established model organism to study flagellar assembly, structure, and function [196]. There are many advantages of using *Chlamydomonas* to study flagellar dynamics and functions such as a simple life cycle, easy isolation of mutants, and applicable techniques for targeted gene silencing and gene editing. When considering using Chlamydomonas flagella as a template to synthesize biomolecules, the following advantages should be highlighted. First, Chlamydomonas is easy to culture synchronously in a large volume in the laboratory. Second, flagella can be easily detached and isolated for biochemical assays. Flagella can be detached and regenerated several times to increase the yield. After flagella detach, it only takes 1-2 hours to regenerate full-length flagella. Third, the flagellar proteome is completely sequenced. It is easy to do genetic modifications of any protein of interest. Fourth, there is an extensive collection of flagella protein null-mutations available, which can be used to express fusion genes without the background of endogenous proteins. Fifth, the target protein amount can be calculated precisely due to the known structural components of the axoneme. Lastly, no protease exists in the *Chlamydomonas* flagellar compartment. Therefore, the target protein should maintain its activity with no degradation after flagella are isolated. The advantages above make *Chlamydomonas* a promising biosynthetic template.

Structure of Chlamydomonas flagellum

Axoneme, as a backbone structure of *Chlamydomonas* flagellum, has been studied for over 30 years. The axoneme is composed of nine doublets microtubule (DMTs) surrounding two central singlet microtubules. Besides microtubules, there are many other proteins or complexes necessary for its function. The 9 + 2 structure of the axoneme has a basic longitudinal repeat unit of 96 nm. Within each unit, there are periodically anchored four inner dynein arms (IDAs), several outer dynein arms (ODAs), one dynein regulatory complex (DRC), as well as two or three pairs of radial spokes (RS) [197] (Figure 1-4). This periodica nano-architecture of the axoneme makes it an excellent template for synthetic biology.

Radial spoke is a T-shaped complex containing a stalk and a head that is composed of at least 23 proteins. The stalk is anchored to the DMTs adjacent to the IDAs and projects toward the central pair of microtubules and the terminal globular head connect those two together [198]. In the paralyzed flagella mutant *pf14*, the defective gene product of radial spoke protein 3 (RSP3) results in the lack of all the other spoke components. *In vitro* experiments showed that amino acids 1-85 of RSP3 is necessary for axoneme binding, and fusion of amino acid 1-85 of RSP3 to an unrelated protein confers complete binding activity to the axoneme [199]. The results indicate that RSP3 is critical for the assembly of the entire spoke and may bind to axoneme directly.

Each DMT consists of one complete A-tubule that composed of 13 tubulin protofilaments (PFs) and one incomplete C-shaped B-tubule composed of 10 PFs. The junctions between A- and B-tubules are structures of the inner junction and outer junction. The outer junction is a closed structure formed by unusual interaction between three PFs [200]. The inner junction (IJ) is a

bridge structure between A- and B-tubules formed by a smaller subunit of non-tubulin proteins [201]. Conventional electron microscope results showed that *Chlamydomonas* FAP20 mutant axonemes lack the IJ, and the further study revealed that labeled FAP20 localizes at the IJ. Lack of FAP20 will have motility defects with an abnormal symmetrical waveform. Immune-fluorescent (IF) results showed that FAP20 localizes along the entire length of DMTs, and estimated that there is one FAP20 per 8 or 4 nm of DMT through comparing the fluorescence intensity of FAP20-GFP and RSP3-GFP [201].

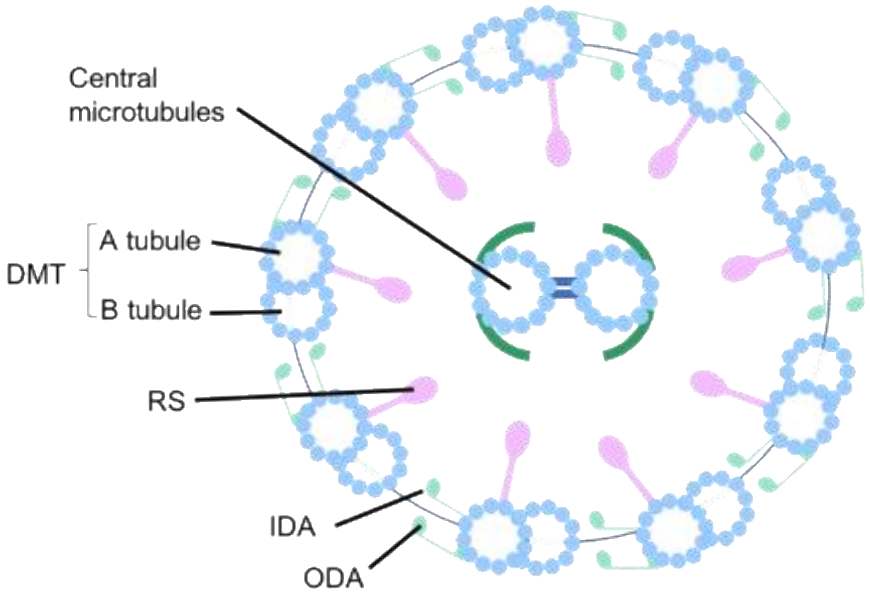

Figure 1- 4 Schematic presentation cross-section structure of axoneme.
The flagella axoneme is composed of nine doublet microtubules and a pair of central singlet microtubules. Several appendages structures involved in regulating axoneme motility are attached on the DMT, such as inner dynein arms, outer dynein arms, and radial spoke. DMT, doublet microtubules; RS, radial spoke; IDA, inner dynein arm; ODA, outer dynein arm.

Chlamydomonas flagellar regeneration

Flagella regeneration in *Chlamydomonas* was discovered fifty years ago [202]. When both flagella of *Chlamydomonas* are removed, they reassembled immediately in favorable conditions.

Interestingly, if only one flagellum is removed, the other intact flagellum shortens at first while the amputated one regenerates, then both flagella approach to full length at the same rate after they attain an equal intermediate length [42]. The results indicate the flagellar regeneration is regulated by internally [202]. Generally, flagella start to extend rapidly after deflagellation by pH 4.5 shock, then bringing the pH back to 7.0 and can reach their full length within two hours. The deflagellation and regeneration can repeat several times (Figure 1-5).

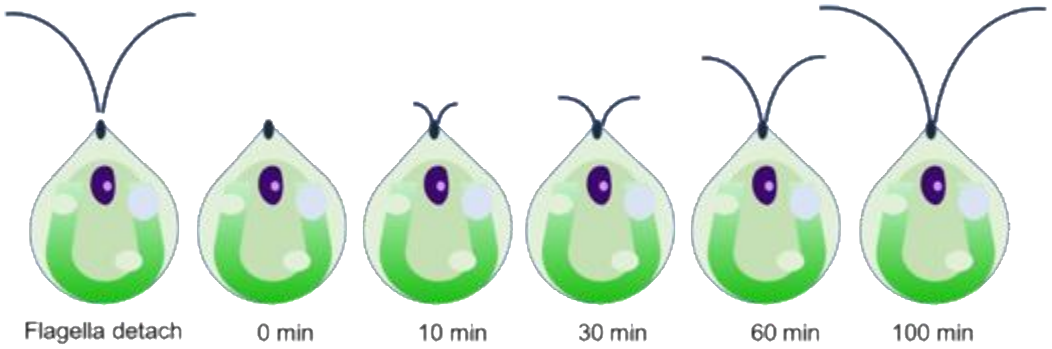

Figure 1- 5 Flagella regeneration.
Original flagella are detached by pH 4.5 shock then return the pH back to 7.0. Cell bodies keep culturing in aerobic environment to induce flagella regeneration. The process of flagella regeneration is monitored. The flagellar assembly is finished in about 90-120 min. Different strains or culture conditions may cause time deviation.

Summary

In the second part of the introduction, I discussed the application of engineering flagellar axoneme as a biosynthetic template. There are several advantages to do so. For example, Chlamydomonas cells are easy to culture in a large volume, flagella can be repeatedly detached and regenerated, fully sequenced flagellar proteome, nontoxic, and the well-studied axoneme structures enable precise calculation of amounts of final products. Then I introduced the axoneme appendages structures of RS and IJ. The RS and IJ components of RSP3 and FAP20 have been used as adaptors to expression the fusion proteins in the mutant strains *pf14* and *im5*.

The hypothesis is supported by the success expression of RPS3-GFP and FAP20-GFP on the axoneme.

CHAPTER II

O-GLCNACYLATION LEVELS REGULATE PRIMARY CILIARY LENGTH BY PROMOTING MICROTUBULE DISASSEMBLY*

Introduction

Ciliary length in any specific type of cell falls within a narrow range. However, the lengths of different types of cilia vary much more widely. Therefore, the cell-specific length of cilia is obviously critical for cells to properly transmit sensory signals and generate directional motion if the cilia are motile. For instance, ciliary length in particular has been predicted to be a critical parameter in the model of the fluid dynamics of left-right patterning. Both longer and shorter ciliary length induce compromised left-right pattern establishment through affecting fluid flow [203] . Indeed, defective ciliogenesis and abnormal ciliary length have been widely implicated in ciliopathies. Many ciliopathies, such as (BBS), nephrononphthisis (NPHP), and Joubert Syndrome, are caused by abnormal ciliogenesis or failure to maintain assembled cilia [93]. A large number of disease genes are associated with syndromes including BBSome components, NPHP1-9, and Inositol polyphosphate-5-phosphatase E (INPP5E) [204]. Excessively long cilia are also associated with ciliopathies, for example, juvenile cystic kidney disease and tuberous sclerosis patients have much longer cilia than normal [93]. Additionally, defective ciliogenesis has been recently found to play important roles in cancer development. The ciliation frequency is greatly decreased in breast cancer tissues, and ciliary loss is prevalent in variety of kidney cancers [205].

*Reprinted with permission from "O-GlcNAcylation Regulates Primary Ciliary Length by Promoting Microtubule Disassembly" by Jie L. Tian and Hongmin Qin, 2019. *iScience*, 12, 379-391, Copyright [2019] by Copyright Clearance Center, Inc.

Primary cilia are present on almost all differentiated human cells, such as kidney cells, fibroblasts, neurons and Schwann cells [206]. They play crucial roles, including sensing environment cues, transducing extracellular signals within the cells, processing developmental signals, and tissue hemostasis. Dysfunction of primary cilia contributes to a large spectrum of human genetic diseases and disorders, including PKD and BBS, retinal degeneration, brain malformations, obesity and diabetes. They collectively are termed ciliopathies [207].

Protein O-linked β-N-acetylglucosamine (O-GlcNAc) modification (O-GlcNAcylation) on serine and threonine residues is one of the most abundant metazoan nuclear-cytoplasmic post-translational modifications. The addition and removal of O-GlcNAc are catalyzed by two enzymes: O-GlcNAc transferase (OGT) and O-GlcNAcase (OGA), respectively [208]. UDP-GlcNAc, as a nucleotide sugar donor of enzyme OGT, is derived from hexosamine biosynthetic pathway (HBP), which consumes 2-5% total glucose [162]. The HBP metabolic pathway integrates multiple metabolites, such as carbohydrates, amino acids, fat and nucleotides, to produce UDP-GlcNAc [125, 209, 210]. Therefore, O-GlcNAc is sensitive to nutrient flux, and the abundance of O-GlcNAc reflects the internal cellular nutrient level. O-GlcNAc modulates basic biological functions and plays broad roles in multifaceted biological processes, such as gene expression [211, 212], signal transduction [141, 213], protein degradation [214], cell cycle [215, 216], autophagy [217, 218], and cellular stress [135]. Perturbation of O-GlcNAcylation alters biological homeostasis, which is involved in a plethora of human pathologies, such as diabetes, obesity, neuron degenerative diseases, and cancer [208].

O-GlcNAcylation regulates the activity of various components critical for metabolism and energy homeostasis, such as Protein kinase B (AKT), glycogen synthase kinase-3β (GSK3β), hypoxia-inducible factor 1-alpha (HIF-1α) and its transcriptional target glucose transporter (GLUT1). O-GlcNAcylation affects these proteins' activity or their stability [180, 219]. Interestingly, the above proteins are all either localized to cilium or cilium related structures, or essential for ciliogenesis [141, 220-222]. The observations that these proteins either rely on the ciliary structure to function or are required for ciliary assemble, intrigue us to ask whether there is a crosstalk between O-GlcNAc and cilium.

Primary cilia are microtubule-based organelles that extend from the surface of many types of cells and enriched with receptors, channels, and signaling molecules [2, 223, 224]. These ubiquitous structures, acting as "antenna" to transduce various extracellular signals, equip cells with diverse sensory functions. Many important signaling pathways, for instance, Hedgehog signaling pathway and Wnt signaling pathway, rely on primary cilia for proper function [210, 225]. A wide range of ciliopathies arises due to defective cilia disrupting embryo development or tissue homeostasis [11, 226, 227].

The backbone of cilia, axoneme, with lengths normally ranging from 1 to 9 μm in human [228]. Axonemal microtubules are highly stable and subjected to elaborate post-translational modifications (PTMs). Tubulin acetylation is the best-studied PTM on ciliary axoneme [71, 229]. Acetylation of axonemal microtubules is catalyzed by α-tubulin acetyltransferase 1 (αTAT1), a conserved enzyme exclusively expressed in ciliated organisms and required for primary cilium assembly [230, 231]. The αTAT1 activity is antagonized by histone deacetylase 6

(HDAC6), which is a tubulin deacetylase. Once activated, HDAC6 deacetylates acetylated axonemal microtubules. The deacetylated microtubules are unstable causing axonemal disassembly [31]. The deacetylase activity of HDAC6 is necessary and essential for ciliary microtubule disassembly [31, 232].

The tubulin deacetylase activity of HDAC6 is regulated by phosphorylation. Aurora kinase A (Aur A) phosphorylates and actives HDAC6. The activated HDAC6 is then localized to the basal body and cilium by forming a complex with the scaffolding protein HEF1 [31]. The activation of Aur A-HDAC6-HEF1 cascade is consistent with the two waves of primary cilia disassembly occurred post serum addition to G0 cells at 2 h and 18 h, which correspond to G1 and mitosis phase, respectively. We reasoned that since O-GlcNAcylation and phosphorylation, these two prominent protein modifications, often tune protein's activity by competing for the same Serine and Threonine residues, or modifying the residues in defined patterns [233], it is possible that the enzymatic activity of HDAC6 is regulated by O-GlcNAcylation as well. Indeed, in a prior LC-MS proteomic analysis, HDAC6 is found to be an O-GlcNAcylated protein [234].

In this study, in cultured hTERT-RPE1 and IMCD3 cells, we demonstrate that the length of primary cilium negatively correlates with the cellular O-GlcNAc level. We also provide evidence that O-GlcNAcylation of either tubulin or HDAC6 promote axonemal microtubule disassembly. The cells appear to be able to attenuate the signaling response by limiting the size of cilium when nutrients are abundant. Clearly, the crosstalk between O-GlcNAc and cilium puts the cell in a better position for fine-tuning the cellular response to nutrients.

Results

Reduction of O-GlcNAc caused ciliary length elongation and increased the percentage of ciliated cells in cultured hTERT-RPE1

OGT is the sole enzyme for addition of O-GlcNAc onto targeted proteins. To investigate the relationship between cilia and O-GlcNAc, we used small interference RNA (siRNA) to knockdown the expression of the enzyme OGT in hTERT-RPE1 cells (Figure 2-1 A). Immunoblotting (IB) of whole cell lysates verified that the level of O-GlcNAcylated proteins was significantly reduced when OGT expression was knocked down by si*OGT*, but remained expressed in cells transfected with a negative control siRNA to Firefly Luciferase GL2 (siGl2) (Figure 2-1 A1). Then we checked how reduction of protein O-GlcNAcylation affected ciliary length and percentage of ciliated cells. Immunofluorescence (IF) staining with antibodies against ciliary marker proteins acetylated-tubulin and IFT88 (Figure 2-1 A2) were used to highlight the ciliary structures. Since the staining with anti-IFT88 marked the ciliary base and tip well, we used it to measure the ciliary length. In cells transfected with the negative control siGl2, 24.18 ± 6.8% of cells were ciliated. In contrast, in cells transfected with si*OGT*, the percentage of ciliated cells was increased to 55.38 ± 8.8% (Figure 2-1 A3). Additionally, the mean ciliary length of cells treated with si*OGT* was 5.07± 0.012 μm, which was significantly longer than that of the cells treated with siGl2 (3.62 ± 0.322 μm) (Fig. 2-1 A4). Therefore, a lower cellular level of O-GlcNAcylation affected positively on ciliary assembly, promoting both cilia formation and elongation.

To verify that the effects seen in si*OGT* treated cells were indeed caused by the reduction of protein O-GlcNAcylation, a si*OGT* resistant OGT (HA-OGT-rescue) [235] was expressed in

si*OGT* cells (Figure 2-1 B1&2). Based on the band intensity on immunoblots of whole cell lysates, the expression of the endogenous OGT was decreased ~75% in cells treated with si*OGT*, but not in cells transfected with siGl2. The si*OGT* resistant HA-OGT-rescue, however, was successfully expressed when endogenous OGT was silenced, as shown by the IB with an antibody against HA (Figure 2-1 B1). We then checked whether the expression of HA-OGT in si*OGT* knockdown cells shortened the ciliary length or not (Figs. 2- 1 B2&3). Indeed, expression of HA-OGT in OGT depleted si*OGT* treated cells restored the ciliary length to normal. The mean ciliary length of cells expressed HA-OGT-rescue was at 3.9 ± 0.36 μm, which was statistically shorter than the si*OGT* cells (4.99 ± 0.31 μm). These results confirmed that protein O-GlcNAcylation catalyzed by OGT was responsible for the elongated cilia seen in si*OGT* cells.

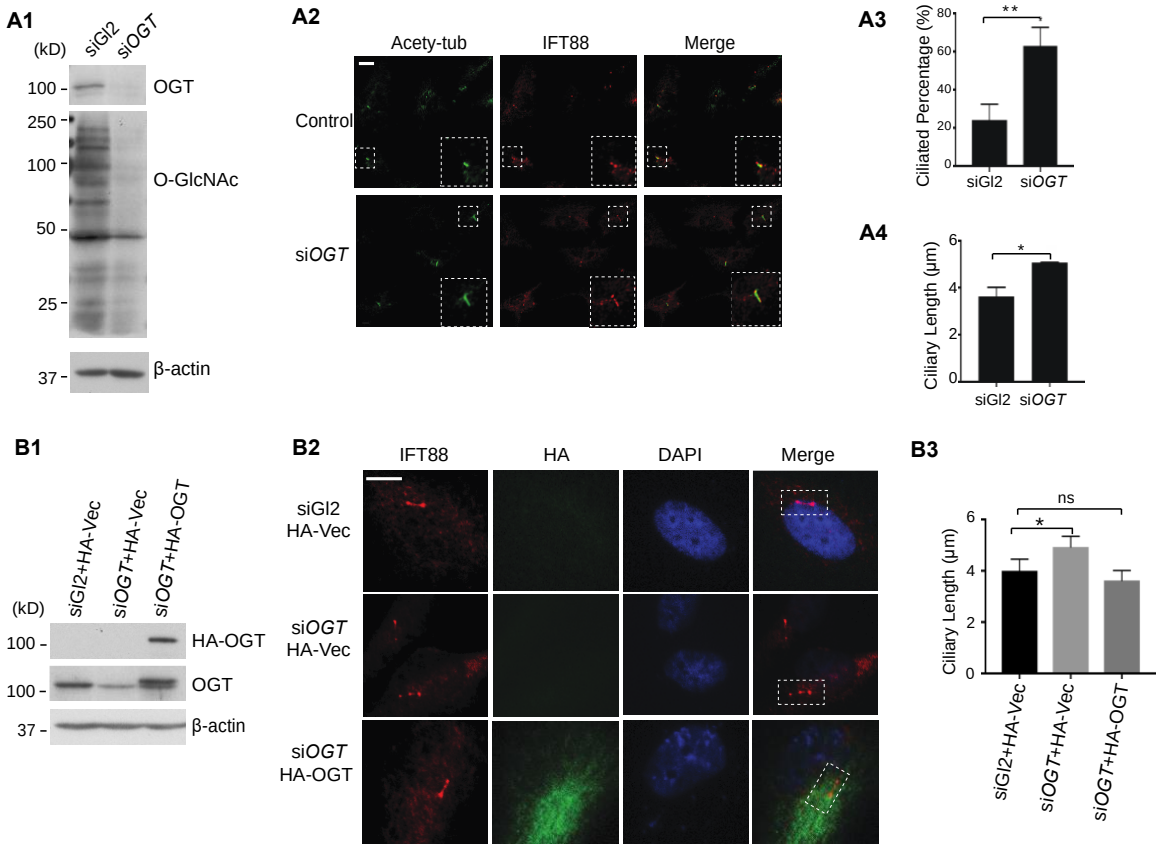

Figure 2- 1 Cilium length and percentage of ciliated cells were increased when O-GlcNAc level was reduced in hTERT-RPE1 cells.

(A) The si*OGT* transfected cells were used to check the effects of O-GlcNAc reduction on ciliary length and percentage of ciliated cells. The siGl2 was the negative control. Three independent replicates were performed. The representative results are shown here. (A1) Immunoblots of cell lysates with indicated antibodies. (A2) Confocal images of cells co-immunostained with antibodies against acetylated-tubulin and IFT88. (A3) Bars represent the percentage of cells with primary cilia in siGl2 and si*OGT* cells (**$p < 0.01$ ($p= 0.006$)). (A4) The mean lengths of cilia in siGl2 and si*OGT* knockdown cells (*$p < 0.05$ ($p = 0.0126$)). (B) Expression of HA-OGT-rescue in si*OGT* knockdown cells restored ciliary length to normal. (B1) IB analysis of endogenous OGT and exogenous HA-OGT-rescue expressions. (B2) Confocal images of cells co-immuno-stained with antibodies against IFT88 and HA. (B3) The mean length of cilia in groups as indicated on the graph (*$p < 0.05$ ($p_{siOGT/HA-Vec} = 0.044$, $p_{siOGT/HA-OGT} = 0.33$), *ns*, not significant). β-actin was used to show equal protein loadings on immunoblots. Scale bar equals 5 μm. All data are mean ± SD.

The O-GlcNAcylation mediated ciliary length regulation was not hTERT-RPE1 specific, but also seen in IMCD3 cells

To evaluate whether the effect of O-GlcNAcylation on ciliary length was cell line specific, we examined whether changes of OGT expression regulated length of cilia in another cell line, IMCD3. Consistent with the results seen in hTERT-RPE1 cells (Figure 2- 1 A), the IMCD3 cells assembled longer length cilia when protein O-GlcNAcylation was inhibited by si*OGT* (Figure 2-2 A). We did not detect a significant change of the percentage of ciliated cells when OGT expression was inhibited. The percentage of ciliated cells remained at about 40%.

We reasoned that since O-GlcNAcylation inhibition induced ciliary elongation, it is possible that an elevated O-GlcNAcylation would lead to shorter length cilia. To test this idea, we transiently overexpressed an HA tagged OGT in IMCD3 cells. The increased protein O-GlcNAcylation in HA-OGT overexpressed cells was verified by IB (Figure 2-2 B1). The mean length of HA-OGT positive cells was 1.55 ± 0.18 μm, which was significantly shorter than that of control cells (2.61 ± 0.4μm) (Figure 2-2 B2&3). Taken together, in both hTERT-RPE1 and IMCD3 cells**,** there is a negative correlation between O-GlcNAcylation and ciliary length: the higher cellular O-GlcNAcylation, the shorter the ciliary length.

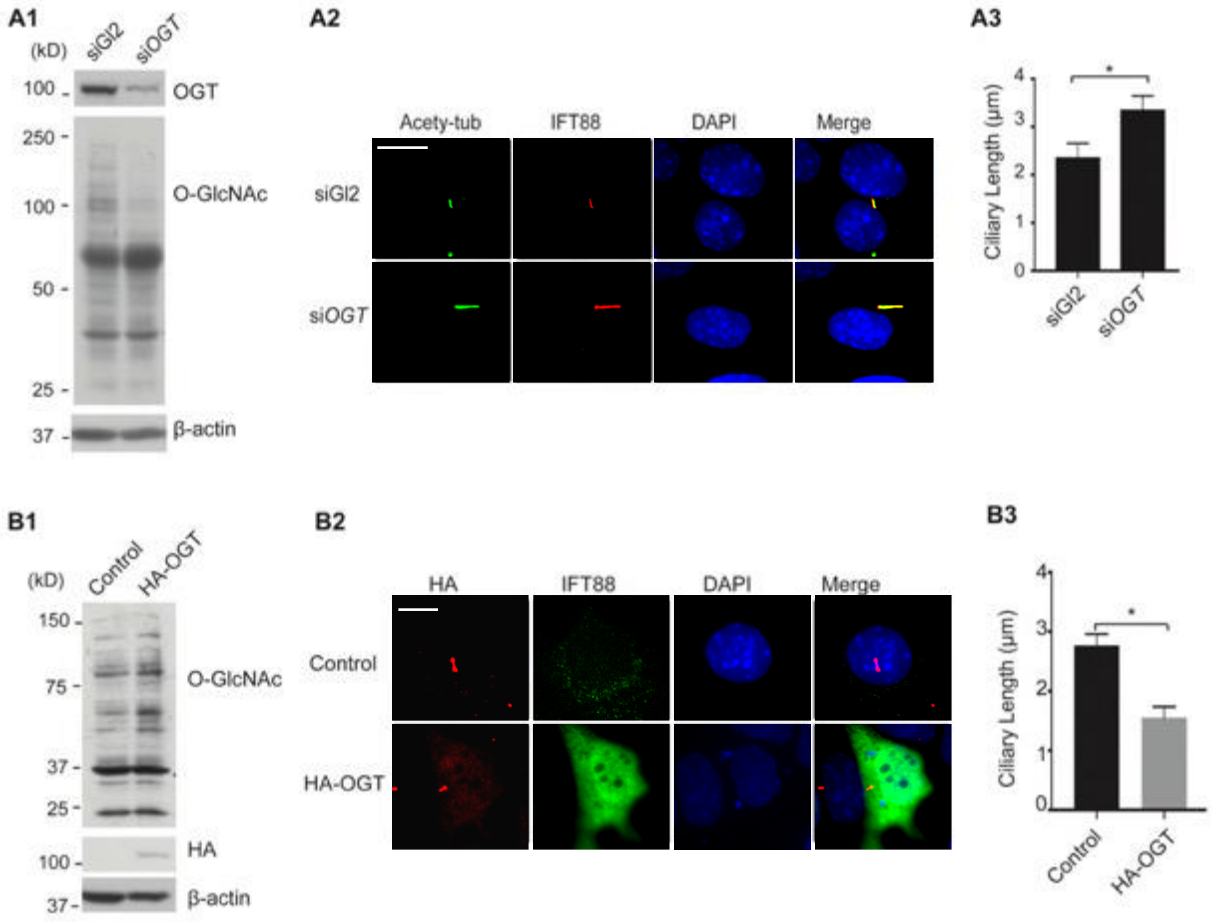

Figure 2- 2 Knockdown of OGT increased ciliary length, while HA-OGT overexpression decreased ciliary length in IMCD3.

(A) The cells transfected with si*OGT* or the negative control siGl2 were used for analysis. Three independent replicates were performed. The representative results were shown here. (A1) IB analysis of O-GlcNAc levels in siGl2 and si*OGT* transfected cells with indicated antibodies. (A2) Confocal images of cells co-immunostained with antibodies against acetylated tubulin and IFT88. (A3) The si*OGT* knockdown cells had longer length cilia (*$p < 0.05$ ($p = 0.0126$)). (B) Overexpression of HA-OGT decreased ciliary length. (B1) IB analysis of O-GlcNAc levels in HA-Vector and HA-OGT overexpressed cells. (B2) Confocal images of cells co-immunostained with antibodies against acetylated tubulin and IFT88. (B3) The ciliary length was shorter when cells overexpressed HA-OGT (*$p < 0.05$ ($p = 0.017$)). Scale bar equals 5 μm. All data are mean ± SD.

Inhibition of OGT or OGA by small chemical inhibitors confirmed the negative regulatory role of O-GlcNAcylation on ciliary length

We selected three specific small chemical inhibitors: Thiamet G (TG) [236] and GlcNAcstatin G (SG) for OGA [237, 238], and Alloxan (Alxn) for OGT [189], to treat both IMCD3 and hTERT-RPE1 cells. The efficiency of these inhibitors on protein O-GlcNAcylation was first confirmed by IB against an anti-O-GlcNAc antibody (Figure 2-3 A1&B1). Consistent with prior published results, Alxn treatment decreased overall protein O-GlcNAcylation, while TG or SG treatment increased cellular O-GlcNAcylation. Then the length of cilia was measured using IF staining of ciliary marker protein IFT88. The length of cilia in either IMCD3 or hTERT-RPE1 was longer with Alxn treatment. The mean length of Alxn treated IMCD3 cells was 4.36 ± 0.32 μm, which was significantly longer than that of the control group (4.0 ± 0.37 μm). The mean length of Alxn treated hTERT-RPE1 cells was 3.79 ± 0.09 μm; while the length of control cells was 3.26 ± 0.2 μm. Conversely, the ciliary lengths were significant shorter in cells treated with TG or SG. The mean length was shortened to 2.88 ± 0.24 μm with TG treatment, and to 2.72 ± 0.32 μm with SG treatment in IMCD3 cells. The TG and SG treatments caused the lengths of hTERT-RPE1 cells shorten to 2.73 ± 0.11μm, and 2.64 ± 0.09μm, respectively (Figure 2-3 A2&3, and B2&3). These small chemical treatment results were consistent with the observations obtained by perturbing the expression of OGT and OGA (Figure 2-1 & 2-2).

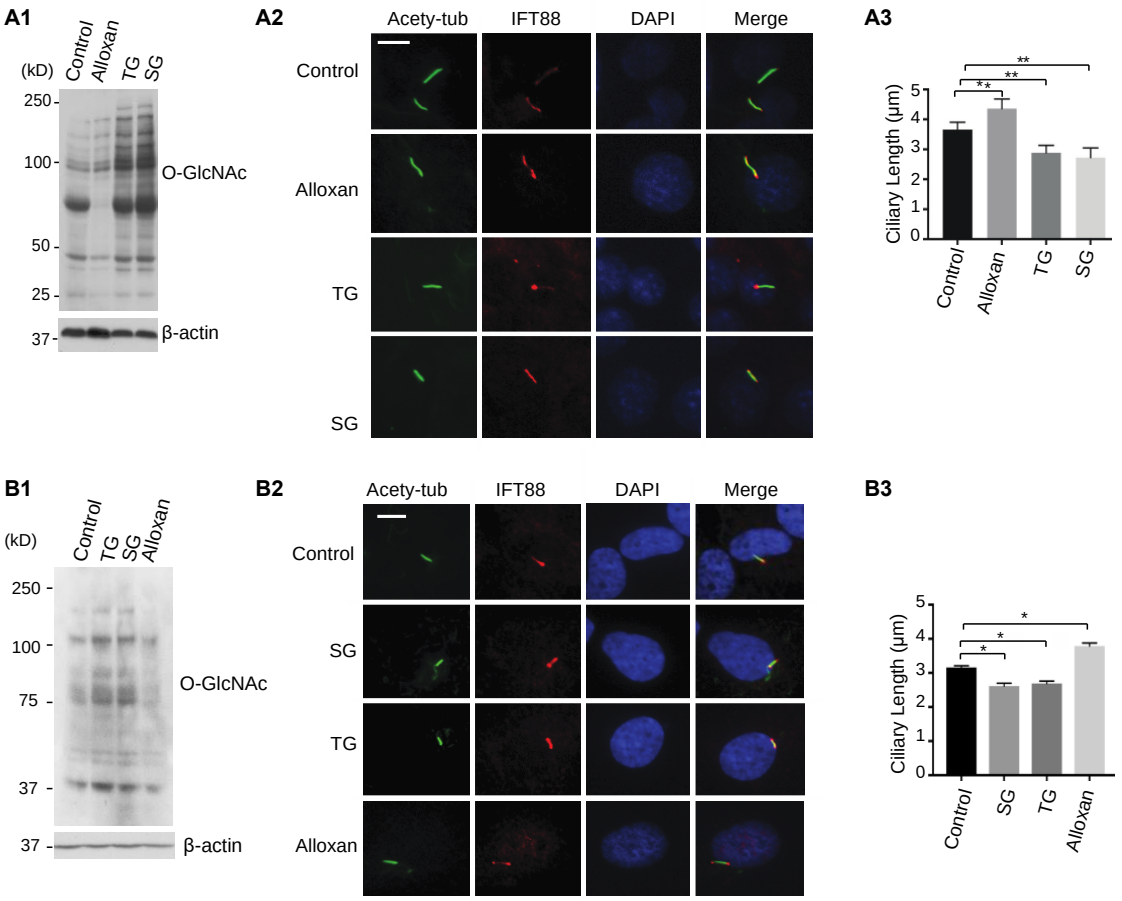

Figure 2- 3 The negative correlation between O-GlcNAcylation level and ciliary length verified by treating cells with OGT and OGA inhibitors.
The IMCD3 (panel A) and hTERT-RPE1 (panel B) cells were subjected to OGT inhibitor Alloxan, or OGA inhibitor TG or SG, or control DMSO (A1&B1). IB analysis of O-GlcNAc levels in treated cells. β-actin was used to show equal protein loadings. (A2&B2) Confocal images of cells co-immunostained with antibodies against acetylated tubulin and IFT88. Scale bar equals 5 μm. (A3&B3) The graph shows the statistical analysis of ciliary lengths of treated groups (*$p < 0.05$, **$p < 0.01$, A3: $p_{Alloxan} = 0.009$, $p_{TG} = 0.0014$, $p_{SG} = 0.004$, B3: $p_{SG} = 0.018$, $p_{TG} = 0.016$, $p_{Alloxan} = 0.039$). All data are mean ± SD.

O-GlcNAcylation of α-tubulin promoted ciliary axoneme disassembly

The ciliary length is determined by the rate of microtubule assembly and disassembly in the axoneme. In order to understand how O-GlcNAcylation affects ciliary length, we asked which proteins, once O-GlcNAcylated, could regulate axonemal microtubule dynamics. A previous

study showed that O-GlcNAcylated α-tubulin fails to incorporate into microtubules [239], suggesting an inhibitory role of tubulin O-GlcNAcylation in microtubule assembly. Using immuno-purified endogenous α-tubulin, we confirmed that α-tubulin was O-GlcNAcylated in hTERT-RPE1 cells (Figure 2-4 A). We then used a direct *in vitro* O-GlcNAcylation assay to examine how tubulin O-GlcNAcylation affects the stability of axonemal microtubules. HA-OGT was overexpressed in hTERT-RPE1 cells for 48 h, and then purified with anti-HA antibody attached to protein A beads. We then checked if the purified HA-OGT could catalyze O-GlcNAcylation of axonemal microtubules *in vitro*, and if O-GlcNAcylation promoted axonemal microtubules disassembly (Figure 2-4 B1). The results showed that the amount of O-GlcNAcylated α-tubulin increased in reactions added with HA-OGT, indicating α-tubulin is a substrate of OGT. Moreover, the amount of free α-tubulin in the supernatants was increased compared to the reaction without HA-OGT. The supernatant contained a higher amount of disassembled free tubulin in reaction prolonged for 2 hours than for just 1 hour (Figure 2-4 B2). This result indicated that O-GlcNAcylation of α-tubulin promoted disassociation of tubulin from axonemal microtubules.

We reasoned since O-GlcNAcylation promoted axonemal microtubule disassembly, cilia undergoing disassembly were likely to have a higher level of O-GlcNAcylation. To test this prediction, we turned to a temperature sensitive flagellar mutant *fla10$_{ts}$* of the green algae *Chlamydomonas reinhardtii*. The mutant *fla10$_{ts}$* harbors a point mutation in the kinesin-II motor subunit FLA10, and is functionally normal in flagellar assembly at the permissive temperature (18°C) but abolishes the anterograde Intraflagellar transport (IFT) at the non-permissive temperature (32°C). The inactivation of IFT at 32°C induces flagellar axonemal disassembly [57,

240]. We checked the levels of protein O-GlcNAcylation in *fla10ts* flagella that were undergoing disassembly. The results showed that O-GlcNAcylation was increased in disassembly active flagella (Figure 2-4 C).

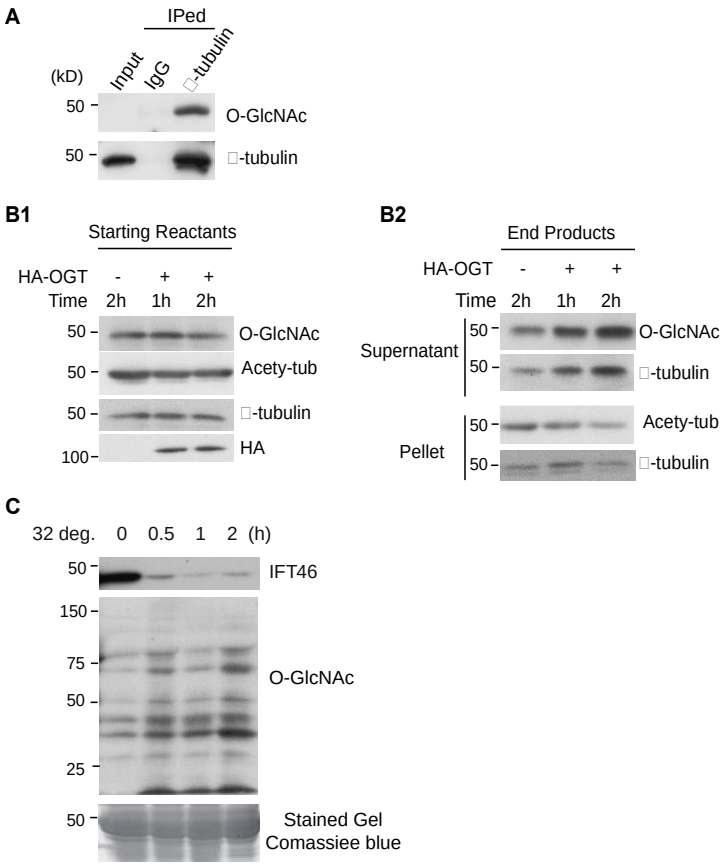

Figure 2- 4 O-GlcNAc of α-tubulin related to instability of flagellar axoneme.
(A) Endogenous α-tubulin was immune-precipated and subjected to IB with anti-α-tubulin and anti-O-GlcNAc antibodies. (B1) Purified HA-OGT was incubated with flagellar axonemes for 1 h or 2 h. IB analysis showed the relative amounts of input reactants of HA-OGT (probed with anti-HA), axonemes (blotted with antibodies against α-tubulin and acetylated-tubulin), and the base level of O-GlcNAc modification of axonemal microtubules (labeled as O-GlcNAc). (B2) After 1 h or 2 h, the supernatants and pellets were separated for IB analysis. (C) Flagella of *fla10ts* harvest after cells were incubated at 32°C for 0, 0.5, 1, and 2 h were used for IB analysis. The levels of O-GlcNAc were increased in *fla10ts* flagella from cells incubated at 32°C. The disappearance of IFT46 was used to verify that flagella were undergoing disassembly.

O-GlcNAcylation of HDAC6 involved in ciliary length shortening

HDAC6 plays an important role in cilia assembly. Recent proteomic analysis shows that HDAC6 is an O-GlcNAcylated protein [234]. It is possible that O-GlcNAcylation activates HDAC6 deacetylase activity, which leads to cilia shortening. If this is true, we reasoned that ciliary shortening induced by elevated protein O-GlcNAcylation should be blocked by inhibition of HDAC6. To test this idea, the hTERT-RPE1 cells were treated with HDAC6 inhibitor Tubacin [241] or together with OGA inhibitor TG or SG (Figure 2-5 A). The ciliary length analysis showed that inhibition of HDAC6 activity indeed prevented cells from shortening caused by TG or SG treatment (Figure 2-5 B). This result suggested that the elevated HDAC6 deacetylase contributed to the shorter length cilia induced by high O-GlcNAcylation.

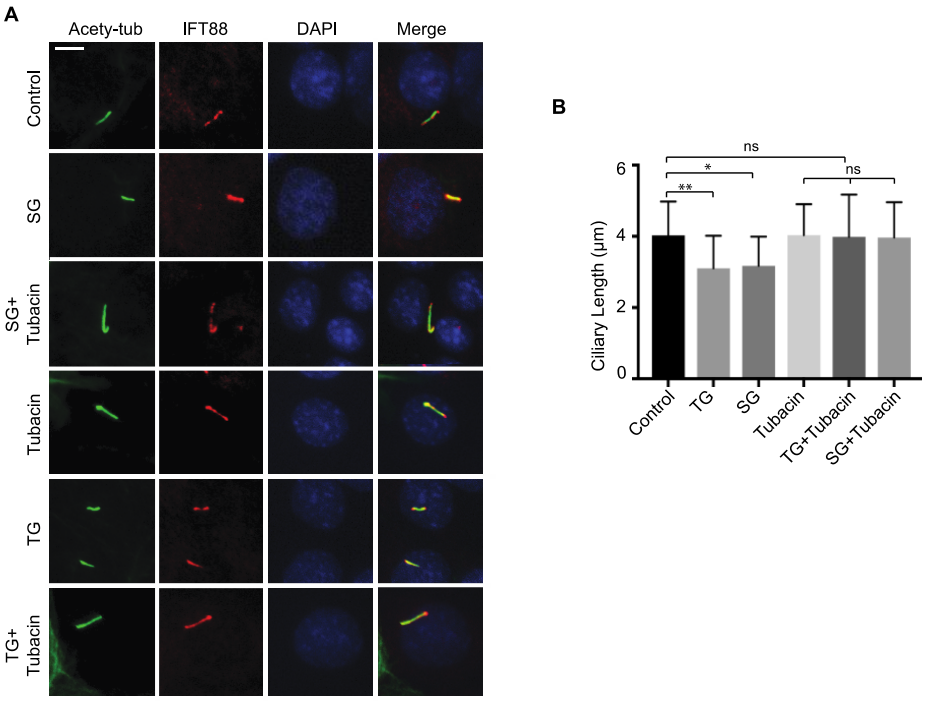

Figure 2- 5 Inhibition of HDAC6 suppressed ciliary resorption induced by TG or SG treatment.
The hTERT-RPE1 cells were subjected to TG, SG, TG + Tubacin, SG + Tubacin, or control DMSO treatment. (A) Confocal images of cells co-immunostained with antibodies against acetylated tubulin and IFT88. Scale bar equals 5 μm. (B) The mean length of cilia of cells with different treatments (*$p < 0.05$, **$p < 0.01$ ($p_{TG} = 0.001$, $p_{SG} = 0.017$, $p_{Tubacin} = 0.97$, $p_{TG/Tubacin} = 0.8$, $p_{SG/Tubacin} = 0.74$)). Data are mean ± SD.

To examine the underlying mechanisms of how O-GlcNAcylation affected HDAC6, we first checked whether HDAC6 and OGT interacted *in vivo*. Immunoprecipitation using either anti-HDAC6 or anti-OGT antibody confirmed that these two proteins could be co-immune-precipitated reciprocally from lysates of hTERT-RPE1 cells (Figure 2-6 A). The immune-precipitated HDAC6 was O-GlcNAcylated (Figure 2-6 B), confirming the prior mass

spectrometry proteomic data [234]. Collectively, these results showed that HDAC6 was a substrate of OGT.

O-GlcNAcylation could potentially increase the HDAC6 deacetylase activity by two means: increasing the protein amount, or increasing the actual enzymatic activity. We confirmed that the amount of HDAC6 protein was higher when O-GlcNAcylation was promoted by OGT overexpression (Figure 2-6 C), or by OGA inhibition (Figure 2-6 D). We then checked whether O-GlcNAcylation of HDAC6 affected its deacetylase activity (Figure 2-6 E). The HDAC6 protein was Immune-precipitated from the lysates of hTERT-RPE1 cells treated with either TG or SG. Equal amounts of purified HDAC6 protein from cells with various treatments were incubated with axonemal microtubules purified from *Chlamydomonas* for 1 h at 37°C. HDAC6 from cells treated with TG or SG had a higher tubulin deacetylation activity compared to the protein from control cells. This result hinted that O-GlcNAc modification of HDAC6 enhanced its deacetylase activity. Taken together, the increased activity of HDAC6 in cells with high O-GlcNAc levels may come from changes of its protein amount as well as from increased enzymatic activity.

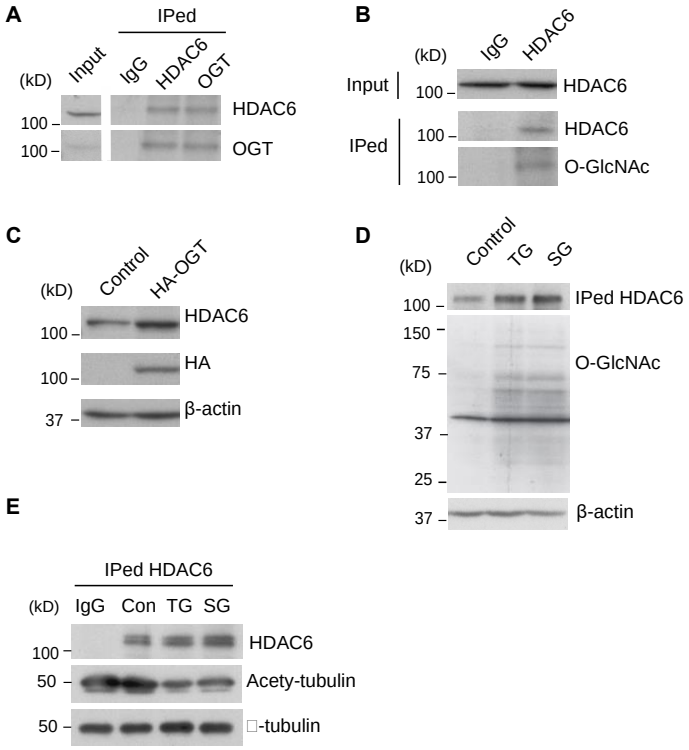

Figure 2- 6 HDAC6 was O-GlcNAcylated and O-GlcNAc modification of HDAC6 enhanced its deacetylase activity.

(A) Protein OGT and HDAC6 were reciprocally co-immune-precipitated together from cell lysates. IB analysis of HDAC6 and OGT in immune-precipitates using anti-HDAC6, anti-OGT, or control rabbit IgG. (B) HDAC6 protein was O-GlcNAcylated. HDAC6 protein was immune-precipitated from cell lysates and then subjected to IB with antibodies against HDAC6 and O-GlcNAc. (C) The amount of HDAC6 level in HA-OGT overexpression cells was increased. (D) The amount of HDAC6 immune-precipitated using the same amount of anti-HDAC6 antibody from TG or SG treated cell lysates was higher than that from the control treated with DMSO (Con) lysates. (E) The same amount of immunopurified HDAC6 proteins from TG or SG treated, or DMSO (control) cell lysates were used in Tubulin Deacetylase (TDAC) assays. After reactions were ended, the samples were subjected to IB to check the levels of indicated proteins. The levels of acetylated-tubulin were reduced in samples containing HDAC6 purified form TG or SG treated cell lysates.

O-GlcNAcylation of INPP5E did not affect its ciliary localization in hTERT-RPE1

Inositol polyphosphate 5-phosphatase (INPP5E) is a ciliopathy disease protein involved in Joubert and MORM syndromes [242, 243]. INPP5E plays an important role in the stability of primary cilia through affecting the ciliary membrane lipid composition [244, 245]. Moreover, both HDAC6 and INPP5E are substrate of AurA kinase [246]. We asked whether INPP5E is O-GlcNAcylated and whether its function is affected by O-GlcNAcylation. We first checked whether INPP5E was a substrate of OGT (Figure 2-7). INPP5E and OGT could be co-Immune-precipitated reciprocally. INPP5E was O-GlcNAcylated, confirming it was a substrate of OGT (Figure 2-7 A&B). However, the amount of O-GlcNAcylated INPP5E did not change even when the overall O-GlcNAcylated protein amount increased with OGA inhibitor treatments (Figure 2-7 C). Moreover, the ciliary localization of INPP5E appeared to be normal in either OGT loss or gain function cells (Figure 2-7 D&E).

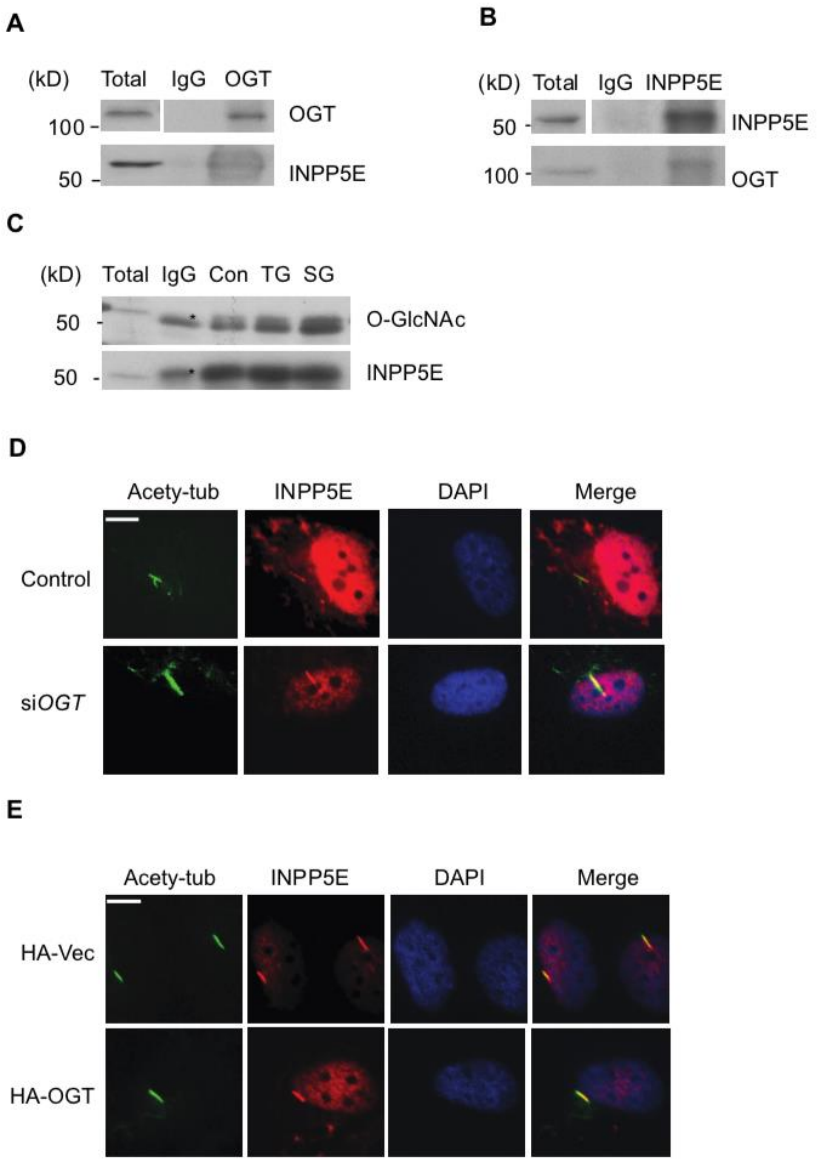

Figure 2- 7 O-GlcNAcylation of INPP5E does not affect ciliary localization in hTERT-RPE1 cells.

(A) Endogenous OGT was Immune-precipitated and subjected to IB with OGT and INPP5E antibodies. (B) Endogenous INPP5E was Immune-precipitated and subjected to IB with INPP5E and OGT antibodies. (C) INPP5E was O-GlcNAcylated. The hTERT-RPE1 cells were first treated with mock DMSO (Con), or OGA inhibitors TG or SG, to modulate intracellular O-GlcNAc levels. Then the endogenous INPP5E was Immune-precipitated and subjected to IB with O-GlcNAc and INPP5E antibodies. (D) Representative confocal images of hTERT-RPE1 cells (*siOGT* treatment) immunostained with anti-INPP5E and anti-acetylated-tubulin antibodies. Scale bar equals 5 μm. (E) Representative images of cells immunostained with anti-INPP5E and anti-acetylated- tubulin. The hTERT-RPE1 cells were transfected with HA-Vector or HA-OGT. Scale bar equals 5 μm.

Discussion

This study uncovered a negative regulatory role of O-GlcNAcylation on primary ciliary length in both hTERT-RPE1 and IMCD3 cells. In OGT gain-of-function cells, ciliary length was shortened, while ciliary length was elongated in OGT loss-of-function cells. O-GlcNAcylation of α-tubulin promoted its disassociation from the axoneme, which might promote the disassembly of axoneme. O-GlcNAcylation of HDAC6 activated its deacetylase activity to deacetylate axonemal microtubule, which was likely causing cilia to resorb. Based these results, we concluded that the ciliary length is sensitive to the cellular level of O-GlcNAc. We propose that the constant cross-talk between the primary cilium and O-GlcNAc is an important mechanism for cells fine-tuning the cellular responses to nutrients (Figure 2-8).

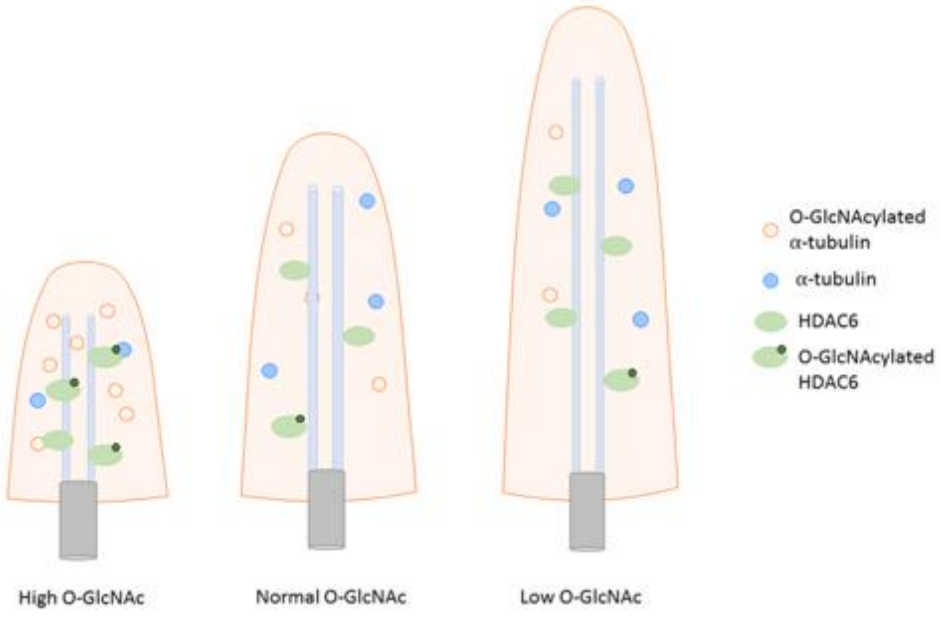

Figure 2- 8 Molecular model of O-GlcNAc in regulating ciliary assembly and disassembly. When the cellular O-GlcNAc level is high, more axonemal α-tubulin are O-GlcNAcylated. These tubulins disassociate from axonemal microtubules, which promotes axonemal disassembly. O-GlcNAcylation of HDAC6 also enhances its deacetylase activity, which leads to axonemal disassembly. Collectively, the ciliary length is shorter in a high O-GlcNAc cellular condition. Conversely, a low O-GlcNAc level stabilizes axonemal microtubules which allow longer cilia to assemble. Therefore, the cross- talk at the molecular level between O-GlcNAc and cilium puts the cell in a better position for fine-tuning the cellular response to nutrients.

This study uncovers O-GlcNAc as an important input signal to ciliary assembly and function. Primary cilia act as a cellular ‘antenna’ that receives diverse signals from the extracellular environment, including chemical and mechanical stimuli. The past studies of a wide spectrum of human ciliopathies, for example, polycystic kidney disease, Bardet-Biedl syndrome and orofaciodigital syndrome [11, 225], demonstrate that the cilium is an essential organelle for almost every aspect of development and tissue homeostasis. The negative feedback regulation of ciliary length by the key nutrient sensor O-GlcNAc shown by this study appears to be a mechanism of sensory signal adaptation. The elongation of the cilium is to increase its signal detection when nutrients are scarce, while the resorption is to limit its responsiveness to external signals. By adjusting their size depending on the abundance of nutrients, cilia allow cells to tune out random nutrient flux fluctuations, and to upregulate or downregulate cilia sensitivity to nutritive environment. Obviously, the constant dialogue between cilia and O-GlcNAc is beneficial to maintain O-GlcNAc homeostasis, which is critical to many cellular processes including cell cycle progress, stress response, and gene transcription [247]. Disruptions in O-GlcNAc homeostasis are proposed to lead to the development of diseases, such as cancer, diabetes, and Alzheimer’s disease [208, 247-250].

A wide range of signals from cell cycle, protein synthesis, autophagy, and cytoskeletons not only rely on cilia to function, but also regulate the assembly and resorption of cilia [225]. For example, these pathways modulate the activity of HDAC6 [232], OFD1 [34], mTOR [251], GSK3β [252], or other enzymes and regulatory proteins that are important for the ciliogenesis [204]. However, very little is known on which one of the signaling proteins or messengers integrates these diverse signals, or whether there is a hierarchical order of these signal inputs on

cilium length regulation. In this study, we showed that the level of protein O-GlcNAcylation negatively regulates the length of cilia. Since O-GlcNAcylation integrates multiple metabolites, such as carbohydrates, amino acids, fat and nucleotides, it is well-suited to tell the nutritive state of an organism. Future research is required to examine whether several ciliary signal inputs converge on O-GlcNAc to regulate ciliary length.

Biochemical analysis of isolated flagella from *Chlamydomonas* showed many flagellar axonemal proteins were O-GlcNAcylated (Figure 2-4 C). Moreover, the overall O-GlcNAc level was much higher in flagella undergoing disassembly (Figure 2-4 C), supporting that upregulated O-GlcNAc leads to ciliary resorption. In this study we checked a couple of proteins with well-established functions in ciliogenesis on how their O-GlcNAcylation affects axonemal microtubules. Although INPP5E was O-GlcNAcylated, we failed to link this modification to its ciliary function (Figure 2-7). We found that O-GlcNAcylation of α-tubulin promoted its disassociation from axonemal microtubules (Figure 2-4 B). The axonemal microtubules are heavily post-translational modified with acetylation, glycylation, and glutamylation [253]. Tubulin acetylation and glycylation stabilize axonemal microtubules. In contrast, polyglutamylation plays an opposite role, destabilizing axonemal microtubule [254, 255]. Here, we showed that O-GlcNAcylation is another MT destabilizer. Balanced tubulin post-translational modifications are important for ciliary length regulation. Future research on whether O-GlcNAcylation of tubulin coordinates with other tubulin PTMs will be of particular interest to ciliary length regulation and ciliogenesis.

In this study, we showed that HDAC6 was subjected to O-GlcNAcylation, and O-GlcNAc modification of HDAC6 promoted its enzymatic activity. HDAC6 is a key regulator of tubulin acetylation and functions in regulating MT stability [232]. The activation of HDAC6 involves its phosphorylation by Aur A kinase. Once activated, HDAC6 deacetylates acetylated MTs, leading to axonemal resorption. The mechanism of how O-GlcNAcylation of HDAC6 enhances its tubulin deacetylase activity is currently unknown. Since interplays between phosphorylation and O-GlcNAcylation are common, future research will be able to test whether O-GlcNAcylation of HDAC6 has a synergic effect on its phosphorylation, which in turn upregulates its activity.

Methods and materials

Cell culture

The mammalian hTERT-RPE1 (ATCC CRL-4000) and IMCD3 (ATCC CRL-2123) cells were grown in DMEM-F12 (Gibco) supplemented with 10% FBS (Gibco) and 1% penicillin-streptomycin (Gibco) at 37 °C in a 5% CO2 incubator. Cilia formation was induced by serum starvation for 24 h when cells reached 80% confluency.

The Chlamydomonas wild type *cc125* and *fla10ts* strains were obtained from the Chlamydomonas Center (http://chlamycollection.org/). Strains were cultured and maintained on Tris-acetate-phosphate (TAP) plates. Unless otherwise specified, liquid cultures used TAP media with constant aeration in a Conviron environmental chamber at 21°C with continuous light.

Transfection

Mammalian expression vectors pcDNA3.0-HA-OGT and pcDNA3.0-HA-OGT-rescue plasmids were used for transfections. For IP experiments, the hTERT-RPE1 cells were first grew to 50-

60% confluency. For each 10 cm Petri dish, cells were transfected with 5 μg plasmids using the TurboFect transfection reagent (Thermo Scientific) and then cultured for 48 h before collected and prepared for immunoprecipitation (IP) using antibodies as indicated in the results part. For IF experiments, the hTERT-RPE1 cells were transfected with 1 μg plasmids for each 3.5 cm Petri dish as described above. The IMCD3 cells were transfected with 1 μg plasmids with Polyethylenimine (PEI) (Polysciences) reagent and then cultured for 48 h before used for IF analysis.

RNA interference and inhibitor treatment

The small RNA interference experiments were carried out using the same method as described in a prior publication. The transfection of the hTERT-RPE1 cells was carried out by using the LipofectamineTM RNAiMax Reagent (Invitrogen) according to the manufacture's protocol. A mixture of two OGT oligonucleotides (siOGT 1# and siOGT 3#) at 1:1 ratio was used. All oligonucleotides including the control siGl2 (5'- CGUACGCGGAAUACUUCGAdTdT-3') and the siOGT duplexes were synthesized by Dharmacon.

The concentrations and durations of chemical inhibitor treatments used in all experiments were: TG (5 μM, 24 h), SG (1 mM, 24 h), Alloxan (5 mM, 18 h), and Tubacin (2 μM, 24 h). The solvent DMSO was used as control for each inhibitor treatments.

Rescue with HA-OGT-rescue

The hTERT-RPE1 cells were first transfected with the HA-OGT-rescue plasmid, or a control construct expressing the HA tag only, and then cultured for 24 h followed by a 12 h treatment of

siGl2 or siOGT. After starving in DMEM for 24 h, the cells were harvested for immunoblotting (IB) or IF analysis (Figure 2-1 B).

Immunoprecipitation (IP)

For IP, cells were lysed with IP buffer (50 mM Tris·Cl, pH 7.4, 150 mM NaCl, 5 mM EDTA, 0.5% NP40) supplemented with a Protease Inhibitor Cocktail (Roche). Lysates were incubated with protein A/G sepharose beads (Santa Cruz) for 2 h for pre-clearing of non-specific bindings prior to incubation with primary antibodies overnight at 4 °C. The beads in the pellets were then subjected to IB analysis.

Antibodies and immunoblotting (IB) assay

Table S1 contains information of primary antibodies used in this study. The methods for SDS-PAGE and IB assays were the same as previous described. Chemiluminescence was used to detect the primary antibodies.

Immunofluorescence staining

Cells grown on glass coverslips were fixed with 4% paraformaldehyde for 10 min, followed by fixation in ice-cold methanol for 3 min. The cells were permeabilized with 1% Triton X-100 in PBS for 10 min before blocked in PBS with 3% BSA. Primary antibodies are listed in Table S1. Secondary antibodies of Alexa-488 and Alexa-561 were purchased from Invitrogen. Images were captured with an Olympus IX81 microscope (Olympus, Tokyo, Japan) with a Yokogawa CSU-X1 Spinning Disk Unit (Andor Technology, CT, USA).

Flagella isolation and axoneme preparation

Flagella were isolated as previously described [240]. Flagellar membrane was removed by incubating isolated flagella in 1% NP40 for 30 min on ice.

Tubulin deacetylase (TDAC) assay

Endogenous HDAC6 proteins were Immune-precipitated from lysates of hTERT-RPE1 cells treated with TG, SG, or control DMSO. The IPs by rabbit IgG and anti-HDAC6 (Con) from control treated cell lysates were used as negative controls. TDAC assays were carried out as previously described (Hubbert et al., 2002). Briefly, Chlamydomonas flagella axonemes (~ 40 μg) and HDAC6 were incubated together in 200 μl TDAC buffer (20 mM Tris-Cl pH 8.0, 20 mM NaCl) at 37 °C for 2 h, and then transferred to ice for 15 mins. Pellets containing protein-A beads were collected by centrifugation. The pellets were analyzed by IB with anti-HDAC6 antibody and the supernatants were analyzed with anti-α-tubulin and anti-acetylated-tubulin antibodies.

In vitro tubulin O-GlcNAcylation assay The in vitro tubulin O-GlcNAcylation assays were performed as described previously [256] with minor modifications. HA-OGT expressed in hTERT-RPE1 cells was purified by IP using anti-HA antibody. The reaction mixture for in vitro glycosylation contained 50mM Tris·Cl, pH 8.0, 5 mM MgCl2, 2 mg HA-OGT, 6 μl flagella axonemes, and 1 mM of UDP- GlcNAc (Sigma-Aldrich) in a reaction volume of 50 μl. The reactions were performed at 25 °C for 1 h or 2 h. The axonemes and beads were collected by centrifugation. Both the pellets and the supernatants were analyzed by IB with antibodies indicated in results.

Percentages of ciliated cells and ciliary length measurements

For counting the percentages of ciliated cells, only the cells clearly IF stained by antibodies against acetylated-tubulin and IFT88 were considered as ciliated. No less than 150 random selected cells combined from three independent experiments were used. The IF staining of IFT88 was used to measure the ciliary length since the staining clearly marked the base and the tip of a cilium. The segmented line selection tool of Image J (Java 1.8.0_172, https://imagej.nih.gov/ij) was used for length measurements. For all ciliary length measurements, 150 cilia combined from three independent experiments were used for statistical analysis.

Statistical analysis

Statistical analyses were performed using the software GraphPad Prism 7.0e (GraphPad software, San Diego, California, USA). Results were shown as mean standard deviation. Statistical analyses between two groups were performed using the student's t-test. p-value less than 0.5 was considered significant. The mark "*" represents $p<0.05$, **represents $p<0.01$, and "ns" represents no significant difference.

CHAPTER III

EXPLORING THE FLAGELLA AXONEME OF *CHLAYMYDOMONAS REINHARDTII* AS A PROTEIN SYNTHESIS PLATFORM

Introduction

Biosynthesis is a multi-step enzymatic intracellular process to produce complex products in living organisms. Biosynthetic pathways typically use monomers as building blocks to build macromolecules, such as proteins, nucleotides, and lipid membrane components. Proteins, one of the essential components in all organisms, have multiple functions such as enzyme catalysis, immune-defense, transport/storage, and regulation. Given the important function of proteins, they have been studied intensively and applied widely in medicine, research, and biotechnology. With the desire for increased protein production, multiple biotechnological methods have been developed [257]. The typical one is the recombinant molecular biology. Briefly, the gene encoding a specific protein is cloned into an expression vector then the vector transformed into a system that expresses the protein. Expression systems include, but are not limited to, bacteria, yeast, insects, and mammalian cells [258-260]. There are tremendous advantages to using organisms as an expression system, such as allowing bacteria to quickly produce a large number of proteins to determine protein structures; yeast to produce proteins with significant PTMs; and insect and mammalian cell lines to execute mRNA splicing similar to human cells. However, there are some limitations when considering the function and quality of the target protein. For example, bacteria often express non-functional proteins or insoluble proteins in inclusion bodies due to misfolding; eukaryotic expression systems like mammalian cells have very low yield, the products can be toxic to the host cells; and the intracellular space is limited [261]. The eukaryotic

unicellular green alga *Chlamydomonas reinhardtii* is an ideal protein production system because it can provide high yield and mathematically calculated products. Other advantages include easy isolation of flagella, stability during storage, and low cost. Thus, the flagella axoneme is an ideal platform for constructing protein arrays.

Chlamydomonas flagella are motile structures that extend from the anterior surface. Flagella are composed of a microtubule-based axoneme underneath an extended plasma membrane. The axoneme consists of nine doublet microtubules (DMTs) surrounding one pair of singlet microtubules with multiple appendage structures attached to render flagella motility, such as radial spokes, inner and outer dynein arms, and nexin. The appendage structures' components and arrangement on the axoneme are well studied. The axoneme is about 12 μm long and the structural components are repeated every 96 nm on the axoneme [262]. For instance, radial spoke is a T-shaped complex and contains a stalk and a head that is composed of at least 23 proteins. The stalk is anchored to the doublet microtubules and globular head toward the central pair of singlet microtubules, the connection between these two gives the mechanical movement of the flagella. In each of 96 nm periodic structure, there are two complete radial spokes and one truncated spoke [263]. The inner junction is a bridge structure between A- and B-tubules of the doublet microtubules, which is formed by a smaller subunit of non-tubulin proteins. FAP20 is one protein of the inner junction and plays a role in the symmetrical waveform of the flagella. FAP20 localizes along the entire length of the axoneme, and there are 12 or 24 FAP20 molecules per 96 nm periodic structures [201].

Because protein synthesis can only happen in the cytoplasm, flagellar proteins are transported and assembled on the axoneme by the molecular machinery named intraflagellar transport (IFT). The IFT recognizes flagellar proteins then transports them into the flagella compartment and incorporates them onto the appropriate positions of the axoneme. This unique structure and self-assembly mechanism of flagella axoneme makes it an excellent template to assemble an exogenous protein array. It can be achieved by expressing a construct that contains a fusion gene of an axoneme protein and an exogenous protein in the cytoplasm. The axoneme protein can serve as an adaptor to carry the exogenous protein onto the axoneme.

The availability of using flagellar axoneme as a protein self-assembly scaffold is supported in several ways. First, the genome and flagella proteome of Chlamydomonas are entirely sequenced. Therefore, it is approachable to do any genetic modifications to express the fusion construct. Second, there are many axoneme protein null mutant strains available, which allows fusion proteins to be expressed and incorporated into the axoneme without the endogenous protein. Third, there are many examples in which tagged axoneme proteins have been successfully expressed and assembled on the axoneme and rescued the phenotypes of the mutant strains, such as HA, GFP, and BCCP tagged axoneme proteins FAP20 and RSP3 [201]. In addition, transformants can be identified quickly by observing their swimming motility. This is because appendage structures are necessary for flagella motility, but adaptor-null mutants are usually non-motile. When the fusion protein is expressed and incorporated onto the axoneme, swimming motility is recovered and easily distinguished.

Simultaneously, flagella axoneme serves as a protein production template, which benefits from all advantages of the natural assembly attributes. First, flagella are easily isolated and produced in large quantities. Chlamydomonas cells have two flagella and are easy to grow on a large scale at low cost. Flagella are easily detached from the cell body by lowering pH to 4.5 then isolated by centrifugation. The target protein anchored to the axoneme as a whole can serve as an immobilized enzyme, or the target protein can be released from the axoneme by protease cleavage. Second, the target protein should be arranged on the axoneme in a high density and periodic manner due to the fusion with an axoneme protein, and the yield of the products can be calculated. Furthermore, the target protein yield can be increased by flagella regeneration. After flagella are detached, cell bodies can regenerate full-length flagella within two hours and the regeneration can repeat multiple times. Finally, isolated flagella are stable and easily stored. Because no protease exists in the flagellar compartment, proteins would not be degraded and protein activity is therefore stable.

Here we investigated using axoneme proteins FAP20 and RSP3 as adaptors to transport and incorporate target proteins to the axoneme. These two adaptors were chosen to take advantage of existing FAP20 and RSP3 null mutant strains *im5* and *pf14*, as well as rescue constructs pBS-FAP20-GFP and pKF-RSP3-GFP. Also, the spatial patterns of FAP20 and RSP3 on the axoneme are clear, which enables estimates of target protein yield. To test the hypothesis of using flagella axoneme as a biosynthetic template, we first modified the rescue constructs to express fusion proteins. The GFP gene in the original rescue constructs pBS-FAP20-GFP and pKF-RSP3-GFP was replaced with the target protein gene estrogen receptor alpha (ERα) or beta-lactamase (Bla), due to the molecular size of these two proteins is similar to the size of GFP. Meanwhile, a TEV

linker was added to connect the adaptor and the target protein genes. Second, the fusion constructs were transformed to the mutant strains *im5* and *pf14*, and the transformants were identified based on the rescue of swimming motility and confirmed by WB. Furthermore, flagella were purified to test the target protein enzymatic activity and stability. Ultimately, we demonstrated that fusion proteins assembled on the axoneme and rescued the phenotype of the mutant strains. Furthermore, target protein yield can be increased by flagellar regeneration. Finally, axoneme-anchored target proteins were enzymatically active and were resistant to freeze-thaw treatment. This study provides a key fundamental step towards the development of using flagellar axoneme as a protein self-assembly template.

Results

Designing the of use of flagellar axoneme as a template to dock the protein of interest

The axoneme proteins FAP20 and RSP3 were chosen as adaptor proteins to transport target proteins for two reasons. First, we have FAP20-loss-of-function mutant strain *im5* and RSP3-deficient mutant strain *pf14* on hand, as well as their rescue constructs of pBS-FAP20-GFP and pKF-RSP3-GFP [201]. Both constructs can rescue the expression of FAP20 and RSP3 to WT levels. The FAP20-GFP fluorescence intensity is three times that of RSP3-GFP, which indicates three times more FAP20 on the axoneme than RSP3. Also, the rescued strains recovered axoneme motility, which indicates that the GFP tag does not affect the adaptor protein function [201].

We modified the rescue constructs by substituting the *GFP* gene with the target protein gene in both pBS-FAP20-GFP and pKF-RSP3-GFP. First, the original *Eco*RV linker and *GFP* gene were

deleted. In the pKF-RSP3-GFP construct, the C-terminal 140 amino acids of RSP3 were also deleted to generate more space for the target protein because the last 140 amino acids of RSP3 do not affect either recruitment of radial spoke proteins assembled on the axoneme or the motility of flagella [199] (Figure 3-1 A&B). Furthermore, the target protein genes following the TEV linker were inserted behind the adaptor protein gene. The target protein can be released from the axoneme by TEV enzyme digestion (Figure 3-1 C&D). In the rescued strains, the fusion protein should be arranged on the axoneme in a high density and periodic manner, and the yield of the fusion protein can be calculated precisely based on the arrangement of the adaptor protein (Figure 3-1 E).

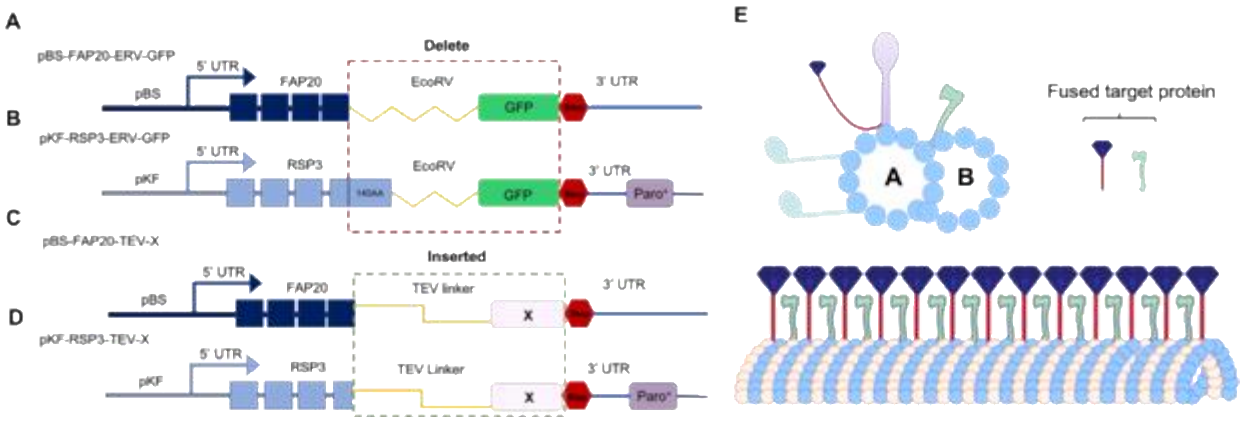

Figure 3- 1 Design of applying flagellar axoneme as a biosynthetic template.
(A) The construct of pBS-FAP20-GFP and pKF-RSP3-GFP were modified to express the fusion proteins of FAP20/RSP3 and the target protein. The fusion proteins were connected by a TEV-linker. The EcoRV-linker and GFP gene were deleted in both of the original constructs of pBS-FAP20-GFP and pKF-RSP3-GFP. In addition, the C-terminal 140 amino acids of RSP3 were deleted as well in the pKF-RSP3-GFP construct. Then replaced with a TEV-linker and the target gene. (B) The schematic structure of flagella axoneme showed the expression of the fusion proteins. The target protein is fused with an axoneme protein, such as FAP20 and RSP3. The axoneme protein is serving as an adaptor to transport and locate the target protein onto the axoneme and form a protein array in a high density and periodic manner.

Prescreening of rescued strains based on the phenotype of motility and flagellar assembly

To increase the potential of the fusion proteins assembled on the axoneme, we chose two small target proteins, the ligand-binding domain of estrogen receptor alpha (ERαLBD) and beta-lactamase (Bla). Both proteins are of a similar molecular weight as GFP (~ 30 kD). Also, the substrates of both target proteins are hydrophobic so can easily pass through the flagellar membrane. Therefore, it is possible to test the target protein enzymatic activity without removing the flagellar membrane.

The rescue constructs that express fusion proteins include: pBS-FAP20-TEV-ERαLBD, pBS-FAP20-TEV-Bla, pKF-RSP3-TEV-ERαLBD, and pKF-RSP3-TEV-Bla (shortened as FAP20-ERα, RSP3-ERα, FAP20-Bla, and RSP3-Bla). The constructs of FAP20-ERα and FAP20-Bla were transformed into the *im5* strain, and RSP3-ERα, RSP3-Bla were transformed into the *pf14* strain. Because both *im5* and *pf14* strains have defects in swimming motility and flagellar assembly, it was efficient to identify the transformants based on their motility and flagellar assembly. All antibiotic-resistant colonies achieved on the TAP plate after transformation were transferred to a 96-well plate with a liquid TAP medium and cultured with continuous light. Then cell motility was checked under a light microscope after a 1-day culture. The motile cells were transferred to a test tube with 3 ml TAP medium and cultured for another two days to ensure motility and flagellar assembly (The flagellar assembly results are not listed here) (Figure 3-2). The movies are included as separate files. The expression of the target protein in the transformants screened in the first step were further confirmed by biochemical tests.

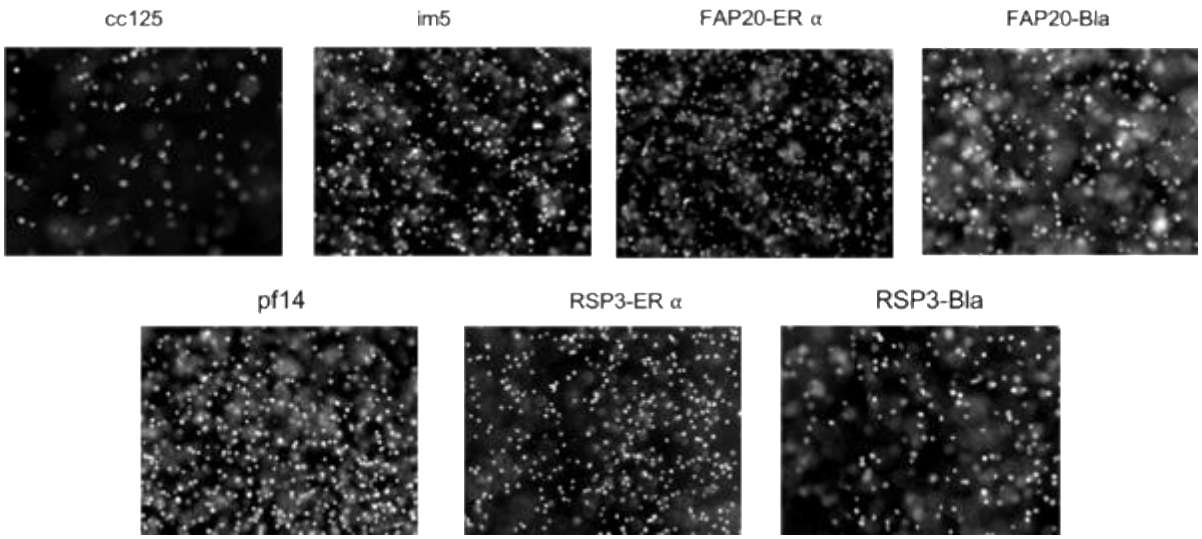

Figure 3- 2 Swimming motility of various strains.
Swimming motility of WT strain *cc125*, mutant strains *im5* and *pf14*, and rescues strains FAP20-ERα, Bla and RSP3-ERα, Bla were taken in real time.

Confirming the positive transformed strains by WB

To confirm the expression of the fusion proteins in the transformants I wanted to use WB. To increase sensitivity, flagella from all transformants with swimming motility were isolated and prepared for WB. We got five flagella samples of FAP20-ERα 6, 9, 12, 13, and 14; and five flagella samples of RSP3-ERα 7, 9, 10, 11, and 14. All samples were subjected to WB. The IB results of ERα showed that the expression levels of ERα protein varied significantly in all flagella samples. FAP20-ERα 12, 14 have relatively higher ERα expression levels compared to others, and RSP3-ERα 10 is the only one with the ERα expression. To further confirm the expression of the fusion protein, flagella samples were immune-blotted with anti-axoneme protein antibodies FAP20 and RSP1. Because of the deletion of 140 amino acids at the C-terminal, RSP3 antibody would not recognize the truncated RSP3. However, the other radial spoke proteins, such as RSP1, can only present when expression of RSP3 is rescued. Therefore, the radial spoke protein RSP1 was used to indicate rescued expression of RSP3. The WB results

showed that FAP20 is expressed in the rescue strains, but the protein level is much lower than in WT. In contrast, the expression of RSP1 was close to WT levels in all flagella samples. These results indicated that the target protein is restricted to the flagellar compartment (Figure 3-3 A&C). Here, FAP20-TEV-ERα 14 and RSP3-TEV-ERα 10 were chosen as the rescued strains.

In parallel, we obtained four samples of FAP20-Bla 2, 3, 4, and 5; and five samples of RSP3-Bla 7, 8, 9, 10, and 11. The immune-blotting (IB) results of Bla showed that beta-lactamase was expressed in FAP20-Bla sample 4 and all samples of RSP3-Bla. The IB results of FAP20 and RSP1 showed that the expression of FAP20 is still much lower in the rescued strain than the WT, while RSP1 expression levels are equivalent to WT (Figure 3-3 B&D). Here, FAP20-Bla 4 and RSP3-Bla 10 were chosen as the rescued strains.

Flagellar length was also measured in each of the rescued strains. WT cells had average flagellar length of 13.4 μm; whereas the mutant cells of *im5* and *pf14* had lengths of 10 μm and 8.2 μm, respectively, which indicated their flagellar assembly defects. These defects were recovered in the rescue strains. The FAP20-ERα 14 and FAP20-Bla 4 assembled the flagellar length of 13.1 μm and 10.7 μm, RSP3-ERα 10 and RSP3-Bla 10 assembled flagellar length of 13.5 μm and 12.3 μm (Figure 3-3 E&F). The results suggest the fusion proteins expressed and targeted to the axoneme.

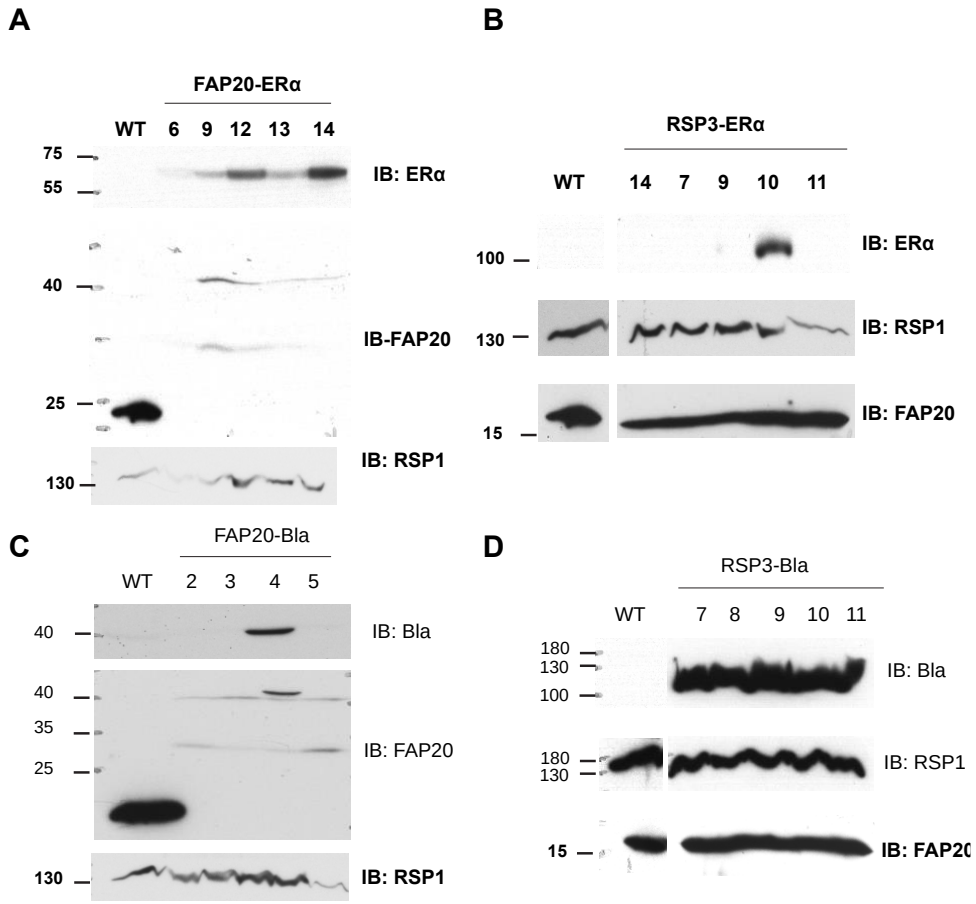

Figure 3- 3 Confirmation of the rescued strains from the candidates of prescreening.
(A-D) Flagella samples were prepared from each of the transformants with swimming motility, and WT used as a negative control. All samples were subjected to WB. The FAP20-ERα and RSP3-ERα samples were blotted with ERα, FAP20, and RSP1 antibodies to detect the expression of both the axoneme protein and the target protein. The FAP20-TEV-Bla and RSP3-TEV-Bla samples were blotted with beta-lactamase, FAP20, and RSP1 antibodies to detect the expression of the fusion proteins. The final candidates for each transform were chosen based on the expression of the axoneme protein and the target protein. (E) The pictures of cc125 and the rescued strains showed the assembly of flagella. Error bar equals 10 μm. (F) The statistical results showed the flagellar length in each of control strains, *cc125, im5, and pf14*, and the rescued strains, FAP20-ERα 14, Bla 4 and RSP3-ERα 10, Bla 10. The error bar showed the flagella length deviation. About 60 flagella were measured for each of the samples.

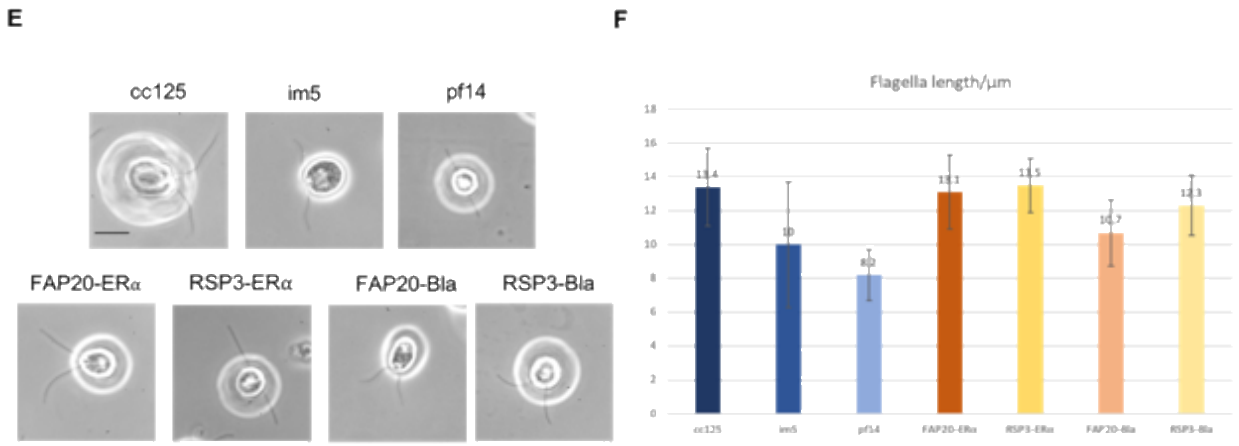

Figure 3-3 Continued.

Quantifying the expression of the target proteins

After confirming the rescue strains, I purified flagella to test the enzymatic activity of the target proteins. FAP20-ERα and RSP3-ERα as one group will be discussed first. FAP20-Bla and RSP3-TEV-Bla as another group will be discussed later. WT, FAP20-ERα, and RSP3-ERα strains were cultured in 4 L TAP medidum to get enough flagella for conducting ERα binding assay. Flagella were harvested as described, and an equal volume of flagella from each sample was used to prepare samples for protein level quantification. Standard BSA concentration samples were used as a reference, and the quantification results showed that the acetylate-tubulin concentration of WT, FAP20-ERα, and RSP3-ERα samples was 2.4 μg/μl, 0.8 μg/μl, and 1.45 μg/μl, respectively (Figure 3-4 A). To ensure the equal amount of the flagella in the following binding assay, the concentration of all samples was adjusted to 0.8 μg/μl then subjected to WB. The IB results showed that the expression of ERα in the FAP20-ERα is about 2.4 times of the RSP3-ERα, and acetylate-tubulin was used as a loading control (Figure 3-4 B). The result is consistent with the previous finding that the fluorescent intensity of FAP20-GFP is three times of RSP3-GFP [201].

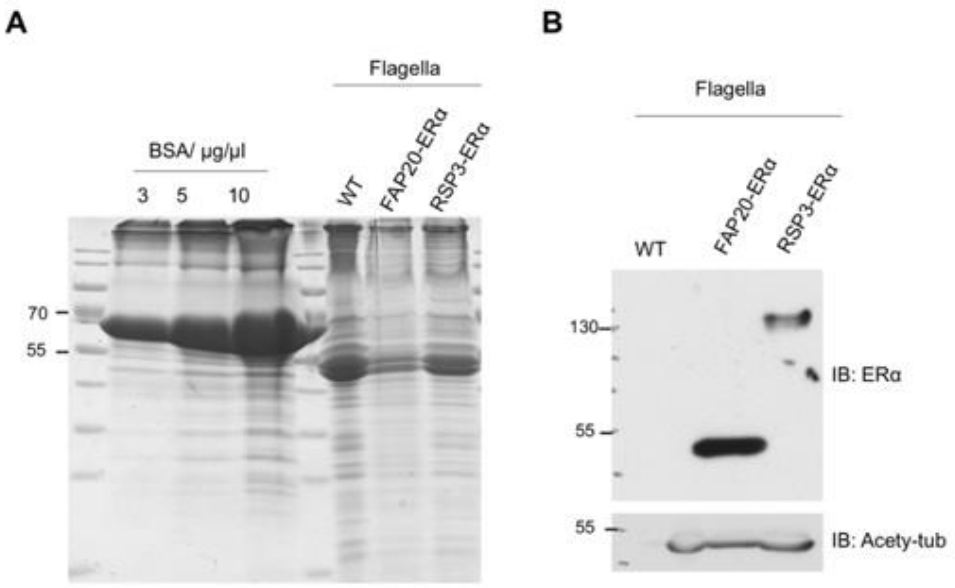

Figure 3- 4 FAP20-ERα and RSP3-ERα flagella isolation and quantification.
(A) Coomassie blue staining showed the intensity of BSA standard samples and WT, FAP20-ERα and RSP3-ERα flagella samples. The quantification results by measuring the main band intensity showed the concentration of flagella samples are 2.4 µg/µl, 0.8 µg/µl, and 1.45 µg/µl separately. (B) The concentration of flagella samples was adjusted to 1 µg/µl with the dilution of HMDEK buffer and subjected to WB. The IB of ERα showed the protein expression levels in each of the flagella samples and IB of acetylate-tubulin showed the equal loading of each sample.

Analyzing the ability of FAP20-ERα and RSP3-ERα flagella to bind to estrogen compounds

To test whether axoneme-tethered ERα can bind to estrogenic compounds, the system of *S. cerevisiae* BLYES was applied to detect the existence and concentration of estrogen compounds. In principle, estrogen compounds will bind to the human estrogen receptor (hERα) and initiate the transcription of estrogen response element (ERE) followed by the expression of a bioluminescent bioreporter gene. All three genes were expressed in *S. cerevisiae*. The bioluminescent intensity positively correlates to the concentration of estrogen compounds [264]. In our experiments, 17-β estradiol, one type of estrogen, was used to conduct the flagellar ERα

binding assay. The concentration of 17-β estradiol was measured before and after incubation with flagella samples. The concentration reduction can reflect the flagella affinity for estrogen compounds.

A standard curve was built first to indicate the relationship between the concentration of 17-β estradiol and bioluminescent. The BLYES system can detect substrate concentration from 10^{-9} M to 10^{-5} M. The 50% effective concentration (EC50) value is around 10^{-7} M and this was used as the starting concentration in the following binding assays. All three flagella samples of WT, FAP20-ERα, and RSP3-ERα were incubated with 10^{-7} M 17-β estradiol in a total 5 ml volume system. At the time points of 1, 3, 6, 24, and 48 hours, 800 μl reactants were taken to measure the 17-β estradiol concentration using the BLYES system (Figure 3-5). The results showed that WT flagella, a negative control, decreased 26% of 17-β estradiol, while FAP20-ERα and RSP3-ERα flagella decreased 17-β estradiol by 47% and 39% separately after incubation of 48 hours. The results indicate that the target protein ERα on the axoneme of FAP20-ERα and RSP3-ERα are enzymatically active.

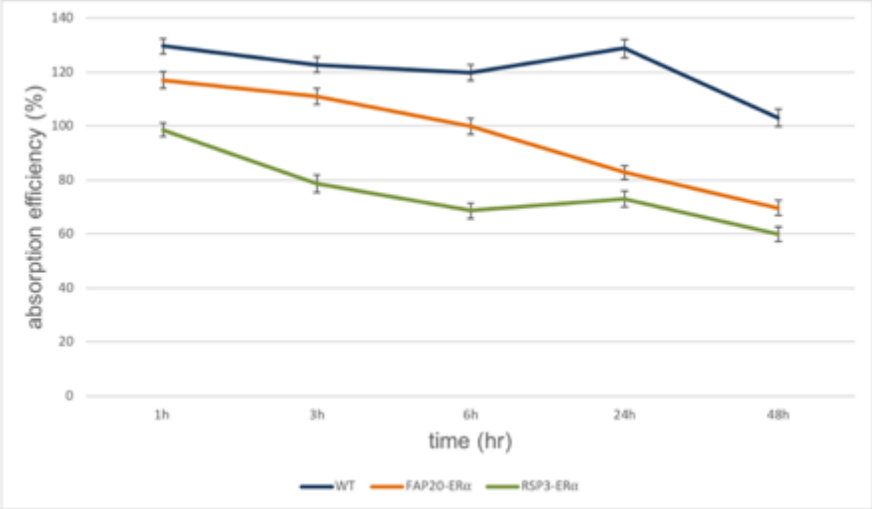

Figure 3- 5 FAP20-TEV-ERα and RSP3-TEV-ERα flagella ERα binding assay.
200 μl each of WT, FAP20-TEV-ERα, and RSP3-TEV-ERα flagella were incubated with 10^{-7} M 17-β-estradiol in a total volume of 5 ml system. 800 μl reactants were taken out to conduct the BLYES assay at the incubation time points of 1, 3, 6, 24, 48 hours. The bio-luminance at each time points were measured. The decreased bio-luminance indicates the binding amount of 17-β-estradiol to flagella.

Regenerating of FAP20-TEV-Bla and RSP3-TEV-Bla flagella

One advantage of using flagellar axoneme as a biosynthetic template is that the yield of products can be easily accumulated by flagella regeneration. We used WT, FAP20-Bla, and RSP3-Bla strains to test the yield accumulation by flagellar regeneration. The original flagella were detached by lowering pH to 4.5, then separated from cell bodies by gentle centrifugation. The flagella in the supernatant were further concentrated by sucrose underlaying as described in the method. The cell bodies were resuspended in HEPES buffer and cultured for another 2 hours to regenerate flagella. Cell status and flagellar assembly were checked before harvesting the regenerated flagella. Due to the different flagellar regeneration time, FAP20-Bla flagella were only regenerated once, and RSP3-Bla flagella were regenerated twice. All original and regenerated flagella samples were observed under a light microscope, and flagellar lengths were measured (Figure 3-6 A). Flagellar length of WT was 13.4 μm; the lengths of FAP20-Bla

original and regenerated flagella were 10.8 μm and 11.1 μm; the lengths of RSP3-Bla original, 1st, and 2nd time regenerated flagella were 12.5 μm, 11.6 μm, and 12.1μm (Figure 3-6 B). Overall, the lengths of original and regenerated flagella were consistent.

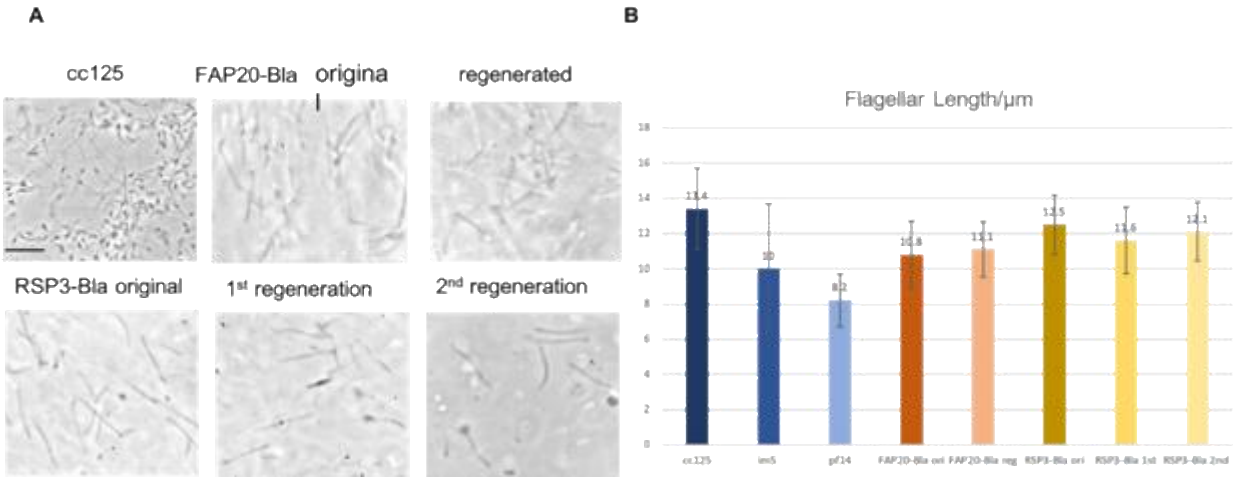

Figure 3- 6 Isolation of FAP20-Bla and RSP3-Bla original and regenerated flagella.
(A) *Chlamydomonas* strains of WT, FAP20-Bla and RSP3-Bla were cultured in the 4 L bubbly system. Cells were collected for flagella isolation when the concentration reached 10_6/ml. Original flagella were detached from the cell body by lowering pH to 4.5 transiently then bringing back to pH 7.0. The flagella and cell bodies can be separated easily by gently centrifuging at 2000 rpm. The flagella can be purified according to the protocol as described, and cell bodies were suspended and cultured in HEPES buffer to regenerate flagella. Then the regenerated flagella were collected in the same way. The pictures showed the purified flagella under 100x of a light microscope. Scale bar equals 10 μm. (B) The statistical results showed the flagellar length in each of the strains. The error bar showed the flagella length deviation. About 60 flagella were measured for each of the samples.

Quantifying protein levels of FAP20-Bla and RSP3-Bla original and regenerated flagella

The protein concentration of all flagella samples was quantified by comparing to BSA standard samples. The concentration of WT, FAP20-Bla original, regenerated, RSP3-Bla original, 1st, and 2nd time regenerated flagella was 3.2 μg/μl, 2.2 μg/μl, 2 μg/μl, 4 μg/μl, 3 μg/μl, and 3 μg/μl, respectively. (Figure 3-7 A). The concentration of each sample was adjusted to 1.6 μg/μl and then subjected to WB. IB of acetylate-tubulin confirmed that all samples had equal loading. The

protein level of Bla in FAP20-Bla flagella is approximately 1.5 times that of RSP3-Bla (Figure 3-7 B). However, the Bla protein levels were similar in each of the original and the regenerated flagella samples, which indicate that the yield of the product can be accumulated by flagella regeneration.

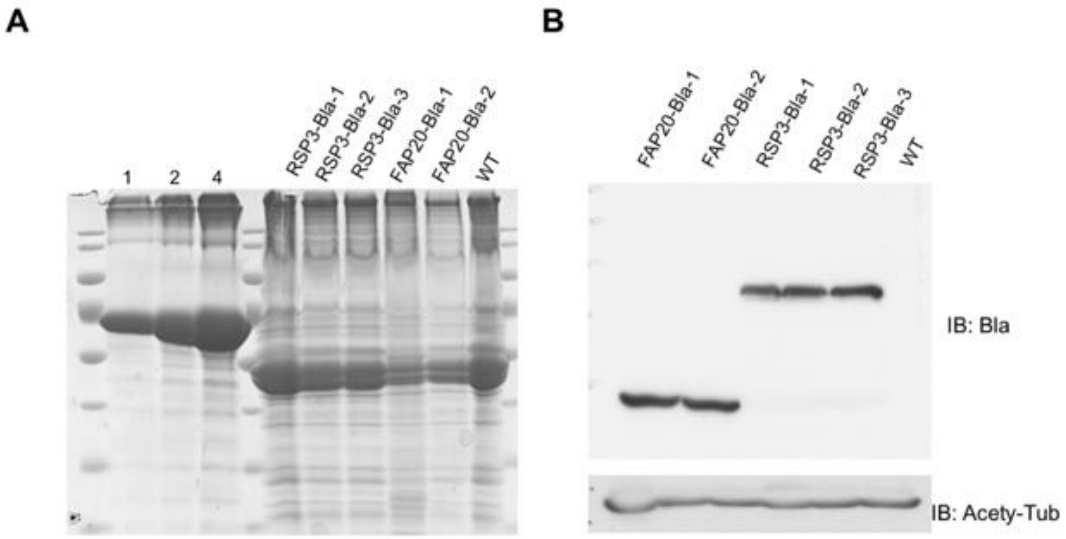

Figure 3- 7 FAP20-TEV-Bla and RSP3-TEV-Bla flagella isolation and quantification.
(A) Coomassie blue staining showed the intensity of BSA standard samples and RSP3-TEV-Bla original, 1st, 2nd regenerated flagella, FAP20-TEV-Bla original, regenerated flagella and WT flagella samples. The quantification results by measuring the main band intensity showed the flagella samples' concentrations are 4 μg/μl, 3 μg/μl, 3 μg/μl, 2.2 μg/μl, 2 μg/μl and 3.2 μg/μl separately. (B) The concentration of flagella samples was adjusted to 1.6 μg/μl with the dilution of HMDEK buffer and subjected to WB. The IB of beta-lactamase showed the protein expression levels in each of the flagella samples and IB of acetylate-tubulin showed the equal loading of each sample.

Detecting and quantifying Bla enzyme activity

The activity of beta-lactamase was detected using the colorimetric Beta Lactamase Activity Assay Kit (ab197008). The assay is based on the enzymatic hydrolysis of the substrate nitrocefin, which results in the generation of a colored product that is detected by absorbance at OD 490nm (Abs 490nm). The amount of product is directly proportional to the enzymatic activity. A

standard curve was built to show the proportion between the concentration of the product and Abs 490nm, standard line equation is y=0.0185x + 0.0318 (Figure 3-8 A). Theoretically, 1 Unit Beta-Lactamase activity is defined as the amount of enzyme that generates 1.0 μmol of nitrocefin per minutes at pH 7.0 at 25°C. Sample Beta-Lactamase activity can also be expressed as mU/μg, which means nmol/min hydrolyzed nitrocefin generated per μg of protein. Based on the amount of hydrolyzed nitrocefin produced per minutes, the enzyme activity of Bla flagella can be calculated.

For each of the original and regenerated flagella samples, I did two parallel assays of Bla activity by adding 5 μl flagella for each test, then measured the absorbance at OD 490nm every minute for overall 20 minutes. Then calculate the enzymatic activity. The results showed that all FAP20-Bla and RSP3-Bla original and regenerated flagella have Bla enzymatic activity (Figure 3-8 B).

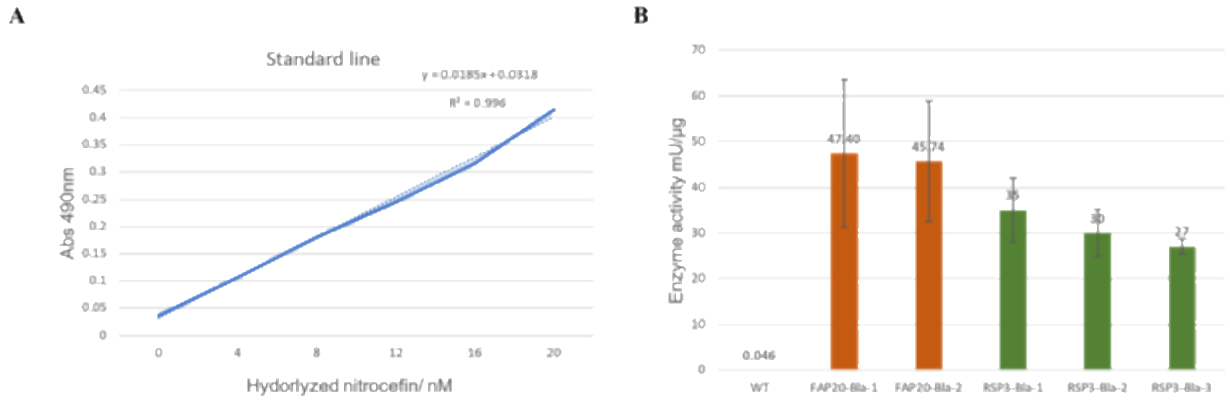

Figure 3- 8 FAP20-Bla and RSP3-Bla flagella beta-lactamase enzymatic activity assay.
(A) A standard curve of enzymatic activity and absorbance at OD 490 nm. (B) Flagella samples were subjected to beta-lactamase activity assay. For each sample, 5 μl flagella were added and incubated with 40 nM Nitrocefin in 100 μl system and measured the absorbance of 490 every minute, then calculate the enzyme activity. 2 replicates were performed for the beta-lactamase activity assay.

Analyzing the enzymatic activity of recycled flagella

One advantage of the fixed enzyme is that the enzyme can be isolated from the reactants compared to soluble enzymes. Therefore, we want to know whether Bla flagella can be recycled to catalyze a new reaction. The flagella from the reactions were isolated by centrifuging at the maximum speed, 10,000 rpm for 10 minutes. The flagella were washed twice with 1x HMDEK buffer to remove the chemicals attached to the flagella. Then the flagella were subjected to a new reaction. The results showed that recycled flagella still have enzymatic activity but with subtle decreased (Figure 3-9). This may be caused by the flagella lost during the washing or the substrate from the previous reaction attached to the flagella.

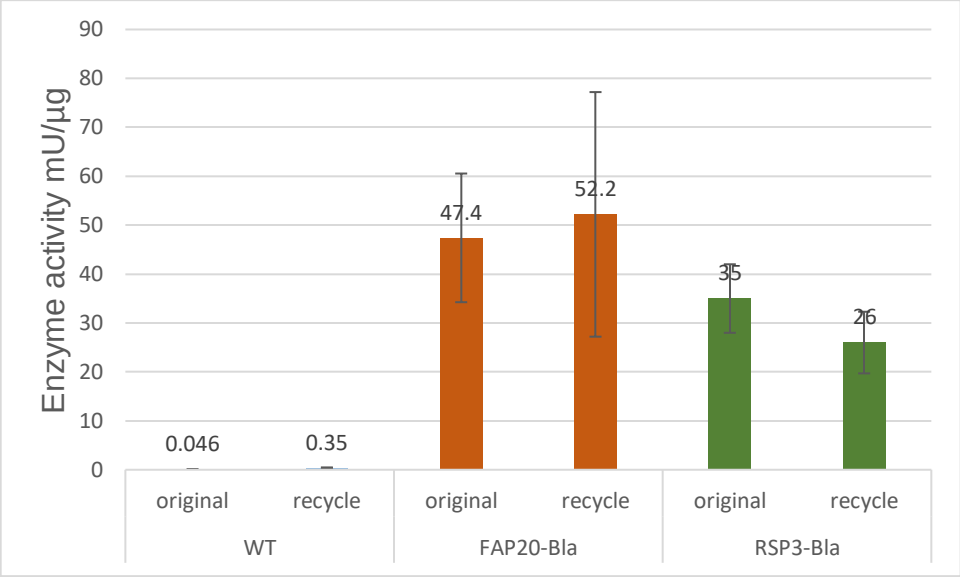

Figure 3- 9 Recycled flagella are still enzymatically active.
The flagella from the first reaction were collected and re-subjected to a new reaction. The absorbance of 490nm were measured and calculate the enzyme activity. Two replicates were performed for the enzymatic activity assay.

The Bla flagella enzyme is resistant to freeze-thaw treatment and durable at room temperature, but is heat sensitive

We showed that both FAP20-Bla and RSP3-Bla flagella express Bla with enzyme activity and flagella axoneme is a suitable enzyme carrier that can be recycled and regenerated. Now we want to know whether the enzyme tethering to the axoneme can have more properties compared to the soluble enzyme, such as higher catalytic efficiency and more stability during storage. First, we compared the catalytic efficiency between the commercial beta-lactamase enzyme and FAP20-Bla and RSP3-Bla flagella. Either 5 μl of commercial enzyme or flagella were added to the reaction system, and the kinetics were recorded within 20 minutes. Furthermore, because the commercial enzyme is usually sensitive to repetitive freeze and thaw, we want to test whether the fixed enzyme is resistant to freeze-thaw treatment. Therefore, we freeze-thaw both the commercial enzyme and flagella four times between -20 °C and 20 °C, then test the enzymatic activity with the same set up as before. The results showed that freeze-thaw treatment significantly decreased the commercial enzymatic activity about 32%, while both the flagella bound enzyme FAP20-Bla and RSP3-Bla have almost the same enzymatic activity compared to the un-treatment control (Figure 3-10). The results strongly indicate that the fixed enzyme is more resistant to the significant temperature change of freeze-thaw. Inspired by the results, we boiled the enzymes at 42°C for 10 min to test whether the fixed enzymes are more heat stable. However, the results showed the opposite results as expected. Commercial Bla enzymatic activity only decreased by about 8.3% while the FAP20-Bla and RSP3-Bla enzymatic activity were decreased by 50.5% and 23%, separately (Figure 3-10). Even though the flagella cooperated enzymes are freeze-thaw resistance, their activity is easily denatured at a higher temperature. At last, all enzymes were kept at room temperature for 48 hours to test the

enzyme's stability then measured the enzymatic activity. The result showed that the enzymatic activity of the fixed enzyme maintained the same as untreated controls after 48 hours, the commercial enzyme showed slightly decreased enzymatic activity about 3.2% (Figure 3-10). Overall, the results suggest that the fixed enzymes are more stable below the denature temperature, especially the fixed enzyme is resistant to freeze-thaw treatment.

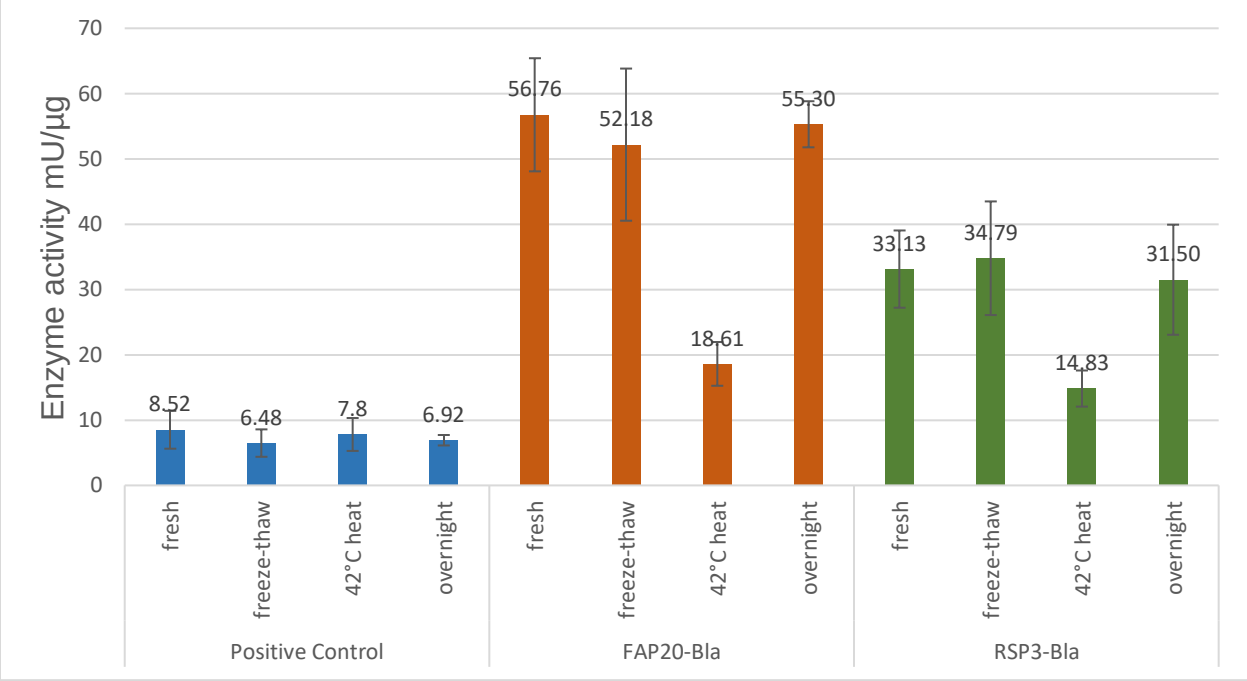

Figure 3- 10 Flagella enzymatic activity assay under different treatments.
Standard Bla enzyme, FAP20-Bla and RSP3-Bla flagella were freeze-thaw for 4 times between -20 and 20°C, boil 10 mins at 42°C, or kept at room temperature for 48 hours. 5 µl commercial beta-lactamase enzyme and flagella from each sample were subjected to beta-lactamase activity assay. The untreated fresh samples were used as a positive control. The graph showed the enzyme activity. Two replicates were performed for the enzymatic activity assay.

Discussion

In this study, we showed the designing the *Chlamydomonas* flagellar axoneme as a biosynthetic template to synthesize enzymatically active biomolecules. The constructs of pBS-FAP20-TEV-ERα, pBS-FAP20-Bla and pKF-RSP3-TEV-ERα, pKF-RSP3-TEV-Bla were made to express fusion proteins in the loss-of-function mutant strains *im5* and *pf14*. Axonemal proteins FAP20

and RPS3 are transported into the flagella compartment specifically by the IFT. Simultaneously, the target proteins of ERα and Bla should be transported together at the time. Indeed, our results showed that target proteins are successfully expressed in the rescued strains and localized to the axoneme. Also, the target protein ERα and Bla showed a similar expression ratio of the axoneme proteins FAP20 and RSP3, which indicate the high incorporation efficiency of the target protein to the axoneme. Further studies showed that target proteins ERα and Bla are both enzymatically active. In the ERα binding assay, FAP20-ERα and RSP3-ERα flagella showed a 30% decrease of the ERα binding chemical after the incubation, while WT flagella did not show any affinity to the ERα binding chemical. The results of beta-lactamase activity assay showed all original and regenerated flagella samples of FAP20-Bla and RSP3-Bla are enzymatically active, and they are more resistant to freeze-thaw treatment compared to the commercial soluble beta-lactamase enzyme.

Compared to other models for synthesizing biomolecules, the application of using flagella axoneme as a biosynthetic template is unique in several aspects. First, the target protein assembled on the axoneme happened automatically and in a high density. Because the axoneme assembly is a cellular process that happened naturally, the target protein could self-assemble on the axoneme only if the construct carrying the gene of fusion protein expressed appropriately. Second, the components and arrangement of the axoneme structure are well studied. Therefore, the number of target proteins on a single axoneme can be calculated precisely, which should be the same as the adaptor protein. Third, the isolation of flagella is much easier compared to other systems. Since the target protein has already incorporated into the axoneme, to acquire the protein array of the target protein only need to isolate the flagella. Flagella were easily detached

from cell bodies when the pH was lowered to 4.5 and purified by sucrose concentration gradient centrifugation due to different sediment of flagella and cell bodies. Unlike other systems, either the target proteins need to be purified from intracellular or need to be linked into the scaffold. Fourth, the regeneration of the flagella increases the yield of the target protein. Instead of increasing culture volume, flagella can repeatedly undergo deflagellation and regeneration for several cycles to accumulate the final products as showed by FAP20-Bla and RPS3-Bla flagellar regeneration. The regeneration can be done within 2 hours. Also, the flagella samples do not need to be collected every time. Because there is no protease in the flagella, there is no need to worry proteases will degrade the axoneme proteins. Flagella from multi-regeneration can be harvested together. Last but not least, flagella are easily stored, and their stability is maintained. Flagella kept at -20°C are stable for several months. Also, axoneme anchored enzymes are more stable compared to the soluble enzymes. The fixed enzyme almost has the same enzymatic activity after multiple freeze-thaw treatments, while the soluble enzyme decreased activity by 40%. Even leaving the flagella at RT for 48 hours, the enzymatic activity stays the same.

In the ERα binding assay, our results showed that both FAP20-ERα and RSP3-ERα flagella bind and remove about 30% of 17-β-estradiol in the solution. However, the binding efficiency of FAP20-ERα is lower than the RSP3-ERα (Figure 3-4), even though the WB results showed that FAP20-ERα has protein levels two times more than RSP3-ERα in an equal amount of flagella samples (Figure 3-5 C-D). The phenomenon indicates that axoneme ERα may have already bound to estrogen compounds that existed in the medium. It makes sense because FAP20-ERα protein density is higher in a single axoneme than RSP3-ERα. Therefore, FAP20-ERα binds more estrogen compounds in the medium, which causes the lower the binding efficiency in the

ERα binding assay. In the future, in order to increase the binding efficiency, the original flagella should be discarded and regenerated flagella in the pure HEPES buffer may help.

Furthermore, our results showed that both the original and regenerated flagella of FAP20-Bla and RSP3-Bla have the same target protein expression levels and enzymatic activity, which support our hypothesis that flagella regeneration increases the yield of the target proteins. However, the small volume of flagella makes it harder to calculate the flagella number per microliter. We can only estimate the enzyme activity based on the amount of the products catalyzed by flagella samples. Theoretically, 1 Unit Beta-Lactamase activity is defined as the amount of enzyme that generates 1.0 μmol of nitrocefin per minutes at pH 7.0 at 25°C. Sample Beta-Lactamase activity can also be expressed as mU/mg, which means nmol/min hydrolyzed nitrocefine generated per mg of protein. Based on the standard line equation y=0.0185x + 0.0318, when the A490nm equals 0.5, the hydrolyzed nitrocefine amount is 25.3nM. The enzyme activity of Bla in flagella amount of 5μl reactions is around 250mU/mg (Figure 3-8 B). The enzyme activity of positive control soluble enzyme is around 1600mU/mg (Figure 3-10 B). The huge activity difference between the fixed enzyme and the soluble enzyme are mainly due to two reasons. One reason is that the flagella resuspension buffer HMDEK generates a huge background of 0.35, which disables the flagella to catalyze all substrate. The other reason is that the existence of flagella membrane dampens the turnover efficiency of substrate and products, even though nitrocefin is a hydrophobic molecule that can easily pass through the membrane. The improvements would be re-suspend flagella axoneme in beta-lactamase assay buffer for the activity assay.

In addition, the axoneme anchored enzyme is more resistant to freeze-thaw treatment. We did several temperature variables to test the stability of the fixed enzyme compared to the soluble enzyme. Because soluble enzymes are susceptible to freeze-thaw, one variable we chose is freeze-thaw enzymes for four times then measure the enzyme activity. The results showed that the fixed enzyme is resistant to freeze-thaw compared to the control. However, the fixed enzyme is sensitive to high temperature. The enzyme activity decreased dramatically when heated at 42°C for 10 minutes. While keep the fixed enzyme at RT for two days does not affect the enzyme activity. Overall, the results may indicate that when the temperature is not beyond to denature proteins, the axoneme can stabilize the enzyme.

Overall, this paper discussed the possibility of using flagellar axoneme as a biosynthetic template. We tested our hypothesis by expressing the constructs of pBS-FAP20-ERα, Bla and pKF-RSP3-ERα, Bla to rescue the mutant strains of *im5* and *pf14*. Our preliminary data showed that both target proteins of ERα and Bla could express and localize to flagella with enzymatic activity. Also, the fixed enzyme is resistant to freeze-thaw treatment, and flagella regeneration increases the output of the target protein. Although the target protein incorporation efficiency and enzymatic assay method still need to be improved, this research provides a new perspective for applying the axoneme as a biosynthetic template.

Method and materials

Strains and cultures conditions

The strains of *cc125, im5, pf14,* and the rescue strains *im5::FAP20-TEV-ERαLBD, im5::FAP20-TEV-Bla, pf14::RSP3-TEV-ERαLBD,* and *pf14::RSP3-TEV-Bla* were made in this study. Strains were maintained on the Tris-acetate-phosphate (TAP) plates. Cells were cultured in the TAP

medium with agitation or constant aeration in a Conviron environmental chamber at 21°C with continuous light.

Constructs and antibodies

All constructs used for rescue experiments are purchased from GeneScript, including pBS-FAP20-TEV-ERαLBD, pBS-FAP20-TEV-Bla, pKF-RSP3-TEV-ERαLBD, and pKF-RSP3-TEV-Bla.

Rescue of im5 and pf14

The plasmids of pBS-FAP20-TEV-ERαLBD and pBS-FAP20-TEV-Bla were used to rescue the *im5* strain. The plasmids were linearized with Ssp1 enzyme before they are transformed together with the paromomycin-resistant pSI103 plasmid for selection. The plasmids of pKF-RSP3-TEV-ERαLBD and pKF-RSP3-TEV-Bla were used to rescue the pf14 strain. Both plasmids were linearized with the enzyme SspI. The electroporation technique was applied to transform *Chlamydomonas* cells. Briefly, *im5* or *pf14* cells were cultured in 100 ml TAP medium to dark green, then transferred to 1 L TAP medium with constant aeration. Check the concentration of the cells about 20 hours later. When the concentration reaches 10_6/ml, the cells are ready to be transformed. Totally, 10_8 cells were collected and re-suspended in 1 ml TAP liquid media containing 60 mM sorbitol. 300ul cells' suspension was transferred to a 4 mm electroporation cuvette. For the *im5* cells, 600ng linearized pBS-FAP20-TEV-ERαLBD to pBS-FAP20-TEV-Bla together with 300 ng PSI103 plasmids were added and mixed evenly. For the *pf14* cells, 600 ng linearized pKF-RSP3-TEV-ERαLBD or pKF-RSP3-TEV-Bla plasmids were added cells and mixed evenly. Because pKF constructs are with a pre-inserted paromomycin-resistant gene, it is

no need to co-transform with PSI103 plasmids. The mixture of plasmids and cells in the cuvettes were chilled on ice for 5 minutes and then electroporated with an ECM630 electroporator (BTX, USA) with the setup parameters of capacitance 50 μF, resistance 650 Ω, and the voltage 825 V. The cells were recovered on the ice for 15 minutes after electroporation and then transferred to 10 ml TAP medium with 60 mM sorbital and culture 24 hours in a low light environment for furthermore recovery. The next day, cells were collected and plated on TAP plates containing 10 ng/μL paromomycin to grow 4-5 days to obtain transformants.

Prescreening rescue colonies by observing cells' motility and flagellar assembly

After 4- or 5-days' culturing, colonies resistant to paromomycin antibiotic should be visible on the plate. The next step is to screen the rescue colonies with the expression of the target protein. Because of the motility deficiency of *im5* and *pf14* cells, the most direct way to screening the rescued strains is to observe the motility of the cells. In order to do so, all colonies on the TAP plate were transferred to 96-well plates with liquid TAP medium. Observe cells' motility under the Olympus inverted microscope CKX53 after 24 hours of culture. In order to further ensure the cells' motility and flagellar assembly, motile cells from the last step were cultured in 3 ml TAP medium in a test tube for two days, then record the cell's motility with an Axioplan phase contrast microscope (Carl Zeiss, Oberkochen, Germany) and 4x objective (Olympus, Tokyo, Japan). Movies were taken with a phantom High-Speed Mico-eX2 camera and processed using the Cine Viewer software (version 2.6, Vision Research Inc, Prince Edward Island (P.E.I), Canada). Movies were imported to Image J for analysis. In order to measure the flagellar length, cells were fixed with 1% glutaraldehyde. Images were taken on the Axioplan phase contrast microscope with a 100x oil Plan-Apochromat objective (Olympus, Tokyo, Japan). The

segmented line selection tool of Image J (Java 1.8.0_172, https://imagej.nih.gov/ij) was used for length measurements.

Flagella isolation and stock solutions

There are two stock solutions need to be prepared ahead, including 25% sucrose in HMDE buffer and 10 x HMDEK buffer. The recipes of each solution are listed below. Below the recipe is the protocol of flagella isolation.

25% sucrose in HMDE (Store at 4°C)

10nM HEPES

5mM MgSO4

1mM DTT (add 1000x stock solution right before use)

0.25mM EGTA

25% sucrose

10x HMDEK (Store at 4°C)

10nM HEPES

5mM MgSO4

1mM DTT (add 1000x stock solution right before use)

5mM EDTA

25mM KCl

1. Make fresh cultures of the cells for flagella isolation on TAP plate.
2. Inoculate 100 ml TAP media with fresh cultures from plates and let it grow for 2-3 days and turns to dark green.

3. Inoculate to 4 L volume of TAP media with the above culture with bubbling for 3-4 days until it turns dark green.
4. Harvest cells by spinning them down at 2200 rpm for 7 minutes at 18°C (Beckman Coulter, USA).
5. Resuspend the cells in 500 ml 10 mM HEPES pH 7.5.
6. Allow flagella regenerate in HEPES with bubbling for 1 hour in low light conditions.
7. Check the cells under 100x objective microscope that all cells have flagella.
8. Spin cells down in 250 ml conical tubes at 2200 rpm for 7 minutes at 18°C (Beckman Coulter, USA) and resuspend the cells in 100 ml HEPES.
9. Deflagellate by adding 0.5 M acetic acid to pH 4.5. Quickly check cells under the microscope to make sure that deflagellation is complete and then quickly bring the pH to 7.0 by adding drops of 0.5 M KOH.
10. Keep cells on ice immediately after deflagellation and orderly adding the following stock solutions to yield the respective final concentration (Table 3-1):

    Table 3-1 Reagents added to the solutions

Stock solution	Final concentration	Volume/100ml
1M MgSO4 (200X)	5mM	0.5ml
1M DTT (1000)	1mM	0.1ml
50% sucrose (10X)	5% sucrose	10ml
0.5M EGTA (2000X)	0.25mM	50μl
100mM PMSF (100)	1mM	1ml

11. Underlay the cells with 40 ml 25% sucrose in HMDE buffer.

12. Centrifuge at 2200 rpm for 7 minutes at 4°C.
13. Collect the supernatant to 50 ml round-bottom tubes and collect flagella by centrifuge at 10,000 rpm for 10 min at 4°C with a SW 32 Ti motor (Beckman Coulter, USA).
14. Resuspend the flagella in 1x HMEDK buffer and store the isolated flagella at -20°C.

Flagella regeneration

The protocol of flagella regeneration is modified slightly upon the flagella isolation method. Instead of underlay with 25% sucrose immediately after step 10, the flagella and cell bodies were separated by centrifuging at 2000 rpm, 5 minutes, 18°C. The supernatant is containing the flagella and subjected to the 25% sucrose underlay to collect flagella, while the cell bodies were resuspended in 500 ml HEPES to culture 1-2 hours in bubbling to regenerate flagella. Repeat this repeat if needed to regenerate flagella for more than one time.

ERα binding assay

FAP20-ERα and RSP3-ERα flagella were subjected to the ERα binding assay. Bioluminescence estrogen assay was conducted first to build the standard line [264]. 17-β-estradiol was used as the substrate of the estrogen receptor binding chemical. Briefly, different dilutions of 17-β-estradiol ranged from 10^{-9} M to 10^{-5} M were incubated with BLYES strain and then measure the bioluminescence in a Perkin-Elmer Victor. Based on the standard line, 10^{-7} M of 17-β-estradiol is the half effective concentration. This concentration is used in the following ERα binding assay. 200 μl flagella of WT, FAP20-ERα and RSP3-ERα were incubated with 10^{-7} M of 17-β-estradiol in a 5ml volume system for overall 48 hours. Each reaction has a duplicate. At the time points of 0, 1, 3, 6, 24, and 48 hours, 800 μl reactants were taken out to conduct the bioluminescence

estrogen assay. The flagella were removed by centrifuging at 10,000 rpm before the assay. The concentration of rest 17-β-estradiol in the supernatant can be calculated based on the standard line.

Beta-lactamase activity assay

The assay is conducted following the protocol of Beta Lactamase Activity Assay Kit (Colorimetric) (ab197008). The principle of the assay is based on the hydrolysis of the substrate Nitrocefin, which generates a colored product that can be detected at OD490 nm. The absorbance of A490 is directly proportional to the amount of beta-lactamase activity. First, set up a standard curve. Prepare a various dilution of hydrolyzed Nitrocefin solutions, 0 nM, 4 nM, 8 nM, 12 nM, 16 nM, and 20 nM, measure output immediately on a colorimetric microplate reader at OD 490 nm to obtain the corresponding absorbance. Secondly, prepare flagella samples for enzymatic activity assay. FAP20-Bla, RSP3-Bla, WT flagella are subjected to the beta-lactamase activity assay. The flagella of WT are used as a negative control. In order to ensure the readings are within the standard value range, each of the flagella samples was diluted 10, 20, and 100 times in the final volume of 100 μl to perform the test. The reaction mix set up is according to the protocol. The flagella suspension buffer HMDEK was used as a negative control. Measure absorbance on a microplate reader at OD 490 nm in a dynamic mode, every 1-2 minute, for 20 minutes at RT protected from light.

Flagella recycle done by centrifuging the reactant at 10,000 rpm, 10 minutes, 4°C. The supernatant was discarded, and the flagella were washed two times with HMEDK buffer to remove the colorimetric products attached on the flagella. At last, flagella were suspended in 45

μl Beta-Lactamase Assay buffer and 5 μl HMDEK buffer to keep the same setup with the previous reaction and catalyze a new reaction.

Beta-Lactamase Activity were expressed as nmoles/min hydrolyzed Nitrocefin generated per μg of protein (mU/μg). The protein amount of each sample per reaction were calculated as below:

- Commercial Bla: Recombinant protein equals 0.5 μg/μl, added 5 μl per reaction, total protein amount equals 0.5 μg/μl x 5 μl = 2.5 μg.
- WT flagella: 1.6 μg/μl x 5 μl = 8 μg.
- FAP20-Bla flagella: First, ratio of FAP20 and α-tubulin numbers were calculated in the 96 nm repetitive axoneme structure. FAP20 repeat every 8 nm and distributed along 9 doublet microtubules, therefore number of FAP20 equals (96/8) x 9 = 108. The number of Bla equals FAP20, which is 108. α, β-tubulin dimers are 8 nm long and compose 9 doublet microtubules and a center pair of singlet microtubules. The number of α, β-tubulin dimer equals (96/8) x [(13+9) x 9 + 13x2] = 2688. Second, because the molecular weight of FAP20-Bla is 40 kd and molecular weight of dimer is 100 kd, the mass ratio of Bla and α, β-tubulin dimer equals (2688/108) x (100/40) = 62. Finally, the mass of Bla in the FAP20-Bla flagella sample equals (1.6 μg/μl x 5 μl)/62 = 0.13 μg.
- RSP3-Bla flagella: First, ratio of RSP3 and α-tubulin numbers were calculated in the 96 nm repetitive axoneme structure. Radial spoke has an average number of 2.5 every 96 nm and forms a dimer, therefore number of RSP3 equals 2.5 x 2 x 9 = 45. The number of Bla equals RSP3, which is 45. The number of α, β-tubulin dimer equals 2688. Second, because the molecular weight of RSP3-Bla is 100 kd and molecular weight of α, β-

tubulin dimer is 100 kd, the mass ratio of Bla and α-tubulin equals (2688/45) x (100/100) = 60. Finally, the mass of Bla in the RSP3-Bla flagella sample equals (1.6 μg/μl x 5 μl)/60 = 0.13 μg.

Once the commercial Bla enzyme or flagella samples mixed with nitrocefin to start the reaction, the absorbance of 490 nm was measured every minute until the absorbance reach plateau. The concentration of the products can be calculate based on the standard line y = 0.0185x + 0.0318. The enzymatic activity is calculated at 1 min, 2 min, and 3 min, then the final enzymatic activity takes an average of 3 values with standard deviation.

CHAPTER IV

SUMMARY AND FUTURE DIRECTION

Part I

The interplay between O-GlcNAc and primary cilia in regulating energy homeostasis

In this study, we identified that O-GlcNAc is a negative regulator of primary ciliary length. The higher of O-GlcNAcylation levels, the shorter the primary ciliary length. The lower the O-GlcNAcylation levels, the longer the primary ciliary length. Also, the O-GlcNAc modification of α-tubulin and HDAC6 promotes the ciliary disassembly.

O-GlcNAc as a PTM generally happens on Ser/Thr of the target proteins and participates in almost all of the cellular processes. Here, we showed that O-GlcNAc in involved in ciliary length regulation. The O-GlcNAc modification happens on both axoneme protein α-tubulin and key ciliary length regulators, such as HDAC6, and positively regulates ciliary disassembly. Because the previous studies showed that PTMs is one of the major factors involves in ciliary assembly and disassembly through acting on the axoneme proteins and critical regulators, our finding adds a new modification of O-GlcNAc in regulating ciliary length.

Besides O-GlcNAc as a PTM, O-GlcNAc is more function as a nutrient sensor. The cellular O-GlcNAcylation levels highly depend on the metabolite state of the cell [129], which is also a key regulator of ciliary length. Several investigations showed that primary ciliary length regulation is affected by nutrient status and cellular metabolic levels [265]. First, the glucose deprivation, decreased ciliary length but promoted primary cilium formation in cultured cells [131]. Furthermore, the work of Yu et al. showed that primary cilia were fewer and shorter in the

diabetic mouse eyes, trachea, and skin cells compared to wild type, and increased the levels of O-GlcNAcylation of RPE1 cells in culture medium impaired ciliogenesis [130]. In addition, human obese individuals also have shortened and compromised functional primary cilia of adipose-derived mesenchymal stem cells (ASCs). Elevated activity of Aurora A and HDAC6 is contributed to the shortening of the ciliary length [132]. More importantly, in chow-diet-fed lean mice, the primary ciliary length on the hypothalamic arcuate (ARC) neurons is longer by about 5.5 ± 0.44 μm on average. However, average ciliary length reduced by 40%-60% in the hypothalamus of diet-induced obese (DIO) mice that are fed with a high-fat, high-sucrose diet [125]. These results strongly indicate that energy homeostasis is vital for maintaining primary ciliary length. Meanwhile, an intriguing question is arising: whether O-GlcNAc is the factor that contributes to the primary ciliary length regulation in response to nutrient status change?

The importance of hypothalamic neurons in regulating energy homeostasis

In order to answer the question above, it is essential to understand the energy homeostasis regulation first. Recent molecular studies reveal that the hypothalamus of the central nervous system (CNS) is the central hub that balances feeding and energy expenditure and regulates the energy homeostasis in mammals [266, 267]. The hypothalamus is composed of distinct types of nuclei that respond to neuronal hormones in the bloodstream and receive peripheral hormones without blood-brain barrier leaking. The peripheral hormones may include growth hormone, prolactin, insulin, insulin-like growth factor- I and II, and leptin. The ARC in the hypothalamus is critical for sensing and responding to the peripheral circulating metabolic hormones and nutrients signals. The location of ARC is adjacent to the median eminence (ME) and third ventricle, where it has easy access to metabolic signals [268-270]. There are two groups of

neurons in the ARC that respond to orexigenic (which stimulate appetite) and anorexigenic (which inhibit appetite), respectively. One group is the neurons producing neuropeptide Y (NPY) and agouti-related peptide (AgRP), and the other group is the neurons producing pro-opiomelanocortin (POMC) and cocaine- and amphetamine-regulated transcript (CART). These two groups of neurons interact with each other through hormone receptors-mediated signaling transduction to control food intake and energy homeostasis in the hypothalamus [271-274].

Interestingly, all four types of ARC neurons are ciliated and distributed with various receptors to bind and respond to hormones, such as the adipocyte hormone leptin and the pancreatic hormone insulin [275-277]. The leptin receptors (LepR) and insulin receptors (IR) are trafficking to the NpY and the POMC neurons, and are responsive to leptin and insulin to regulate energy metabolic pathways. The binding of leptin to LepR mainly actives the signaling pathways of JAK2-STAT3 and PI3K-PKD1-AKT pathways as well as the downstream effectors FoxO1, AMPK, and mTOR [278-281]. The activation of STAT3 promotes the expression of the POMC, which is a precursor peptide of anorexigenic α-melanocyte-stimulating hormone (α-MSH) while inhibiting the expression of AgRP and NPY to decrease feeding [125, 282-284]. AgRP and α-MSH are ligands acting antagonistically on the same melanocortin 3 and 4 receptors (MC3/4R) on the lateral neurons. The α-MSH activates MC4R to reduce food intake while AgRP inhibiting MC4R to increase feeding [285-287]. Meanwhile, leptin directly increases PI3K activity in POMC neurons but inhibits PI3K activity indirectly in AgRP neurons. FoxO1 is a well-known target of PI3K-PDK1-Akt kinase cascades. FoxO1 acts as an inhibitor of POMC and an activator of AgRP expression in the nucleus. Phosphorylation of FoxO1 by Akt inhibits its translocation from cytoplasm to the nucleus to abrogate the expression of AgRP and increases the expression

of POMC to decrease food intake [288-290]. The other cellular fuel sensors mTOR and AMPK are also the targets of Akt. The mTOR is activated by leptin mediated PI3K-Akt signaling then phosphorylates to inactivate downstream AMPK, and it thereby regulates energy homeostasis. Insulin signaling in the POMC and AgRP neurons is important for glucose metabolism [291]. Once insulin binds to the IR, IRS will be activated and converge with the leptin pathway at the point of PI3K activation [292]. Leptin and insulin interplay through the primary cilia mediated signaling pathway of PI3K-PKD1-Akt-FoxO1 to active or inhibited POMC and AgRP neurons [291, 293-295]. Therefore, hypothalamic primary cilia are crucial in maintaining energy homeostasis through cooperating leptin and insulin signaling pathways. In order to know whether O-GlcNAc involved in ciliary length regulation, we need to know the factors participating in the ciliary length regulation.

The regulation of ciliary length in hypothalamic neurons

Investigations recently showed the primary ciliary length of hypothalamic neurons shorten in either genetic or diet-induced obesity mouse, which further indicates primary ciliary length is tightly correlated with signaling transduction and energy status in the body [210]. For example, diet-induced obese (DIO) mice, leptin-deficient (LEPR-deficient) *ob/ob* mice, and leptin receptor-deficient *db/db* mice all exhibit shorter hypothalamic neuron cilia [125]. Shortening of ciliary length in *ob/ob* mice can be rescued by leptin administrations, which indicate that hypothalamic ciliary length can be regulated dynamically by metabolic conditions in adult mice [125, 210]. Also, *in vitro* experiment showed that leptin treatment of primary hypothalamic neurons cells elongated ciliary lengths [125, 296]. These data suggested that there is an interplay between primary cilia and leptin signaling in regulating energy metabolism. Further studies

showed leptin mediated signaling molecules, such as JAK2 and PI3K, are also involved in ciliary length regulation. Pharmacological inhibits JAK2 and PI3K or genetically knockdown the expression of PI3K blocks leptin-induced primary cilia elongation [296]. Moreover, targets of PI3K downstream signaling such as PTEN, AKT, and GSK3β are also involved in ciliary length regulation. Knockdown of *Pten* and *Gsk3b* increases ciliary length, while overexpression *Pten* and *Gsk3b* decreases the ciliary length and blocks the effects of leptin treatment on hypothalamic neuron cilia [125]. Further work showed that leptin treatment elongates ciliary length by inhibiting PTEN and GSK3β signaling and increasing the expression of IFT proteins [296]. These results strongly suggest that primary ciliary length is critical for stimulating LepR-mediated leptin signaling pathways in hypothalamic neurons. Investigations also showed that insulin might promote ciliary growth in parallel with leptin. Insulin signaling is integrated with the PI3K signaling pathway, and insulin treatment increases ciliary length up to 25% in hypothalamic neurons [125]. It is worth investigating whether O-GlcNAc level is higher in the hypothalamic neurons of obese mice. If it is so, it will build a connection that O-GlcNAc mediates the energy metabolic dysregulation induced ciliary length abnormally. It can be tested by formulating the hypothesis that O-GlcNAc levels regulate the hypothalamic ciliary length mediated by leptin and insulin signaling pathway.

The potential to involve O-GlcNAc in ciliary length regulation in hypothalamic neurons

Even though there is no direct evidence showing the linkage between O-GlcNAc and primary ciliary length in the hypothalamic neurons, current findings showed some hints O-GlcNAc is involved in the regulation of leptin and insulin signaling pathways; hence, it may affect ciliary length indirectly. First, the key components of leptin and insulin signaling are O-GlcNAc

regulated. For example, STAT3, PI3K, PKD1, Akt, FoxO1, AMPK, IR, and IRS are all O-GlcNAcylated and respond to leptin and insulin. For other components, even though they are not O-GlcNAcylated directly, their activity is highly regulated by cellular O-GlcNAcylation levels, such as JAK2 and PI3K/AKT/mTOR axis [137, 141, 297-299]. It is considered that O-GlcNAcylation acts as a negative regulator of insulin and a positive regulator of leptin signaling pathways [131]. Since both primary cilia and O-GlcNAc are intensively involved in leptin and insulin signaling, it is worth to investigate the role of O-GlcNAc in response to energy metabolism in the hypothalamus.

The importance of O-GlcNAc in regulating homeostasis through the hypothalamus

The importance of O-GlcNAc in regulating energy homeostasis through hypothalamic neurons was reflected in the ablation of OGT in AgRP neurons. Once the AgRP neurons were activated by signals such as fasting, browning of the white adipose tissue will be suppressed in order to inhibit energy expenditure. However, abolishing OGT in AgRP neurons failed excitation of AgRP neurons, therefore promoting the browning of white adipose tissue and protecting the mutated mice against diet-induced obesity and insulin resistance. Even though there were a higher OGT expression and O-GlcNAcylation levels in the hypothalamic neurons compared to the peripheral tissues, elevated O-GlcNAc levels is a signal to active AgRP neurons under fasting conditions [300]. However, the other paper reported that *Oga*$^{+/-}$ mice are increased energy expenditure by promoting whited adipose tissue browning [301]. The contradictory phenomenon may be because the mutation target regions are different, OGT KO is induced in AgRP neurons specifically, while OGA heterozygote mice are generated in the whole body. The results indicate that O-GlcNAc mediated signaling is critical for regulation energy homeostasis in the

hypothalamic neurons. Next, it is important to know whether altering of O-GlcNAc levels in response to nutrient status is the reason caused ciliary length changing.

The potential mechanism of O-GlcNAc to regulate hypothalamic ciliary length to maintain energy homeostasis

There are two investigations showing that the potential of O-GlcNAc regulates ciliary length in the hypothalamus neurons. First, the work of Dai et al. showed that conditional knockout neuronal OGT by crossing CaMKIIα-Cre$_{(+)}$ and Ogt$_{loxp(+)/loxp(+)}$ mice led more food intake, body weight gain, insulin resistance, and elevated serum leptin level, which are prediabetic symptoms. The mechanism studies revealed that decreased neuron cells and LepR in the hypothalamic contributed to the up-regulated appetite and insulin/leptin resistance [302]. The results indicate that the correlation between the diminished neuronal O-GlcNAcylation levels, the attenuated leptin and insulin signaling transduction, and the potential dysfunction of primary cilia in neuron cells. Another finding revealed that mutation of LepR induced diabetic (DB) mice (Lepr$_{db}$/Nju) showed both ciliary defects and elevated O-GlcNAcylation levels in multiple tissues of mutant mice [130]. The following in vitro experiments results showed that increasing O-GlcNAcylation levels of RPE1 cells in culture medium impaired ciliogenesis and decreased the ciliary length. It is possible that the elevated O-GlcNAcylation level decreased ciliary length in the DB mice. It is inevitable to notice that lacking or deficient of LepR is the main reason causing obesity or diabetes of the mutant mice in both studies. These observations provide further possibilities that O-GlcNAc may regulate ciliary length through integrating with LepR mediated signaling to maintain energy homeostasis in hypothalamus.

In order to test the hypothesis that O-GlcNAc promotes LepR recruiting to the cilium and actives leptin signaling molecules to regulate ciliary length, several experiments can be done. After knockdown or pharmacological inhibition of the enzyme OGT/OGA in the primary hypothalamic neuron cells, then tests whether the hypothalamic ciliary length changed under different cellular O-GlcNAcylation levels. If O-GlcNAc is involved in the ciliary length regulation in the hypothalamic neurons, then the recruitment of LepR on the primary cilia and leptin signaling activity will be detected. More importantly, the hypothalamic ciliary length should be observed in OGT or OGA heterozygote mutant mice. If there is an interplay between O-GlcNAc and primary ciliary length, it will build a connection of O-GlcNAc and ciliary length in response to nutrients and energy metabolism.

Part II

Advantages of using flagella axoneme as a biosynthetic template

This work described using axoneme proteins FAP20 and RSP3 as an adaptor to link a protein of interest and incorporate the fusion protein on the axoneme. There are several advantages to do so, such as products can be calculated mathematically, isolated simply, regenerated to increase the yield, and made more stable during the storage. In the study, we tested the ability of *Chlamydomonas* expressing the fusion proteins FAP20-ERα, Bla and RSP3-ERα, Bla. Our results showed that the fusion proteins successfully expressed and assembled on the axoneme; the yield of the target protein ratio in two strains is roughly consistent with the ratio of the adaptor protein of FAP20 and RSP3, which indicated the incorporation efficiency of the target protein on the axoneme is high; the yield of the target protein can be accumulated by flagella regeneration; the target proteins are enzymatically active; the axoneme is recyclable; and the stability of the target protein is durable during the storage. These preliminary tests on the hypothesis are inspiring. The results indicate the high possibility of applying flagella axoneme as a biosynthetic template. However, in order to improve the application, refined conditions are needed, specifically, improving the incorporation rate of the target protein on the axoneme, stabilizing the expression of the target in the rescue strains, and quantifying the target protein yield, etc.

REFERENCES

1. Bloodgood, R.A., *From central to rudimentary to primary: the history of an underappreciated organelle whose time has come. The primary cilium.* Methods Cell Biol, 2009. **94**: p. 3-52.
2. Satir, P., L.B. Pedersen, and S.T. Christensen, *The primary cilium at a glance.* J Cell Sci, 2010. **123**(Pt 4): p. 499-503.
3. Worthington, W.C., Jr. and R.S. Cathcart, 3rd, *Ependymal cilia: distribution and activity in the adult human brain.* Science, 1963. **139**(3551): p. 221-2.
4. Wu, J., et al., *Characterization of primary cilia in human airway smooth muscle cells.* Chest, 2009. **136**(2): p. 561-570.
5. Heydeck, W., et al., *The complexity of the cilium: spatiotemporal diversity of an ancient organelle.* Curr Opin Cell Biol, 2018. **55**: p. 139-149.
6. Singla, V. and J.F. Reiter, *The primary cilium as the cell's antenna: signaling at a sensory organelle.* Science, 2006. **313**(5787): p. 629-33.
7. Handel, M., et al., *Selective targeting of somatostatin receptor 3 to neuronal cilia.* Neuroscience, 1999. **89**(3): p. 909-26.
8. Seo, S., et al., *Requirement of Bardet-Biedl syndrome proteins for leptin receptor signaling.* Hum Mol Genet, 2009. **18**(7): p. 1323-31.
9. Bahrenberg, G., et al., *Identification of the critical sequence elements in the cytoplasmic domain of leptin receptor isoforms required for Janus kinase/signal transducer and activator of transcription activation by receptor heterodimers.* Mol Endocrinol, 2002. **16**(4): p. 859-72.

10. Berbari, N.F., et al., *Bardet-Biedl syndrome proteins are required for the localization of G protein-coupled receptors to primary cilia.* Proc Natl Acad Sci U S A, 2008. **105**(11): p. 4242-6.

11. Hildebrandt, F., T. Benzing, and N. Katsanis, *Ciliopathies.* N Engl J Med, 2011. **364**(16): p. 1533-43.

12. Sorokin, S., *Centrioles and the formation of rudimentary cilia by fibroblasts and smooth muscle cells.* J Cell Biol, 1962. **15**: p. 363-77.

13. Sorokin, S.P., *Reconstructions of centriole formation and ciliogenesis in mammalian lungs.* J Cell Sci, 1968. **3**(2): p. 207-30.

14. Hoyer-Fender, S., *Centriole maturation and transformation to basal body.* Semin Cell Dev Biol, 2010. **21**(2): p. 142-7.

15. Kobayashi, T. and B.D. Dynlacht, *Regulating the transition from centriole to basal body.* J Cell Biol, 2011. **193**(3): p. 435-44.

16. Kozminski, K.G., et al., *A motility in the eukaryotic flagellum unrelated to flagellar beating.* Proc Natl Acad Sci U S A, 1993. **90**(12): p. 5519-23.

17. Pedersen, L.B. and J.L. Rosenbaum, *Intraflagellar transport (IFT) role in ciliary assembly, resorption and signalling.* Curr Top Dev Biol, 2008. **85**: p. 23-61.

18. Pazour, G.J. and G.B. Witman, *The vertebrate primary cilium is a sensory organelle.* Curr Opin Cell Biol, 2003. **15**(1): p. 105-10.

19. Hao, L. and J.M. Scholey, *Intraflagellar transport at a glance.* J Cell Sci, 2009. **122**(Pt 7): p. 889-92.

20. Rosenbaum, J.L. and G.B. Witman, *Intraflagellar transport.* Nat Rev Mol Cell Biol, 2002. **3**(11): p. 813-25.

21. Ishikawa, H. and W.F. Marshall, *Ciliogenesis: building the cell's antenna.* Nat Rev Mol Cell Biol, 2011. **12**(4): p. 222-34.

22. Marshall, W.F. and J.L. Rosenbaum, *Intraflagellar transport balances continuous turnover of outer doublet microtubules: implications for flagellar length control.* J Cell Biol, 2001. **155**(3): p. 405-14.

23. Santos, N. and J.F. Reiter, *Building it up and taking it down: the regulation of vertebrate ciliogenesis.* Dev Dyn, 2008. **237**(8): p. 1972-81.

24. Rieder, C.L., C.G. Jensen, and L.C. Jensen, *The resorption of primary cilia during mitosis in a vertebrate (PtK1) cell line.* J Ultrastruct Res, 1979. **68**(2): p. 173-85.

25. Tucker, R.W., A.B. Pardee, and K. Fujiwara, *Centriole ciliation is related to quiescence and DNA synthesis in 3T3 cells.* Cell, 1979. **17**(3): p. 527-35.

26. Vorobjev, I.A. and S. Chentsov Yu, *Centrioles in the cell cycle. I. Epithelial cells.* J Cell Biol, 1982. **93**(3): p. 938-49.

27. Tsou, M.F. and T. Stearns, *Mechanism limiting centrosome duplication to once per cell cycle.* Nature, 2006. **442**(7105): p. 947-51.

28. Lacey, K.R., P.K. Jackson, and T. Stearns, *Cyclin-dependent kinase control of centrosome duplication.* Proc Natl Acad Sci U S A, 1999. **96**(6): p. 2817-22.

29. Spektor, A., et al., *Cep97 and CP110 suppress a cilia assembly program.* Cell, 2007. **130**(4): p. 678-90.

30. Pugacheva, E.N. and E.A. Golemis, *The focal adhesion scaffolding protein HEF1 regulates activation of the Aurora-A and Nek2 kinases at the centrosome.* Nat Cell Biol, 2005. **7**(10): p. 937-46.

31. Pugacheva, E.N., et al., *HEF1-dependent Aurora A activation induces disassembly of the primary cilium.* Cell, 2007. **129**(7): p. 1351-63.

32. Marshall, W.F., et al., *Flagellar length control system: testing a simple model based on intraflagellar transport and turnover.* Mol Biol Cell, 2005. **16**(1): p. 270-8.

33. Qin, H., et al., *Intraflagellar transport protein 27 is a small G protein involved in cell-cycle control.* Curr Biol, 2007. **17**(3): p. 193-202.

34. Tang, Z., et al., *Autophagy promotes primary ciliogenesis by removing OFD1 from centriolar satellites.* Nature, 2013. **502**(7470): p. 254-7.

35. Roe, J.S. and H.D. Youn, *The positive regulation of p53 by the tumor suppressor VHL.* Cell Cycle, 2006. **5**(18): p. 2054-6.

36. Esteban, M.A., et al., *Formation of primary cilia in the renal epithelium is regulated by the von Hippel-Lindau tumor suppressor protein.* J Am Soc Nephrol, 2006. **17**(7): p. 1801-6.

37. Lolkema, M.P., et al., *Allele-specific regulation of primary cilia function by the von Hippel-Lindau tumor suppressor.* Eur J Hum Genet, 2008. **16**(1): p. 73-8.

38. Thoma, C.R., et al., *pVHL and GSK3beta are components of a primary cilium-maintenance signalling network.* Nat Cell Biol, 2007. **9**(5): p. 588-95.

39. Van der Heiden, K., et al., *Endothelial primary cilia in areas of disturbed flow are at the base of atherosclerosis.* Atherosclerosis, 2008. **196**(2): p. 542-550.

40. Broekhuis, J.R., W.Y. Leong, and G. Jansen, *Regulation of Cilium Length and Intraflagellar Transport.* International Review of Cell and Molecular Biology, Vol 303, 2013. **303**: p. 101-138.

41. Coyne, B. and J.L. Rosenbaum, *Flagellar Elongation and Shortening in Chlamydomonas - Reutilization of Flagellar Proteins.* Journal of Cell Biology, 1970. **47**(2): p. A42-+.

42. Rosenbaum, J.L., J.E. Moulder, and D.L. Ringo, *Flagellar elongation and shortening in Chlamydomonas. The use of cycloheximide and colchicine to study the synthesis and assembly of flagellar proteins.* J Cell Biol, 1969. **41**(2): p. 600-19.

43. Niggemann, B., et al., *Abnormal length of cilia--a cause of primary ciliary dyskinesia--a case report.* Eur J Pediatr, 1992. **151**(1): p. 73-5.

44. Smith, L.A., et al., *Development of polycystic kidney disease in juvenile cystic kidney mice: insights into pathogenesis, ciliary abnormalities, and common features with human disease.* J Am Soc Nephrol, 2006. **17**(10): p. 2821-31.

45. Cole, D.G. and W.J. Snell, *SnapShot: Intraflagellar transport.* Cell, 2009. **137**(4): p. 784-784 e1.

46. Cole, D.G., et al., *Isolation of a sea urchin egg kinesin-related protein using peptide antibodies.* J Cell Sci, 1992. **101 (Pt 2)**: p. 291-301.

47. Cole, D.G., et al., *Novel heterotrimeric kinesin-related protein purified from sea urchin eggs.* Nature, 1993. **366**(6452): p. 268-70.

48. Pazour, G.J., C.G. Wilkerson, and G.B. Witman, *A dynein light chain is essential for the retrograde particle movement of intraflagellar transport (IFT).* J Cell Biol, 1998. **141**(4): p. 979-92.

49. Blacque, O.E., et al., *Loss of C. elegans BBS-7 and BBS-8 protein function results in cilia defects and compromised intraflagellar transport.* Genes Dev, 2004. **18**(13): p. 1630-42.

50. Lechtreck, K.F., et al., *The Chlamydomonas reinhardtii BBSome is an IFT cargo required for export of specific signaling proteins from flagella.* J Cell Biol, 2009. **187**(7): p. 1117-32.

51. Nachury, M.V., et al., *A core complex of BBS proteins cooperates with the GTPase Rab8 to promote ciliary membrane biogenesis.* Cell, 2007. **129**(6): p. 1201-13.

52. Mykytyn, K., et al., *Bardet-Biedl syndrome type 4 (BBS4)-null mice implicate Bbs4 in flagella formation but not global cilia assembly.* Proc Natl Acad Sci U S A, 2004. **101**(23): p. 8664-9.

53. Bennett, C.N., et al., *Regulation of Wnt signaling during adipogenesis.* J Biol Chem, 2002. **277**(34): p. 30998-1004.

54. Ou, G., et al., *Sensory ciliogenesis in Caenorhabditis elegans: assignment of IFT components into distinct modules based on transport and phenotypic profiles.* Mol Biol Cell, 2007. **18**(5): p. 1554-69.

55. Piperno, G., K. Mead, and S. Henderson, *Inner dynein arms but not outer dynein arms require the activity of kinesin homologue protein KHP1(FLA10) to reach the distal part of flagella in Chlamydomonas.* J Cell Biol, 1996. **133**(2): p. 371-9.

56. Brown, J.M., et al., *Kinesin-II is preferentially targeted to assembling cilia and is required for ciliogenesis and normal cytokinesis in Tetrahymena.* Mol Biol Cell, 1999. **10**(10): p. 3081-96.

57. Walther, Z., M. Vashishtha, and J.L. Hall, *The Chlamydomonas FLA10 gene encodes a novel kinesin-homologous protein.* J Cell Biol, 1994. **126**(1): p. 175-88.

58. Parker, J.D. and L.M. Quarmby, *Chlamydomonas fla mutants reveal a link between deflagellation and intraflagellar transport.* BMC Cell Biol, 2003. **4**: p. 11.

59. Fouquet, J.P., et al., *Differential distribution of glutamylated tubulin during spermatogenesis in mammalian testis.* Cell Motil Cytoskeleton, 1994. **27**(1): p. 49-58.

60. L'Hernault, S.W. and J.L. Rosenbaum, *Chlamydomonas alpha-tubulin is posttranslationally modified by acetylation on the epsilon-amino group of a lysine.* Biochemistry, 1985. **24**(2): p. 473-8.

61. Rudiger, M., et al., *Beta tubulin of bull sperm is polyglycylated.* FEBS Lett, 1995. **364**(2): p. 147-51.

62. Sherwin, T., et al., *Distinct localization and cell cycle dependence of COOH terminally tyrosinolated alpha-tubulin in the microtubules of Trypanosoma brucei brucei.* J Cell Biol, 1987. **104**(3): p. 439-46.

63. Westermann, S. and K. Weber, *Post-translational modifications regulate microtubule function.* Nat Rev Mol Cell Biol, 2003. **4**(12): p. 938-47.

64. Hammond, J.W., D. Cai, and K.J. Verhey, *Tubulin modifications and their cellular functions.* Curr Opin Cell Biol, 2008. **20**(1): p. 71-6.

65. Zilberman, Y., et al., *Regulation of microtubule dynamics by inhibition of the tubulin deacetylase HDAC6.* J Cell Sci, 2009. **122**(Pt 19): p. 3531-41.

66. Webster, D.R. and G.G. Borisy, *Microtubules are acetylated in domains that turn over slowly.* J Cell Sci, 1989. **92 (Pt 1)**: p. 57-65.

67. Sasse, R. and K. Gull, *Tubulin post-translational modifications and the construction of microtubular organelles in Trypanosoma brucei.* J Cell Sci, 1988. **90 (Pt 4)**: p. 577-89.

68. LeDizet, M. and G. Piperno, *Identification of an acetylation site of Chlamydomonas alpha-tubulin.* Proc Natl Acad Sci U S A, 1987. **84**(16): p. 5720-4.

69. Nogales, E., et al., *High-resolution model of the microtubule.* Cell, 1999. **96**(1): p. 79-88.

70. Reed, N.A., et al., *Microtubule acetylation promotes kinesin-1 binding and transport.* Curr Biol, 2006. **16**(21): p. 2166-72.

71. Janke, C. and J.C. Bulinski, *Post-translational regulation of the microtubule cytoskeleton: mechanisms and functions.* Nat Rev Mol Cell Biol, 2011. **12**(12): p. 773-86.

72. Akella, J.S., et al., *MEC-17 is an alpha-tubulin acetyltransferase.* Nature, 2010. **467**(7312): p. 218-22.

73. Kalebic, N., et al., *Tubulin acetyltransferase alphaTAT1 destabilizes microtubules independently of its acetylation activity.* Mol Cell Biol, 2013. **33**(6): p. 1114-23.

74. Kalebic, N., et al., *alphaTAT1 is the major alpha-tubulin acetyltransferase in mice.* Nat Commun, 2013. **4**: p. 1962.

75. Topalidou, I., et al., *Genetically separable functions of the MEC-17 tubulin acetyltransferase affect microtubule organization.* Curr Biol, 2012. **22**(12): p. 1057-65.

76. Hubbert, C., et al., *HDAC6 is a microtubule-associated deacetylase.* Nature, 2002. **417**(6887): p. 455-8.

77. Matsuyama, A., et al., *In vivo destabilization of dynamic microtubules by HDAC6-mediated deacetylation.* EMBO J, 2002. **21**(24): p. 6820-31.

78. Zhang, Y., et al., *HDAC-6 interacts with and deacetylates tubulin and microtubules in vivo.* EMBO J, 2003. **22**(5): p. 1168-79.

79. North, B.J., et al., *The human Sir2 ortholog, SIRT2, is an NAD+-dependent tubulin deacetylase.* Mol Cell, 2003. **11**(2): p. 437-44.

80. Gundersen, G.G., S. Khawaja, and J.C. Bulinski, *Postpolymerization detyrosination of alpha-tubulin: a mechanism for subcellular differentiation of microtubules.* J Cell Biol, 1987. **105**(1): p. 251-64.

81. Luchko, T., et al., *Conformational analysis of the carboxy-terminal tails of human beta-tubulin isotypes.* Biophys J, 2008. **94**(6): p. 1971-82.

82. Argarana, C.E., H.S. Barra, and R. Caputto, *Release of [14C]tyrosine from tubulinyl-[14C]tyrosine by brain extract. Separation of a carboxypeptidase from tubulin-tyrosine ligase.* Mol Cell Biochem, 1978. **19**(1): p. 17-21.

83. Infante, A.S., et al., *Detyrosinated (Glu) microtubules are stabilized by an ATP-sensitive plus-end cap.* J Cell Sci, 2000. **113 (Pt 22)**: p. 3907-19.

84. Rudiger, M., J. Wehland, and K. Weber, *The carboxy-terminal peptide of detyrosinated alpha tubulin provides a minimal system to study the substrate specificity of tubulin-tyrosine ligase.* Eur J Biochem, 1994. **220**(2): p. 309-20.

85. Webster, D.R., et al., *Assembly and turnover of detyrosinated tubulin in vivo.* J Cell Biol, 1987. **105**(1): p. 265-76.

86. Szyk, A., et al., *Tubulin tyrosine ligase structure reveals adaptation of an ancient fold to bind and modify tubulin.* Nat Struct Mol Biol, 2011. **18**(11): p. 1250-8.

87. Edde, B., et al., *Posttranslational glutamylation of alpha-tubulin.* Science, 1990. **247**(4938): p. 83-5.

88. Rudiger, M., et al., *Class II tubulin, the major brain beta tubulin isotype is polyglutamylated on glutamic acid residue 435.* FEBS Lett, 1992. **308**(1): p. 101-5.

89. Bobinnec, Y., et al., *Glutamylation of centriole and cytoplasmic tubulin in proliferating non-neuronal cells.* Cell Motil Cytoskeleton, 1998. **39**(3): p. 223-32.

90. Janke, C., et al., *Tubulin polyglutamylase enzymes are members of the TTL domain protein family.* Science, 2005. **308**(5729): p. 1758-62.

91. Gagnon, C., et al., *The polyglutamylated lateral chain of alpha-tubulin plays a key role in flagellar motility.* J Cell Sci, 1996. **109 (Pt 6)**: p. 1545-53.

92. Gaertig, J. and D. Wloga, *Ciliary tubulin and its post-translational modifications.* Curr Top Dev Biol, 2008. **85**: p. 83-113.

93. Avasthi, P. and W.F. Marshall, *Stages of ciliogenesis and regulation of ciliary length.* Differentiation, 2012. **83**(2): p. S30-42.

94. Miyoshi, K., et al., *Factors that influence primary cilium length.* Acta Med Okayama, 2011. **65**(5): p. 279-85.

95. Abdul-Majeed, S., B.C. Moloney, and S.M. Nauli, *Mechanisms regulating cilia growth and cilia function in endothelial cells.* Cell Mol Life Sci, 2012. **69**(1): p. 165-73.

96. Besschetnova, T.Y., et al., *Identification of signaling pathways regulating primary cilium length and flow-mediated adaptation.* Curr Biol, 2010. **20**(2): p. 182-7.

97. Burghoorn, J., et al., *Mutation of the MAP kinase DYF-5 affects docking and undocking of kinesin-2 motors and reduces their speed in the cilia of Caenorhabditis elegans.* Proc Natl Acad Sci U S A, 2007. **104**(17): p. 7157-62.

98. Mukhopadhyay, S., et al., *TULP3 bridges the IFT-A complex and membrane phosphoinositides to promote trafficking of G protein-coupled receptors into primary cilia.* Genes Dev, 2010. **24**(19): p. 2180-93.

99. Wang, Q., J. Pan, and W.J. Snell, *Intraflagellar transport particles participate directly in cilium-generated signaling in Chlamydomonas.* Cell, 2006. **125**(3): p. 549-62.

100. Forrest, A.R., et al., *Exploration of the cell-cycle genes found within the RIKEN FANTOM2 data set.* Genome Res, 2003. **13**(6B): p. 1366-75.

101. Belham, C., et al., *A mitotic cascade of NIMA family kinases. Nercc1/Nek9 activates the Nek6 and Nek7 kinases.* J Biol Chem, 2003. **278**(37): p. 34897-909.

102. Caenepeel, S., et al., *The mouse kinome: discovery and comparative genomics of all mouse protein kinases.* Proc Natl Acad Sci U S A, 2004. **101**(32): p. 11707-12.

103. Upadhya, P., et al., *Mutations in a NIMA-related kinase gene, Nek1, cause pleiotropic effects including a progressive polycystic kidney disease in mice.* Proc Natl Acad Sci U S A, 2000. **97**(1): p. 217-21.

104. Liu, S., et al., *A defect in a novel Nek-family kinase causes cystic kidney disease in the mouse and in zebrafish.* Development, 2002. **129**(24): p. 5839-46.

105. Sohara, E., et al., *Nek8 regulates the expression and localization of polycystin-1 and polycystin-2.* J Am Soc Nephrol, 2008. **19**(3): p. 469-76.

106. Thiel, C., et al., *NEK1 mutations cause short-rib polydactyly syndrome type majewski.* Am J Hum Genet, 2011. **88**(1): p. 106-14.

107. Corbit, K.C., et al., *Vertebrate Smoothened functions at the primary cilium.* Nature, 2005. **437**(7061): p. 1018-21.

108. Haycraft, C.J., et al., *Gli2 and Gli3 localize to cilia and require the intraflagellar transport protein polaris for processing and function.* PLoS Genet, 2005. **1**(4): p. e53.

109. Sfakianos, J., et al., *Par3 functions in the biogenesis of the primary cilium in polarized epithelial cells.* J Cell Biol, 2007. **179**(6): p. 1133-40.

110. Nakamura, S., H. Takino, and M.K. Kojima, *Effect of Lithium on Flagellar Length in Chlamydomonas-Reinhardtii.* Cell Structure and Function, 1987. **12**(4): p. 369-374.

111. Wilson, N.F. and P.A. Lefebvre, *Regulation of flagellar assembly by glycogen synthase kinase 3 in Chlamydomonas reinhardtii.* Eukaryot Cell, 2004. **3**(5): p. 1307-19.

112. Miyoshi, K., et al., *Lithium treatment elongates primary cilia in the mouse brain and in cultured cells.* Biochem Biophys Res Commun, 2009. **388**(4): p. 757-62.

113. Christensen, S.T., et al., *The primary cilium coordinates signaling pathways in cell cycle control and migration during development and tissue repair.* Curr Top Dev Biol, 2008. **85**: p. 261-301.

114. Eggenschwiler, J.T. and K.V. Anderson, *Cilia and developmental signaling.* Annu Rev Cell Dev Biol, 2007. **23**: p. 345-73.

115. Kiprilov, E.N., et al., *Human embryonic stem cells in culture possess primary cilia with hedgehog signaling machinery.* J Cell Biol, 2008. **180**(5): p. 897-904.

116. Gerdes, J.M., E.E. Davis, and N. Katsanis, *The vertebrate primary cilium in development, homeostasis, and disease.* Cell, 2009. **137**(1): p. 32-45.

117. Jones, C. and P. Chen, *Primary cilia in planar cell polarity regulation of the inner ear.* Curr Top Dev Biol, 2008. **85**: p. 197-224.

118. Schneider, L., et al., *PDGFRalphaalpha signaling is regulated through the primary cilium in fibroblasts.* Curr Biol, 2005. **15**(20): p. 1861-6.

119. Lemmon, M.A. and J. Schlessinger, *Cell signaling by receptor tyrosine kinases.* Cell, 2010. **141**(7): p. 1117-34.

120. Christensen, S.T., et al., *Primary cilia and coordination of receptor tyrosine kinase (RTK) signalling.* J Pathol, 2012. **226**(2): p. 172-84.

121. Christensen, S.T., et al., *Primary Cilia and Coordination of Receptor Tyrosine Kinase (RTK) and Transforming Growth Factor beta (TGF-beta) Signaling.* Cold Spring Harb Perspect Biol, 2017. **9**(6).

122. Schier, A.F. and M.M. Shen, *Nodal signalling in vertebrate development.* Nature, 2000. **403**(6768): p. 385-9.

123. Saijoh, Y., et al., *Left-right asymmetric expression of lefty2 and nodal is induced by a signaling pathway that includes the transcription factor FAST2.* Mol Cell, 2000. **5**(1): p. 35-47.

124. Suzue, N., et al., *Ubiquitin ligase Cbl-b downregulates bone formation through suppression of IGF-I signaling in osteoblasts during denervation.* J Bone Miner Res, 2006. **21**(5): p. 722-34.

125. Han, Y.M., et al., *Leptin-promoted cilia assembly is critical for normal energy balance.* J Clin Invest, 2014. **124**(5): p. 2193-7.

126. Pugh, T.J., et al., *Medulloblastoma exome sequencing uncovers subtype-specific somatic mutations.* Nature, 2012. **488**(7409): p. 106-10.

127. Nishimura, Y., et al., *Primary Cilia as Signaling Hubs in Health and Disease.* Advanced Science, 2019. **6**(1).

128. Issad, T. and M. Kuo, *O-GlcNAc modification of transcription factors, glucose sensing and glucotoxicity.* Trends Endocrinol Metab, 2008. **19**(10): p. 380-9.

129. Zachara, N.E. and G.W. Hart, *O-GlcNAc a sensor of cellular state: the role of nucleocytoplasmic glycosylation in modulating cellular function in response to nutrition and stress.* Biochim Biophys Acta, 2004. **1673**(1-2): p. 13-28.

130. Yu, F., et al., *Ciliary defects caused by dysregulation of O-GlcNAc modification are associated with diabetic complications.* Cell Res, 2019. **29**(2): p. 171-173.

131. Takahashi, K., et al., *Glucose deprivation induces primary cilium formation through mTORC1 inactivation.* J Cell Sci, 2018. **131**(1).

132. Ritter, A., et al., *Primary Cilia Are Dysfunctional in Obese Adipose-Derived Mesenchymal Stem Cells.* Stem Cell Reports, 2018. **10**(2): p. 583-599.

133. Buse, M.G., *Hexosamines, insulin resistance, and the complications of diabetes: current status.* Am J Physiol Endocrinol Metab, 2006. **290**(1): p. E1-E8.

134. Copeland, R.J., J.W. Bullen, and G.W. Hart, *Cross-talk between GlcNAcylation and phosphorylation: roles in insulin resistance and glucose toxicity.* Am J Physiol Endocrinol Metab, 2008. **295**(1): p. E17-28.

135. Zachara, N., Y. Akimoto, and G.W. Hart, *The O-GlcNAc Modification*, in *Essentials of Glycobiology*, rd, et al., Editors. 2015: Cold Spring Harbor (NY). p. 239-251.

136. Nishikawa, I., et al., *Computational prediction of O-linked glycosylation sites that preferentially map on intrinsically disordered regions of extracellular proteins.* Int J Mol Sci, 2010. **11**(12): p. 4991-5008.

137. Ruan, H.B., et al., *Cracking the O-GlcNAc code in metabolism.* Trends Endocrinol Metab, 2013. **24**(6): p. 301-9.

138. Butkinaree, C., K. Park, and G.W. Hart, *O-linked beta-N-acetylglucosamine (O-GlcNAc): Extensive crosstalk with phosphorylation to regulate signaling and transcription in response to nutrients and stress.* Biochim Biophys Acta, 2010. **1800**(2): p. 96-106.

139. Yi, W., et al., *Phosphofructokinase 1 glycosylation regulates cell growth and metabolism.* Science, 2012. **337**(6097): p. 975-80.

140. Slawson, C. and G.W. Hart, *O-GlcNAc signalling: implications for cancer cell biology.* Nat Rev Cancer, 2011. **11**(9): p. 678-84.

141. Yang, X., et al., *Phosphoinositide signalling links O-GlcNAc transferase to insulin resistance.* Nature, 2008. **451**(7181): p. 964-9.

142. Yuzwa, S.A., et al., *Increasing O-GlcNAc slows neurodegeneration and stabilizes tau against aggregation.* Nat Chem Biol, 2012. **8**(4): p. 393-9.

143. Zhu, Y., et al., *The emerging link between O-GlcNAc and Alzheimer disease.* J Biol Chem, 2014. **289**(50): p. 34472-81.

144. Hardiville, S. and G.W. Hart, *Nutrient regulation of signaling, transcription, and cell physiology by O-GlcNAcylation.* Cell Metab, 2014. **20**(2): p. 208-13.

145. Hart, G.W., M.P. Housley, and C. Slawson, *Cycling of O-linked beta-N-acetylglucosamine on nucleocytoplasmic proteins.* Nature, 2007. **446**(7139): p. 1017-22.

146. Hart, G.W., et al., *Cross talk between O-GlcNAcylation and phosphorylation: roles in signaling, transcription, and chronic disease.* Annu Rev Biochem, 2011. **80**: p. 825-58.

147. Bond, M.R. and J.A. Hanover, *O-GlcNAc cycling: a link between metabolism and chronic disease.* Annu Rev Nutr, 2013. **33**: p. 205-29.

148. Hanover, J.A., M.W. Krause, and D.C. Love, *Bittersweet memories: linking metabolism to epigenetics through O-GlcNAcylation.* Nat Rev Mol Cell Biol, 2012. **13**(5): p. 312-21.

149. Caldwell, S.A., et al., *Nutrient sensor O-GlcNAc transferase regulates breast cancer tumorigenesis through targeting of the oncogenic transcription factor FoxM1.* Oncogene, 2010. **29**(19): p. 2831-42.

150. Park, M.J., et al., *High glucose-induced O-GlcNAcylated carbohydrate response element-binding protein (ChREBP) mediates mesangial cell lipogenesis and fibrosis: the possible role in the development of diabetic nephropathy.* J Biol Chem, 2014. **289**(19): p. 13519-30.

151. Wang, Z., M. Gucek, and G.W. Hart, *Cross-talk between GlcNAcylation and phosphorylation: site-specific phosphorylation dynamics in response to globally elevated O-GlcNAc.* Proc Natl Acad Sci U S A, 2008. **105**(37): p. 13793-8.

152. Soesanto, Y.A., et al., *Regulation of Akt signaling by O-GlcNAc in euglycemia.* Am J Physiol Endocrinol Metab, 2008. **295**(4): p. E974-80.

153. Gandy, J.C., A.E. Rountree, and G.N. Bijur, *Akt1 is dynamically modified with O-GlcNAc following treatments with PUGNAc and insulin-like growth factor-1.* FEBS Lett, 2006. **580**(13): p. 3051-8.

154. Bullen, J.W., et al., *Cross-talk between two essential nutrient-sensitive enzymes: O-GlcNAc transferase (OGT) and AMP-activated protein kinase (AMPK).* J Biol Chem, 2014. **289**(15): p. 10592-606.

155. Kaasik, K., et al., *Glucose sensor O-GlcNAcylation coordinates with phosphorylation to regulate circadian clock.* Cell Metab, 2013. **17**(2): p. 291-302.

156. Wang, Z., A. Pandey, and G.W. Hart, *Dynamic interplay between O-linked N-acetylglucosaminylation and glycogen synthase kinase-3-dependent phosphorylation.* Mol Cell Proteomics, 2007. **6**(8): p. 1365-79.

157. Xu, Q., et al., *AMPK regulates histone H2B O-GlcNAcylation.* Nucleic Acids Res, 2014. **42**(9): p. 5594-604.

158. Du, X.L., et al., *Hyperglycemia-induced mitochondrial superoxide overproduction activates the hexosamine pathway and induces plasminogen activator inhibitor-1 expression by increasing Sp1 glycosylation.* Proc Natl Acad Sci U S A, 2000. **97**(22): p. 12222-6.

159. McDaniel, M.L., et al., *Metabolic and autocrine regulation of the mammalian target of rapamycin by pancreatic beta-cells.* Diabetes, 2002. **51**(10): p. 2877-85.

160. Whiteman, E.L., H. Cho, and M.J. Birnbaum, *Role of Akt/protein kinase B in metabolism.* Trends Endocrinol Metab, 2002. **13**(10): p. 444-51.

161. Hardie, D.G., et al., *Management of cellular energy by the AMP-activated protein kinase system.* FEBS Lett, 2003. **546**(1): p. 113-20.

162. Marshall, S., V. Bacote, and R.R. Traxinger, *Discovery of a metabolic pathway mediating glucose-induced desensitization of the glucose transport system. Role of hexosamine biosynthesis in the induction of insulin resistance.* J Biol Chem, 1991. **266**(8): p. 4706-12.

163. Buse, M.G., et al., *Enhanced O-GlcNAc protein modification is associated with insulin resistance in GLUT1-overexpressing muscles.* Am J Physiol Endocrinol Metab, 2002. **283**(2): p. E241-50.

164. Federici, M., et al., *Insulin-dependent activation of endothelial nitric oxide synthase is impaired by O-linked glycosylation modification of signaling proteins in human coronary endothelial cells.* Circulation, 2002. **106**(4): p. 466-72.

165. Patti, M.E., et al., *Activation of the hexosamine pathway by glucosamine in vivo induces insulin resistance of early postreceptor insulin signaling events in skeletal muscle.* Diabetes, 1999. **48**(8): p. 1562-71.

166. Klein, A.L., et al., *O-linked N-acetylglucosamine modification of insulin receptor substrate-1 occurs in close proximity to multiple SH2 domain binding motifs.* Mol Cell Proteomics, 2009. **8**(12): p. 2733-45.

167. Vosseller, K., et al., *Elevated nucleocytoplasmic glycosylation by O-GlcNAc results in insulin resistance associated with defects in Akt activation in 3T3-L1 adipocytes.* Proc Natl Acad Sci U S A, 2002. **99**(8): p. 5313-8.

168. Nelson, B.A., K.A. Robinson, and M.G. Buse, *High glucose and glucosamine induce insulin resistance via different mechanisms in 3T3-L1 adipocytes.* Diabetes, 2000. **49**(6): p. 981-91.

169. Nakamura, M., et al., *Excessive hexosamines block the neuroprotective effect of insulin and induce apoptosis in retinal neurons.* J Biol Chem, 2001. **276**(47): p. 43748-55.

170. McClain, D.A. and E.D. Crook, *Hexosamines and insulin resistance.* Diabetes, 1996. **45**(8): p. 1003-9.

171. McClain, D.A., et al., *Altered glycan-dependent signaling induces insulin resistance and hyperleptinemia.* Proc Natl Acad Sci U S A, 2002. **99**(16): p. 10695-9.

172. Heiss, W.D., et al., *Abnormalities of energy metabolism in Alzheimer's disease studied with PET.* Ann N Y Acad Sci, 1991. **640**: p. 65-71.

173. Drzezga, A., et al., *Cerebral metabolic changes accompanying conversion of mild cognitive impairment into Alzheimer's disease: a PET follow-up study.* Eur J Nucl Med Mol Imaging, 2003. **30**(8): p. 1104-13.

174. Liu, F., et al., *O-GlcNAcylation regulates phosphorylation of tau: a mechanism involved in Alzheimer's disease.* Proc Natl Acad Sci U S A, 2004. **101**(29): p. 10804-9.

175. Alzheimer, A., et al., *An English translation of Alzheimer's 1907 paper, "Uber eine eigenartige Erkankung der Hirnrinde".* Clin Anat, 1995. **8**(6): p. 429-31.

176. Griffith, L.S., M. Mathes, and B. Schmitz, *Beta-amyloid precursor protein is modified with O-linked N-acetylglucosamine.* J Neurosci Res, 1995. **41**(2): p. 270-8.

177. Kim, C., et al., *O-linked beta-N-acetylglucosaminidase inhibitor attenuates beta-amyloid plaque and rescues memory impairment.* Neurobiol Aging, 2013. **34**(1): p. 275-85.

178. Bendor, J.T., T.P. Logan, and R.H. Edwards, *The function of alpha-synuclein.* Neuron, 2013. **79**(6): p. 1044-66.

179. Marotta, N.P., et al., *O-GlcNAc modification blocks the aggregation and toxicity of the protein alpha-synuclein associated with Parkinson's disease.* Nat Chem, 2015. **7**(11): p. 913-20.

180. Ferrer, C.M., et al., *O-GlcNAcylation regulates cancer metabolism and survival stress signaling via regulation of the HIF-1 pathway.* Mol Cell, 2014. **54**(5): p. 820-31.

181. DeBerardinis, R.J., et al., *The biology of cancer: metabolic reprogramming fuels cell growth and proliferation.* Cell Metab, 2008. **7**(1): p. 11-20.

182. Hanahan, D. and R.A. Weinberg, *Hallmarks of cancer: the next generation.* Cell, 2011. **144**(5): p. 646-74.

183. Marshall, S., *Role of insulin, adipocyte hormones, and nutrient-sensing pathways in regulating fuel metabolism and energy homeostasis: a nutritional perspective of diabetes, obesity, and cancer.* Sci STKE, 2006. **2006**(346): p. re7.

184. Iyer, N.V., et al., *Cellular and developmental control of O2 homeostasis by hypoxia-inducible factor 1 alpha.* Genes Dev, 1998. **12**(2): p. 149-62.

185. Semenza, G.L., *HIF-1: upstream and downstream of cancer metabolism.* Curr Opin Genet Dev, 2010. **20**(1): p. 51-6.

186. Gradilone, S.A., M.J.L. Pisarello, and N.F. LaRusso, *Primary Cilia in Tumor Biology: The Primary Cilium as a Therapeutic Target in Cholangiocarcinoma.* Curr Drug Targets, 2017. **18**(8): p. 958-963.

187. Hahne, H., et al., *Proteome wide purification and identification of O-GlcNAc-modified proteins using click chemistry and mass spectrometry.* J Proteome Res, 2013. **12**(2): p. 927-36.

188. Teo, C.F., E.G. El-Karim, and L. Wells, *Dissecting PUGNAc-mediated inhibition of the pro-survival action of insulin.* Glycobiology, 2016. **26**(11): p. 1198-1208.

189. Konrad, R.J., et al., *Alloxan is an inhibitor of the enzyme O-linked N-acetylglucosamine transferase.* Biochem Biophys Res Commun, 2002. **293**(1): p. 207-12.

190. Nielsen, J. and J.D. Keasling, *Engineering Cellular Metabolism.* Cell, 2016. **164**(6): p. 1185-1197.

191. Kaznessis, Y.N., *Models for synthetic biology.* BMC Syst Biol, 2007. **1**: p. 47.

192. Yang, S.H., K.C. Cheng, and V.H. Liao, *A novel approach for rapidly and cost-effectively assessing toxicity of toxic metals in acidic water using an acidophilic iron-oxidizing biosensor.* Chemosphere, 2017. **186**: p. 446-452.

193. Hassan, S.H., S.W. Van Ginkel, and S.E. Oh, *Detection of Cr6+ by the sulfur oxidizing bacteria biosensor: effect of different physical factors.* Environ Sci Technol, 2012. **46**(14): p. 7844-8.

194. Lutolf, M.P. and J.A. Hubbell, *Synthetic biomaterials as instructive extracellular microenvironments for morphogenesis in tissue engineering.* Nat Biotechnol, 2005. **23**(1): p. 47-55.

195. Park, T.J., et al., *In vivo synthesis of diverse metal nanoparticles by recombinant Escherichia coli.* Angew Chem Int Ed Engl, 2010. **49**(39): p. 7019-24.

196. Harris, E.H., *Chlamydomonas as a Model Organism.* Annu Rev Plant Physiol Plant Mol Biol, 2001. **52**: p. 363-406.

197. Bui, K.H., et al., *Polarity and asymmetry in the arrangement of dynein and related structures in the Chlamydomonas axoneme.* J Cell Biol, 2012. **198**(5): p. 913-25.

198. Yang, P., et al., *Radial spoke proteins of Chlamydomonas flagella.* J Cell Sci, 2006. **119**(Pt 6): p. 1165-74.

199. Diener, D.R., L.H. Ang, and J.L. Rosenbaum, *Assembly of flagellar radial spoke proteins in Chlamydomonas: identification of the axoneme binding domain of radial spoke protein 3.* J Cell Biol, 1993. **123**(1): p. 183-90.

200. Nicastro, D., et al., *Cryo-electron tomography reveals conserved features of doublet microtubules in flagella.* Proc Natl Acad Sci U S A, 2011. **108**(42): p. E845-53.

201. Yanagisawa, H.A., et al., *FAP20 is an inner junction protein of doublet microtubules essential for both the planar asymmetrical waveform and stability of flagella in Chlamydomonas.* Mol Biol Cell, 2014. **25**(9): p. 1472-83.

202. Farrell, K.W., *Flagellar regeneration in Chlamydomonas reinhardtii: evidence that cycloheximide pulses induce a delay in morphogenesis.* J Cell Sci, 1976. **20**(3): p. 639-54.

203. Pintado, P., et al., *Dynamics of cilia length in left-right development.* R Soc Open Sci, 2017. **4**(3): p. 161102.

204. Keeling, J., L. Tsiokas, and D. Maskey, *Cellular Mechanisms of Ciliary Length Control.* Cells, 2016. **5**(1).

205. Lee, H., et al., *Primary cilia in energy balance signaling and metabolic disorder.* BMB Reports, 2015. **48**(12): p. 647-654.

206. Satir, P. and S.T. Christensen, *Structure and function of mammalian cilia.* Histochem Cell Biol, 2008. **129**(6): p. 687-93.

207. Wang, S., et al., *Reciprocal regulation of cilia and autophagy via the MTOR and proteasome pathways.* Autophagy, 2015. **11**(4): p. 607-16.

208. Bond, M.R. and J.A. Hanover, *A little sugar goes a long way: the cell biology of O-GlcNAc.* J Cell Biol, 2015. **208**(7): p. 869-80.

209. Wells, L., K. Vosseller, and G.W. Hart, *A role for N-acetylglucosamine as a nutrient sensor and mediator of insulin resistance.* Cell Mol Life Sci, 2003. **60**(2): p. 222-8.

210. Song, D.K., J.H. Choi, and M.S. Kim, *Primary Cilia as a Signaling Platform for Control of Energy Metabolism.* Diabetes Metab J, 2018. **42**(2): p. 117-127.

211. Zeidan, Q., et al., *O-GlcNAc cycling enzymes associate with the translational machinery and modify core ribosomal proteins.* Mol Biol Cell, 2010. **21**(12): p. 1922-36.

212. Hardiville, S. and G.W. Hart, *Nutrient regulation of gene expression by O-GlcNAcylation of chromatin.* Curr Opin Chem Biol, 2016. **33**: p. 88-94.

213. Vosseller, K., et al., *Diverse regulation of protein function by O-GlcNAc: a nuclear and cytoplasmic carbohydrate post-translational modification.* Curr Opin Chem Biol, 2002. **6**(6): p. 851-7.

214. Ruan, H.B., Y. Nie, and X. Yang, *Regulation of protein degradation by O-GlcNAcylation: crosstalk with ubiquitination.* Mol Cell Proteomics, 2013. **12**(12): p. 3489-97.

215. Capotosti, F., et al., *O-GlcNAc transferase catalyzes site-specific proteolysis of HCF-1.* Cell, 2011. **144**(3): p. 376-88.

216. Wang, Z., et al., *Extensive crosstalk between O-GlcNAcylation and phosphorylation regulates cytokinesis.* Sci Signal, 2010. **3**(104): p. ra2.

217. Wani, W.Y., et al., *Regulation of autophagy by protein post-translational modification.* Lab Invest, 2015. **95**(1): p. 14-25.

218. Guo, B., et al., *O-GlcNAc-modification of SNAP-29 regulates autophagosome maturation.* Nat Cell Biol, 2014. **16**(12): p. 1215-26.

219. Shi, J., et al., *Diverse regulation of AKT and GSK-3beta by O-GlcNAcylation in various types of cells.* FEBS Lett, 2012. **586**(16): p. 2443-50.

220. Suizu, F., et al., *Phosphorylation-dependent Akt-Inversin interaction at the basal body of primary cilia.* EMBO J, 2016. **35**(12): p. 1346-63.

221. Troilo, A., et al., *HIF1alpha deubiquitination by USP8 is essential for ciliogenesis in normoxia.* EMBO Rep, 2014. **15**(1): p. 77-85.

222. Zhang, B., et al., *GSK3beta-Dzip1-Rab8 cascade regulates ciliogenesis after mitosis.* PLoS Biol, 2015. **13**(4): p. e1002129.

223. Wheway, G., L. Nazlamova, and J.T. Hancock, *Signaling through the Primary Cilium.* Front Cell Dev Biol, 2018. **6**: p. 8.

224. Satir, P. and S.T. Christensen, *Overview of structure and function of mammalian cilia.* Annu Rev Physiol, 2007. **69**: p. 377-400.

225. Malicki, J.J. and C.A. Johnson, *The Cilium: Cellular Antenna and Central Processing Unit.* Trends Cell Biol, 2017. **27**(2): p. 126-140.

226. Eguether, T. and M. Hahne, *Mixed signals from the cell's antennae: primary cilia in cancer.* EMBO Rep, 2018.

227. Guo, J., et al., *Developmental disruptions underlying brain abnormalities in ciliopathies.* Nat Commun, 2015. **6**: p. 7857.

228. Dummer, A., et al., *Measuring the primary cilium length: improved method for unbiased high-throughput analysis.* Cilia, 2016. **5**: p. 7.

229. Ke, Y.N. and W.X. Yang, *Primary cilium: an elaborate structure that blocks cell division?* Gene, 2014. **547**(2): p. 175-85.

230. Shida, T., et al., *The major alpha-tubulin K40 acetyltransferase alphaTAT1 promotes rapid ciliogenesis and efficient mechanosensation.* Proc Natl Acad Sci U S A, 2010. **107**(50): p. 21517-22.

231. Li, L., et al., *MEC-17 deficiency leads to reduced alpha-tubulin acetylation and impaired migration of cortical neurons.* J Neurosci, 2012. **32**(37): p. 12673-83.

232. Ran, J., et al., *Deacetylation of alpha-tubulin and cortactin is required for HDAC6 to trigger ciliary disassembly.* Sci Rep, 2015. **5**: p. 12917.

233. van der Laarse, S.A.M., A.C. Leney, and A.J.R. Heck, *Crosstalk between phosphorylation and O-GlcNAcylation: friend or foe.* FEBS J, 2018. **285**(17): p. 3152-3167.

234. Gurel, Z., et al., *Identification of O-GlcNAc modification targets in mouse retinal pericytes: implication of p53 in pathogenesis of diabetic retinopathy.* PLoS One, 2014. **9**(5): p. e95561.

235. Li, Z., et al., *Checkpoint kinase 1-induced phosphorylation of O-linked beta-N-acetylglucosamine transferase regulates the intermediate filament network during cytokinesis.* J Biol Chem, 2017. **292**(48): p. 19548-19555.

236. Ding, N., et al., *Thiamet-G-mediated inhibition of O-GlcNAcase sensitizes human leukemia cells to microtubule-stabilizing agent paclitaxel.* Biochem Biophys Res Commun, 2014. **453**(3): p. 392-7.

237. Dorfmueller, H.C., et al., *GlcNAcstatin: a picomolar, selective O-GlcNAcase inhibitor that modulates intracellular O-glcNAcylation levels.* J Am Chem Soc, 2006. **128**(51): p. 16484-5.

238. Sousa, P.R., et al., *Protein-ligand interaction study of CpOGA in complex with GlcNAcstatin.* Chem Biol Drug Des, 2013. **81**(2): p. 284-90.

239. Ji, S., et al., *O-GlcNAcylation of tubulin inhibits its polymerization.* Amino Acids, 2011. **40**(3): p. 809-18.

240. Cole, D.G., et al., *Chlamydomonas kinesin-II-dependent intraflagellar transport (IFT): IFT particles contain proteins required for ciliary assembly in Caenorhabditis elegans sensory neurons.* J Cell Biol, 1998. **141**(4): p. 993-1008.

241. Haggarty, S.J., et al., *Domain-selective small-molecule inhibitor of histone deacetylase 6 (HDAC6)-mediated tubulin deacetylation.* Proc Natl Acad Sci U S A, 2003. **100**(8): p. 4389-94.

242. Travaglini, L., et al., *Phenotypic spectrum and prevalence of INPP5E mutations in Joubert syndrome and related disorders.* Eur J Hum Genet, 2013. **21**(10): p. 1074-8.

243. Jacoby, M., et al., *INPP5E mutations cause primary cilium signaling defects, ciliary instability and ciliopathies in human and mouse.* Nat Genet, 2009. **41**(9): p. 1027-31.

244. Bielas, S.L., et al., *Mutations in INPP5E, encoding inositol polyphosphate-5-phosphatase E, link phosphatidyl inositol signaling to the ciliopathies.* Nat Genet, 2009. **41**(9): p. 1032-6.

245. Garcia-Gonzalo, F.R., et al., *Phosphoinositides Regulate Ciliary Protein Trafficking to Modulate Hedgehog Signaling.* Dev Cell, 2015. **34**(4): p. 400-409.

246. Plotnikova, O.V., et al., *INPP5E interacts with AURKA, linking phosphoinositide signaling to primary cilium stability.* J Cell Sci, 2015. **128**(2): p. 364-72.

247. Zhang, Z., et al., *O-GlcNAcase Expression is Sensitive to Changes in O-GlcNAc Homeostasis.* Front Endocrinol (Lausanne), 2014. **5**: p. 206.

248. Shi, H., et al., *Skeletal muscle O-GlcNAc transferase is important for muscle energy homeostasis and whole-body insulin sensitivity.* Mol Metab, 2018. **11**: p. 160-177.

249. de Queiroz, R.M., et al., *Changes in O-Linked N-Acetylglucosamine (O-GlcNAc) Homeostasis Activate the p53 Pathway in Ovarian Cancer Cells.* J Biol Chem, 2016. **291**(36): p. 18897-914.

250. Qian, K., et al., *Transcriptional regulation of O-GlcNAc homeostasis is disrupted in pancreatic cancer.* J Biol Chem, 2018. **293**(36): p. 13989-14000.

251. Boehlke, C., et al., *Primary cilia regulate mTORC1 activity and cell size through Lkb1.* Nat Cell Biol, 2010. **12**(11): p. 1115-22.

252. Thoma, C.R., I.J. Frew, and W. Krek, *The VHL tumor suppressor: riding tandem with GSK3beta in primary cilium maintenance.* Cell Cycle, 2007. **6**(15): p. 1809-13.

253. Yu, I., C.P. Garnham, and A. Roll-Mecak, *Writing and Reading the Tubulin Code.* J Biol Chem, 2015. **290**(28): p. 17163-72.

254. Kubo, T., et al., *Reduced tubulin polyglutamylation suppresses flagellar shortness in Chlamydomonas.* Mol Biol Cell, 2015. **26**(15): p. 2810-22.

255. Wloga, D., et al., *Posttranslational Modifications of Tubulin and Cilia.* Cold Spring Harb Perspect Biol, 2017. **9**(6).

256. Kreppel, L.K. and G.W. Hart, *Regulation of a cytosolic and nuclear O-GlcNAc transferase - Role of the tetratricopeptide repeats.* Journal of Biological Chemistry, 1999. **274**(45): p. 32015-32022.

257. Structural Genomics, C., et al., *Protein production and purification.* Nat Methods, 2008. **5**(2): p. 135-46.

258. Baneyx, F., *Recombinant protein expression in Escherichia coli.* Curr Opin Biotechnol, 1999. **10**(5): p. 411-21.

259. Cregg, J.M., et al., *Recombinant protein expression in Pichia pastoris.* Mol Biotechnol, 2000. **16**(1): p. 23-52.

260. Kost, T.A., J.P. Condreay, and D.L. Jarvis, *Baculovirus as versatile vectors for protein expression in insect and mammalian cells.* Nat Biotechnol, 2005. **23**(5): p. 567-75.

261. Keasling, J.D., *Manufacturing molecules through metabolic engineering.* Science, 2010. **330**(6009): p. 1355-8.

262. Ishikawa, T., *Axoneme Structure from Motile Cilia.* Cold Spring Harb Perspect Biol, 2017. **9**(1).

263. King, S.M., *Axonemal Dynein Arms.* Cold Spring Harb Perspect Biol, 2016. **8**(11).

264. Sanseverino, J., et al., *Use of Saccharomyces cerevisiae BLYES expressing bacterial bioluminescence for rapid, sensitive detection of estrogenic compounds.* Appl Environ Microbiol, 2005. **71**(8): p. 4455-60.

265. Anvarian, Z., et al., *Cellular signalling by primary cilia in development, organ function and disease.* Nat Rev Nephrol, 2019. **15**(4): p. 199-219.

266. Morton, G.J., et al., *Central nervous system control of food intake and body weight.* Nature, 2006. **443**(7109): p. 289-95.

267. Myers, M.G., Jr. and D.P. Olson, *Central nervous system control of metabolism.* Nature, 2012. **491**(7424): p. 357-63.

268. Rodriguez, E.M., J.L. Blazquez, and M. Guerra, *The design of barriers in the hypothalamus allows the median eminence and the arcuate nucleus to enjoy private milieus: the former opens to the portal blood and the latter to the cerebrospinal fluid.* Peptides, 2010. **31**(4): p. 757-76.

269. Millan, M.J., et al., *The role of the mediobasal arcuate hypothalamus in relation to opioid systems in the control of ingestive behaviour in the rat.* Brain Res, 1986. **381**(1): p. 29-42.

270. Skipor, J. and J.C. Thiery, *The choroid plexus--cerebrospinal fluid system: undervaluated pathway of neuroendocrine signaling into the brain.* Acta Neurobiol Exp (Wars), 2008. **68**(3): p. 414-28.

271. Luquet, S., et al., *NPY/AgRP neurons are essential for feeding in adult mice but can be ablated in neonates.* Science, 2005. **310**(5748): p. 683-5.

272. Gropp, E., et al., *Agouti-related peptide-expressing neurons are mandatory for feeding.* Nat Neurosci, 2005. **8**(10): p. 1289-91.

273. Xu, A.W., et al., *Effects of hypothalamic neurodegeneration on energy balance.* PLoS Biol, 2005. **3**(12): p. e415.

274. Waterson, M.J. and T.L. Horvath, *Neuronal Regulation of Energy Homeostasis: Beyond the Hypothalamus and Feeding.* Cell Metab, 2015. **22**(6): p. 962-70.

275. Oh, E.C., S. Vasanth, and N. Katsanis, *Metabolic regulation and energy homeostasis through the primary Cilium.* Cell Metab, 2015. **21**(1): p. 21-31.

276. Cowley, M.A., et al., *Leptin activates anorexigenic POMC neurons through a neural network in the arcuate nucleus.* Nature, 2001. **411**(6836): p. 480-4.

277. Prentki, M., F.M. Matschinsky, and S.R. Madiraju, *Metabolic signaling in fuel-induced insulin secretion.* Cell Metab, 2013. **18**(2): p. 162-85.

278. Ebihara, K., et al., *Involvement of agouti-related protein, an endogenous antagonist of hypothalamic melanocortin receptor, in leptin action.* Diabetes, 1999. **48**(10): p. 2028-33.

279. Elias, C.F., et al., *Leptin activates hypothalamic CART neurons projecting to the spinal cord.* Neuron, 1998. **21**(6): p. 1375-85.

280. Friedman, J.M. and J.L. Halaas, *Leptin and the regulation of body weight in mammals.* Nature, 1998. **395**(6704): p. 763-70.

281. Vaisse, C., et al., *Leptin activation of Stat3 in the hypothalamus of wild-type and ob/ob mice but not db/db mice.* Nat Genet, 1996. **14**(1): p. 95-7.

282. Elias, C.F., et al., *Leptin differentially regulates NPY and POMC neurons projecting to the lateral hypothalamic area.* Neuron, 1999. **23**(4): p. 775-86.

283. Elmquist, J.K., C.F. Elias, and C.B. Saper, *From lesions to leptin: hypothalamic control of food intake and body weight.* Neuron, 1999. **22**(2): p. 221-32.

284. Schwartz, M.W., et al., *Central nervous system control of food intake.* Nature, 2000. **404**(6778): p. 661-71.

285. Konner, A.C., T. Klockener, and J.C. Bruning, *Control of energy homeostasis by insulin and leptin: targeting the arcuate nucleus and beyond.* Physiol Behav, 2009. **97**(5): p. 632-8.

286. Cone, R.D., *The Central Melanocortin System and Energy Homeostasis.* Trends Endocrinol Metab, 1999. **10**(6): p. 211-216.

287. Fan, W., et al., *Role of melanocortinergic neurons in feeding and the agouti obesity syndrome.* Nature, 1997. **385**(6612): p. 165-8.

288. Kitamura, T., et al., *Forkhead protein FoxO1 mediates Agrp-dependent effects of leptin on food intake.* Nat Med, 2006. **12**(5): p. 534-40.

289. Kim, K.W., et al., *FOXO1 in the ventromedial hypothalamus regulates energy balance.* J Clin Invest, 2012. **122**(7): p. 2578-89.

290. Kwon, O., K.W. Kim, and M.S. Kim, *Leptin signalling pathways in hypothalamic neurons.* Cell Mol Life Sci, 2016. **73**(7): p. 1457-77.

291. Konner, A.C., et al., *Insulin action in AgRP-expressing neurons is required for suppression of hepatic glucose production.* Cell Metab, 2007. **5**(6): p. 438-49.

292. Niswender, K.D., et al., *Insulin activation of phosphatidylinositol 3-kinase in the hypothalamic arcuate nucleus: a key mediator of insulin-induced anorexia.* Diabetes, 2003. **52**(2): p. 227-31.

293. Hill, J.W., et al., *Acute effects of leptin require PI3K signaling in hypothalamic proopiomelanocortin neurons in mice.* J Clin Invest, 2008. **118**(5): p. 1796-805.

294. Claret, M., et al., *AMPK is essential for energy homeostasis regulation and glucose sensing by POMC and AgRP neurons.* J Clin Invest, 2007. **117**(8): p. 2325-36.

295. van den Top, M., et al., *Orexigen-sensitive NPY/AgRP pacemaker neurons in the hypothalamic arcuate nucleus.* Nature Neuroscience, 2004. **7**(5): p. 493-494.

296. Kang, G.M., et al., *Leptin Elongates Hypothalamic Neuronal Cilia via Transcriptional Regulation and Actin Destabilization.* J Biol Chem, 2015. **290**(29): p. 18146-55.

297. Whelan, S.A., et al., *Regulation of insulin receptor substrate 1 (IRS-1)/AKT kinase-mediated insulin signaling by O-Linked beta-N-acetylglucosamine in 3T3-L1 adipocytes.* J Biol Chem, 2010. **285**(8): p. 5204-11.

298. Very, N., et al., *Cross-Dysregulation of O-GlcNAcylation and PI3K/AKT/mTOR Axis in Human Chronic Diseases.* Front Endocrinol (Lausanne), 2018. **9**: p. 602.

299. Very, N., et al., *Cross regulation between mTOR signaling and O-GlcNAcylation.* J Bioenerg Biomembr, 2018. **50**(3): p. 213-222.

300. Ruan, H.B., et al., *O-GlcNAc transferase enables AgRP neurons to suppress browning of white fat.* Cell, 2014. **159**(2): p. 306-17.

301. Yang, Y.R., et al., *Obesity resistance and increased energy expenditure by white adipose tissue browning in Oga(+/-) mice.* Diabetologia, 2015. **58**(12): p. 2867-76.

302. Dai, C.L., et al., *Neuronal O-GlcNAc transferase regulates appetite, body weight, and peripheral insulin resistance.* Neurobiol Aging, 2018. **70**: p. 40-50.

APPENDIX

Table A-1. Antibodies used in this study

Antibody	Dilution		Source
	WB	IF	
O-GlcNAc (RL2)	1:1000	NA	Santa Cruz sc-59624
OGT (H-300)	1:1000	NA	Santa Cruz sc-32921
HDAC6 (D2E5)	1:1000	NA	Cell Signaling 7558S
IFT88	1:1000	1:200	Proteintech 13967-I-AP
Acetylated-tubulin	1:5000	1:1000	Sigma-Aldrich 017M-4806
α-Tubulin (B-7)	1:100	NA	Santa Cruz sc-5286
HA (3F10)	1:200	1:100	Sigma-Aldrich 12013819001
β-actin (C4)	1:10000	NA	Santa Cruz sc-47778
ERα	1:200	NA	CTS 8644S
Beta-lactamase	1:100	NA	Sc-66062
FAP20	1:2000	NA	homemade
RSP1	1:5000	NA	homemade

IF, immunofluorescence; NA, not application; WB, Western blot.